UNIVERSITY OF TROMSØ UIT

FACULTY OF SCIENCE AND TECHNOLOGY
DEPARTMENT OF GEOLOGY

Holocene sedimentary environments in Smeerenburgfjorden, Spitsbergen

Julie Heggdal Velle

GEO-3900 Master's Thesis in Geology

November 2012

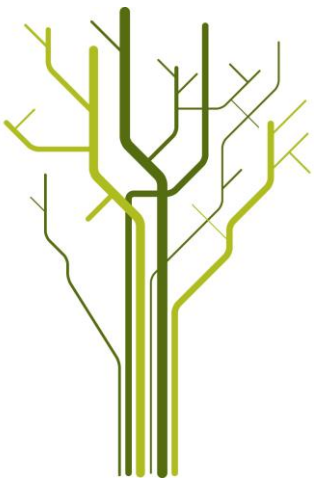

GEO-3900

MASTER'S THESIS IN GEOLOGY

Holocene sedimentary environments in Smeerenburgfjorden, Spitsbergen

Julie Heggdal Velle

November, 2012

FACULTY OF SCIENCE AND TECHNOLOGY
Department of Geology

University of Tromsø

Abstract

Multi-proxy analyses of six sediment cores (including lithostratigraphy, physical properties, granulometric analyses, and XRF scanning), and analyses of swath bathymetry and chirp data were integrated to elucidate the Holocene sedimentary processes and palaeoenvironments in Smeerenburgfjorden, northwest Spitsbergen.

Three basins separated by two sills define the present-day large-scale bathymetry. A transverse ridge in the innermost part of the fjord represents the Little Ice Age (LIA) maximum position of Smeerenburgbreen. Slide scars along the fjord sides and mass transport deposits in the basins indicate repeated mass wasting. Recessional moraines deposited during the last deglaciation suggest a mean annual retreat rate of 140 m/year. Another set of recessional moraines deposited between the maximum LIA position of Smeerenburgbreen and its present day terminus indicate a mean retreat rate of the ice front of ~87 m/year. Although only some of the recessional moraines deposited during the last deglaciation are expressed on the modern seafloor, chirp data reveal that they occur throughout the entire fjord.

Suspension settling, ice rafting and mass wasting are the main sedimentary processes acting in Smeerenburgfjorden. Suspension settling is most important in the inner parts of the fjord, resulting in high sedimentation rates that rapidly decrease with increasing distance from the main sediment sources. Strong out-fjord decreasing trends in magnetic susceptibility and Fe-content indicate that these properties are related to material originating from the Hornemantoppen granite in the catchment of Smeerenburgbreen and are, thus, useful proxies for the reconstruction of the activity of the glacier.

Relatively little ice rafting, most likely related to warmer surface water conditions, occurred between 8650 and 7350 cal. years BP. Ice rafting from both sea-ice and icebergs increased around 6200 cal. years BP and peaked at ~5200 cal. years BP, associated with a regional cooling. Smeerenburgbreen became more active around 2000 cal. years BP. It probably retreated during the Roman Warm Period (50 BC – AD 400) and advanced during the Dark Ages Cold Period (AD 400 – 800). From AD 1300 – 1500 (late Medieval Warm Period; AD 900 – 1500), ice rafting, sedimentation rates and productivity increased in the inner fjord. The Little Ice Age was characterised by reduced ice rafting, possibly linked to an increased sea-ice cover suppressing iceberg drift. An increase in Ice Rafted Debris (IRD) commencing around AD 1880 is suggested to represent the beginning of Smeerenburgbreen's retreat from its LIA maximum towards its present position.

Acknowledgements

First of all, I want to thank my supervisors Prof. Dr. Tore O. Vorren, Dr. Jan Sverre Laberg and Dr. Matthias Forwick for excellent supervision and guidance through writing this thesis. Thank you for sharing your knowledge with me and for inspiring me during this process. A special thanks goes to Matthias; you have been very patient, supportive and encouraging from beginning to end. You deserve endless thanks for always being a source of great inspiration and motivation. Thank you!

Dr. Christian Hass at the Alfred Wegner Institute for Polar and Marine Research in Sylt, Germany, helped me with all the practical and theoretical work concerning both my travel and stay, and, of course, the grain size analyses and statistical programming. Finn Mielck and Nina Wittenberg were also helpful during my stay at the AWI, and made sure I had a great time in Sylt and in the German Bight.

Edel Ellingsen, Ingvild Hald and Trine Dahl were very helpful and answered both practical and theoretical questions during my lab work in Tromsø. Jan P. Holm created the maps and gave me useful tips on creating figures.

I want to thank all my friends and fellow students in brakka, but especially Audun, Morten and Torgeir for all the good times and the good coffee in office 12. A special thanks goes to Torgeir and Malin for the countless hours we have spent together in brakka during these last months. There is never a dull moment with you two around. I also want to thank the lovely Amy Northrop for reading through my thesis and for giving me constructive (and hilarious) comments.

Finally, I have to thank my wonderful family. I could never have completed this without your never ending support and motivation. Thank you.

I am very grateful!

Julie Heggdal Velle
Tromsø, November 2012

Table of contents

1. Introduction

1.1 Objectives

The objectives of this master thesis are

To establish a lithostratigraphic framework and correlate it with acoustic data, and from this

1. describe the sedimentary palaeoenvironment and estimate sedimentation rates in the fjord through the Holocene,
2. identify and define the main sources of sediment to the fjord, and
3. link this to external factors such as climatic-, sea level- and oceanographic changes.

1.2 Background

Fjords are transitions from the terrestrial to the marine environment and are invaluable archives of information about climatic and environmental change. In addition, the often high sedimentation rates of fjords allow us to study such changes with high temporal resolution.

Fjords often contain well-preserved glacimarine sediments and submarine glacial landforms which reveal information on both the style and dynamics of past glaciations, as well as deglaciation history and the following Holocene climatic and oceanographic changes. This information can in turn be used to understand the on-going processes of today and the changes to come in the future (e.g. Elverhøi et al., 1995; Plassen et al., 2004; Landvik et al., 2005; Ottesen et al., 2007; Forwick & Vorren, 2009; Skirbekk et al., 2010; Trusel et a., 2010; Rasmussen et al., 2012).

Spitsbergen fjords are ice-free during the summers and, compared to the fjords of north-eastern Greenland, for example, are easily accessible. They are of special interest, because they i) provide valuable information about the final phase of the decay of the Svalbard-Barents Sea Ice Sheet, ii) archive information about the dynamics of Atlantic Water flow since the last deglaciation, and iii) may be modern analogues of the conditions that have been prevailing in Scandinavia during a late phase of the last glacial and, thus, contribute to understand sedimentary records from Scandinavian fjords.

1.2.1 Glacial history of Spitsbergen

The glacial advances and fluctuations of the Svalbard-Barents Sea Ice Sheet through the last glacial-interglacial cycle and, especially, the configuration and extent of the Late Weichselian ice sheet, have been the subject of multiple studies through the last decades (e.g. Mangerud et al., 1987; Elverhøi et al., 1995; Mangerud et al., 1998, Landvik et al., 1998). During the Late Weichselian, the Svalbard-Barents Sea Ice Sheet is thought to have reached its maximum position at the western Svalbard margin at c. 23.8 cal. ka BP (thousand calendar years before present; Andersen et al., 1996; Jessen et al., 2010). The major fjord systems of Svalbard (e.g. Storfjorden, Bellsund, Isfjorden, Kongsfjorden and Wijdefjorden) acted as pathways channelling fast-flowing ice streams that drained the interior of the ice sheet (Figure 1.1). The ice-streams were separated by areas of thinner, slower moving and dynamically less active ice (Landvik et al 2005; Ottesen et al., 2005, 2007; Ottesen & Dowdeswell, 2009). According to Jessen et al. (2010), the retreat from the outer shelf area began at 20.5 cal. ka BP. The timing of retreat to the western Svalbard coast varies, but in general the ice front had receded to the fjord mouths by 13 cal. ka BP (e.g. Lehman & Forman, 1992; Svendsen & Mangerud, 1992; Elverhøi et al., 1995; Landvik et al., 1998; Ślubowska-Woldengen et al., 2007). For northern Svalbard, it is suggested that the Hinlopen Strait ice and possibly the northern margin of the Svalbard Ice Sheet was deglaciated by ~16.5 cal. ka BP (Koç et al., 2002; Ślubowska-Woldengen et al., 2007).

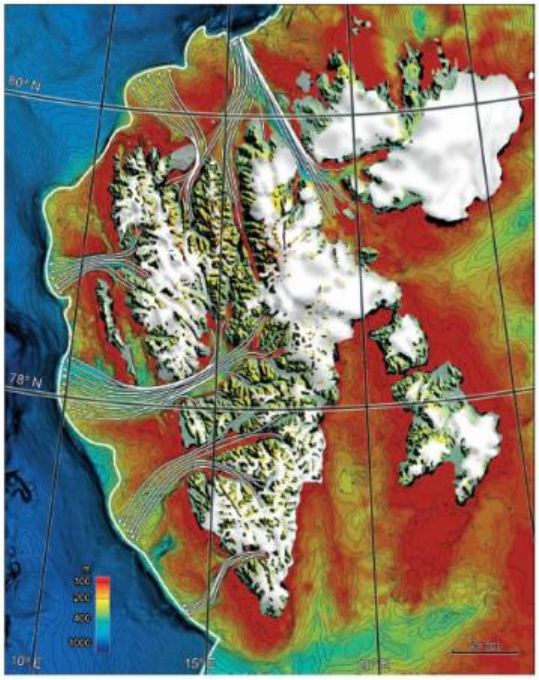

Figure 1.1: *Reconstruction of the palaeo-ice-streams on Svalbard during the Late Weichselian (Ottesen et al., 2007).*

Contrary to Scandinavia and northern Canada (e.g. Andersen et al., 1995; Dyke & Savelle, 2000), no prominent Younger Dryas (YD; 12.9 - 11.6 cal. ka BP) moraines have been found on land on Svalbard. Svendsen & Mangerud (1992) and Mangerud & Landvik (2007) suggested that, in contrast to the Scandinavian ice sheet, the Svalbard-Barents Sea Ice Sheet might not have re-advanced to the west during the Younger Dryas and that the cirque glaciers of Spitsbergen were smaller during the YD than their maximum extent during the Little Ice Age (LIA; AD ~1900). They proposed that starvation of precipitation on western Spitsbergen during the YD might be the reason for the missing re-advances. Some authors (e.g. Forman et al., 1987; Landvik et al., 1987; Lehman & Forman, 1992) identified retarded glacio-isostatic uplift in western Spitsbergen for the Younger Dryas period. Based on this, Landvik et al. (1987) and Svendsen et al. (1996) concluded that the overall recession of the Svalbard-Barents Sea Ice Sheet either came to a halt or re-advanced during the YD. However, so far, no clear evidence has been found. Forwick & Vorren (2009) suggested that a Younger Dryas glacial advance might be archived in proximal glacimarine sediment from central Isfjorden, where it is reflected by an increase in sea-ice formation and -rafting and reduced iceberg-rafting. Furthermore, Forwick & Vorren (2011a) have described moraines and sediment wedges that they suggest might be deposited in relation to a YD glacial re-advance. The final deglaciation was interrupted by multiple halts and/or re-advances and terminated around 11.3 cal. ka BP (Lehman & Forman, 1992; Svendsen & Mangerud, 1992; Elverhøi et al., 1995; Mangerud et al., 1998; Lønne, 2005; Forwick & Vorren, 2009, 2011a; Baeten et al., 2010).

1.2.2 Holocene palaeoclimate of Spitsbergen

Based on a continuous record of Ice Rafted Debris (IRD), Hald et al. (2004), Forwick et al. (2010) and Baeten et al. (2010) proposed that central Spitsbergen never completely deglaciated during the Holocene. Hald et al. (2004) suggested that sea-surface temperatures in the early Holocene (11.2 – 8.8 cal. years BP) were significantly warmer than today and that moderate to low tidewater glaciation characterised the period from 11.2 until ~7.5 cal. years BP. Svendsen & Mangerud (1997) suggested no glacial activity for approximately the same time interval. The occurrence of the mussel *Mytilus edulis* in raised marine sediments (Salvigsen et al., 1990, 1992) and fossils of *Cassiope hypnoides* and *Salix* in Skardtjørna lake sediments both suggest an early- and mid-Holocene climate with temperatures of 1 - 2°C higher than today (Birks, 1991).

After ~9 cal. ka BP, glacial activity increased asynchronously in the Spitsbergen fjords e.g. Van Mijenfjorden from 7.5 cal. ka BP (Hald et al., 2004), outer Isfjorden from 7 cal. ka BP (Forwick & Vorren, 2007), Tempelfjorden and Sassenfjorden from 5.6 cal. years BP (Forwick et al., 2010) and Billefjorden from 5.4 cal. ka BP (Baeten et al., 2010). Svendsen & Mangerud (1997) postulated glacier re-growth in Isfjorden from ~5 cal. ka BP and that the maximum extent was reached during the Little Ice Age. These maximum late Holocene glacial extents were either climatically induced or related to surges (Plassen et al., 2004). Jessen et al. (2010) found increased IRD concentrations in sediment cores off western Spitsbergen in the intervals 7.6 - 6.6 and 5.7 - 2.6 cal. ka BP, also indicating a mid-Holocene glacial advance. A further cooling is suggested from c. 4.7 cal. ka BP, whereas the climate during the last 2.5 cal. ka BP is thought to be relatively close to the present climatic conditions (Birks, 1991; Svendsen & Mangerud, 1997; Ślubowska-Woldengen et al., 2007; Forwick et al., 2010; Skirbekk et al., 2010).

1.2.3 Previous investigations of the study area

The north-western corner of Spitsbergen is situated between two of the Late Weichselian palaeo-ice-streams, Kongsfjorden in the south and Woodfjorden-Wijdefjorden in the north (Ottesen et al., 2007) and was termed an "*inter-ice-stream*" area by Ottesen & Dowdeswell (2009; see below). The glacial-deglacial history and the Holocene palaeoclimate of north-western Spitsbergen and Smeerenburgfjorden are scarcely documented. However, through detailed hydrographic mapping, Liestøl (1972) identified pronounced moraine ridges in the outer shelf area off NW Spitsbergen (Figure 1.2). Three marked ridges were recognised at the mouth of Smeerenburgfjorden as well as morainal ridges at the mouth of Danskegattet and Kobbefjorden (see Figure 1.2 for location). Although no dating was performed, the ridges were interpreted to mark the maximum extent of the Weichselian ice sheet and that the glacier flow in Smeerenburgfjorden at this time had overflows to the west in Danskegattet and Kobbefjorden (Liestøl, 1972). Landvik et al. (1998) suggested that, rather than marking the Late Weichselian maximum extent, the moraines described by Liestøl (1972) may have been deposited during a recessional stage.

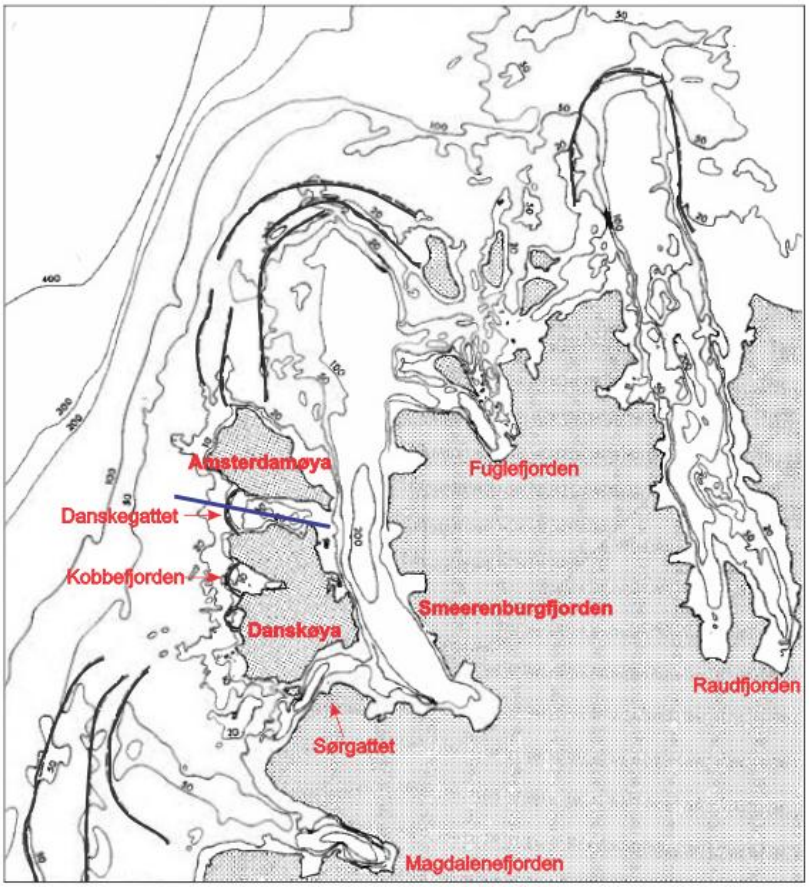

Figure 1.2: *Bathymetric map of north-western Spitsbergen. Moraine ridges are indicated in black lines. The blue line indicates the profile in Figure 1.3. Modified from Liestøl (1972).*

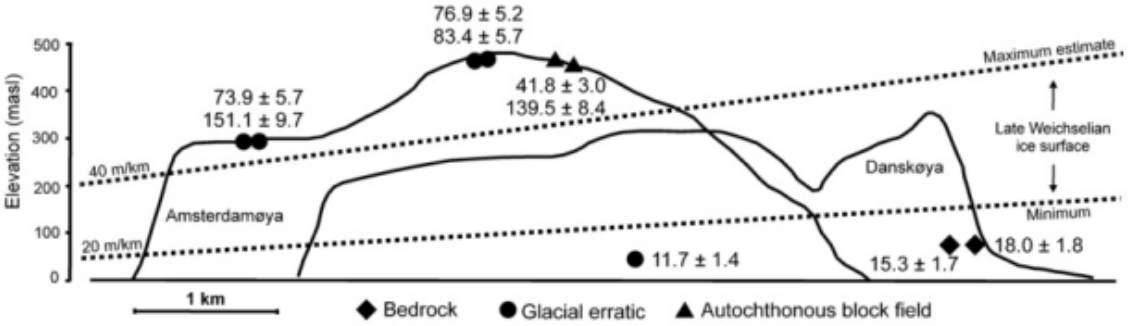

Figure 1.3: *Topographic profiles of Amsterdamøya and Danskøya (profile location is seen in Figure 1.2) with dated samples (in ka; thousand years). The minimum and maximum estimates of the Weichselian ice-sheet surface are indicated in dotted lines (from Landvik et al., 2003).*

Salvigsen (1977) dated marine deposits on Danskøya and Amsterdamøya (see Figure 1.2 for location) and concluded that they belong to two different ages (~40 and 28.5 ^{14}C ka BP) and not to the maximum extent of the last glacial ice cover. The orientation of glacial striae on the two islands was also investigated and showed a general ice flow direction from east to west (Salvigsen, 1977). Based on ^{10}Be exposure dates on bedrock and erratic boulders on Amsterdamøya and Danskøya, Landvik et al. (2003; Figure 1.3) suggested that the plateaus > 300 m.a.s.l. on the two islands had not been covered by ice in the last > 80.000 years. Landvik et al. (2003) also estimated a minimum and maximum Late Weichselian ice-sheet surface gradient of 20 m/km and 40 m/km, respectively (Figure 1.3).

Forman (1990) investigated Late Weichselian and Holocene raised beach sequences and proposed that north-western Spitsbergen was deglaciated early and that it was marginal to any substantial glacial loading during the Late Weichselian. Relatively slow rates (1.5 - 5 m/ka) of post-glacial emergence and two mid- and late-Holocene transgressions were also described for the area (Forman, 1990).

By studying marine-geophysical data, Ottesen & Dowdeswell (2009) identified the submarine landforms on the shelf and in the fjords (Magdalenefjorden, Smeerenburgfjorden and Raudfjorden; see Figure 1.2 for location) on north-western Spitsbergen. Based on this, they created a model of a typical *inter-ice-stream glacial landform assemblage* (Figure 1.4). According to the model, the landforms in inter-ice-stream settings are usually oriented transverse to the palaeo ice-flow direction with small and large retreat moraines, arcuate ridges at the fjord mouth, and more recent LIA moraines and retreat/re-advance ridges in the innermost part of the fjord. Slide scars and –deposits are also a common feature, along with fine-grained basin fills from suspension settling (see also chapter *2.3 Geomorphology*; Ottesen & Dowdeswell, 2009).

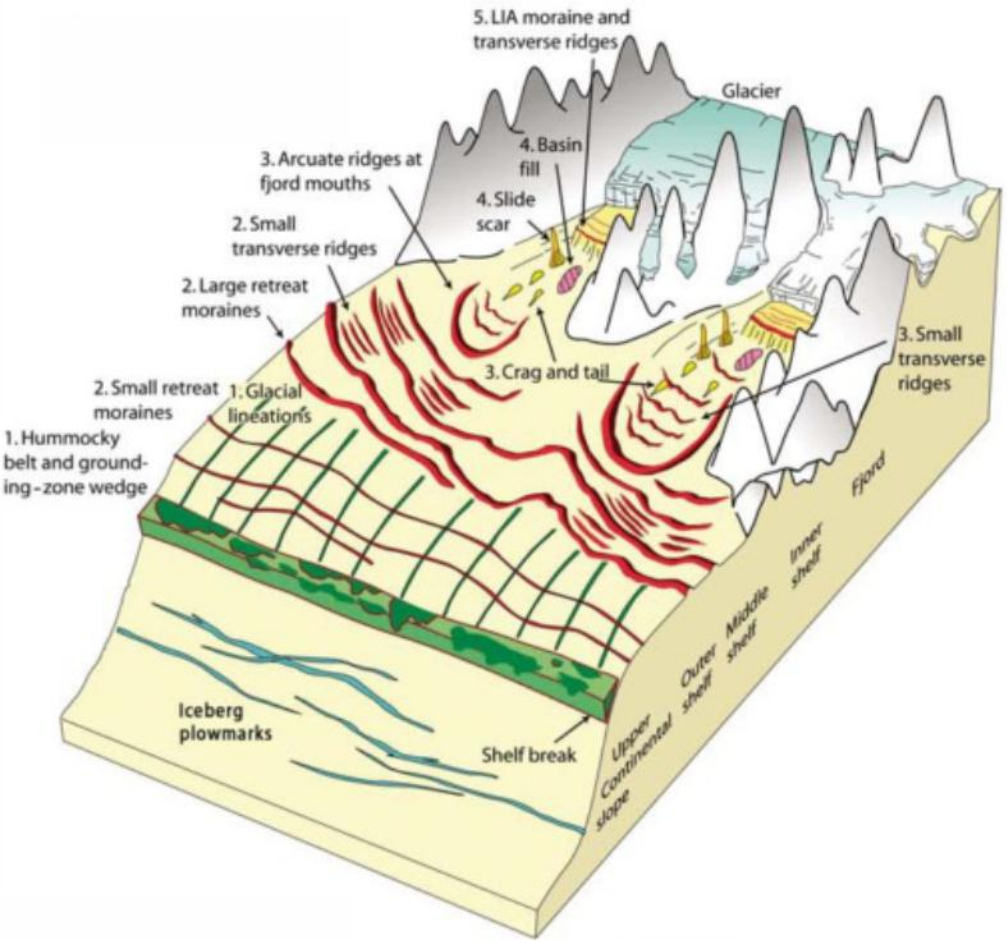

Figure 1.4: *Schematic model of the inter-ice-stream glacial landform assemblage (modified from Ottesen & Dowdeswell, 2009).*

1. Introduction

2. Study area

2.1 Physiographic setting

Svalbard is an Arctic archipelago consisting of all land areas between 74°N - 81°N and 10°E - 35°E (Figure 2.1). With an area of approximately 39,000 km^2, Spitsbergen is the largest of the Svalbard islands and constitutes over half of Svalbard's total area. Western Spitsbergen is characterised by large glacially eroded fjord systems, high mountains (highest mountain: Newtontoppen 1713 m.a.s.l.) but also low-lying coastal strandflat topography (Ingólfsson, 2011).

Smeerenburgfjorden (79°37'N - 79°51'N and 11°00'E - 11°30'E) is located on the north-western corner of Spitsbergen, in the region of Albert I Land (Figure 2.2). The fjord is approximately 20 km long, 2 - 5 km wide and has an N-S orientation in the outer fjord and a NNW-SSE direction in the innermost parts. To the east, the fjord is bordered by the Vasahalvøya peninsula, and by the islands Danskøya and Amsterdamøya to the west. The mouth of Smeerenburgfjorden is called Nordgattet, whereas the sounds Danskegattet (between Amsterdamøya and Danskøya) and Sørgattet (between Danskøya and Spitsbergen) are the western inlets to the fjord. The innermost part of the fjord is named Bjørnfjorden (Figure 2.2).

Figure 2.1: ***A:*** *Overview map of the North Atlantic region.* ***B:*** *Svalbard. Longyearbyen (arrow) and Smeerenburgfjorden (Figure 2.2).*

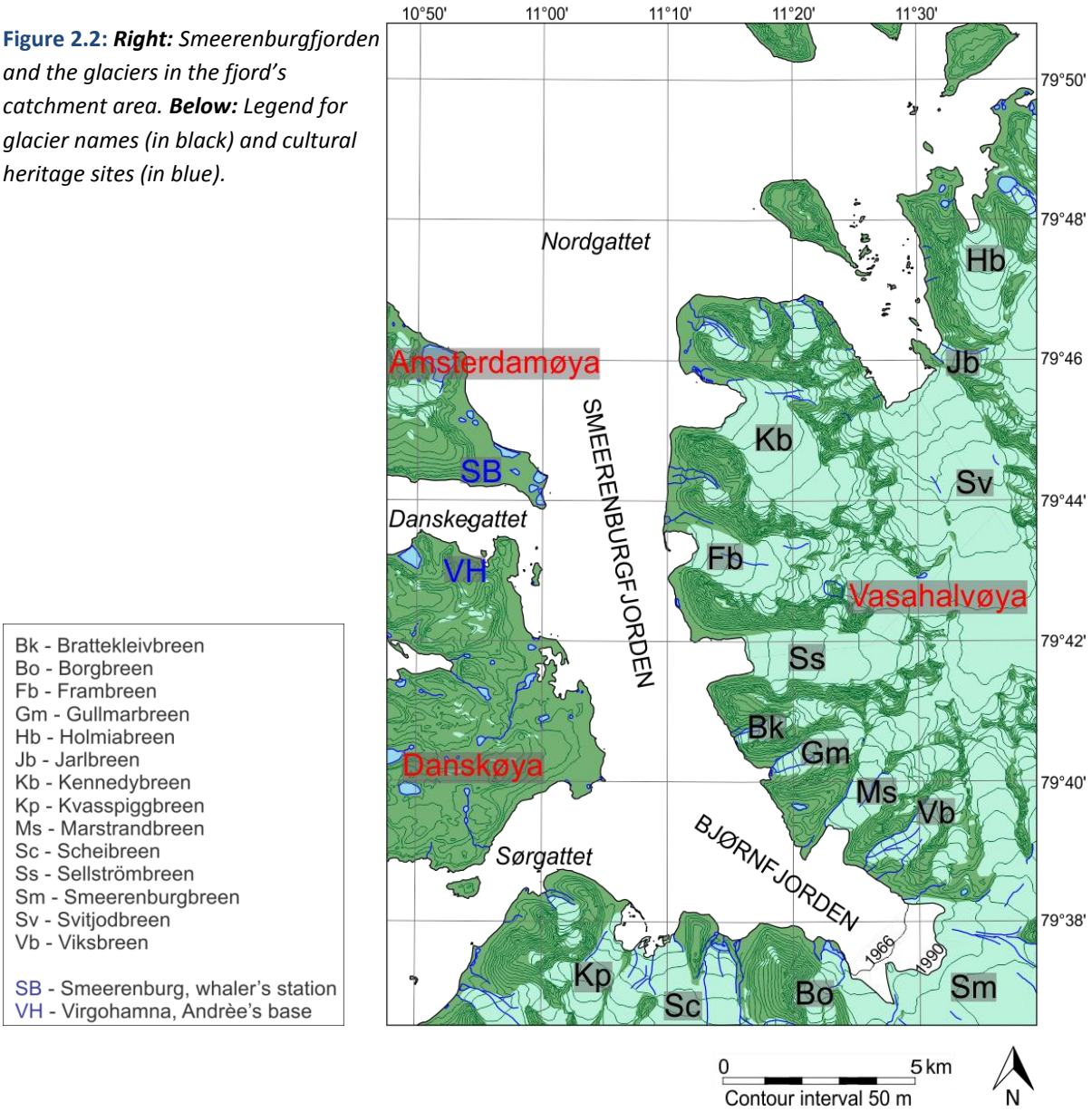

Figure 2.2: ***Right:*** *Smeerenburgfjorden and the glaciers in the fjord's catchment area.* ***Below:*** *Legend for glacier names (in black) and cultural heritage sites (in blue).*

2.2 Bedrock geology

The bedrock in the northern and south-western parts of the catchment area in Smeerenburgfjorden mainly comprise metamorphosed basement (Hecla Hoek) including late-tectonic granite, migmatite and banded gneiss of the Caledonian Smeerenburgfjorden Complex (Mesoproterozoic; Figure 2.3). However, in the inner and south-eastern parts of the fjord, the intrusive Hornemantoppen Granite of the Silurian-Devonian boundary is the most dominant bedrock feature. The N-S orientation of the outer fjord is sub-parallel to the major thrust-faults in the area. However, the inner fjord seems to be sub-parallel to the bedrock boundary separating the Hornemantoppen Granite and the Smeerenburgfjorden Complex (Worsley, 1986; Dallmann et al., 2002; Ohta et al., 2007, 2008; Figure 2.3).

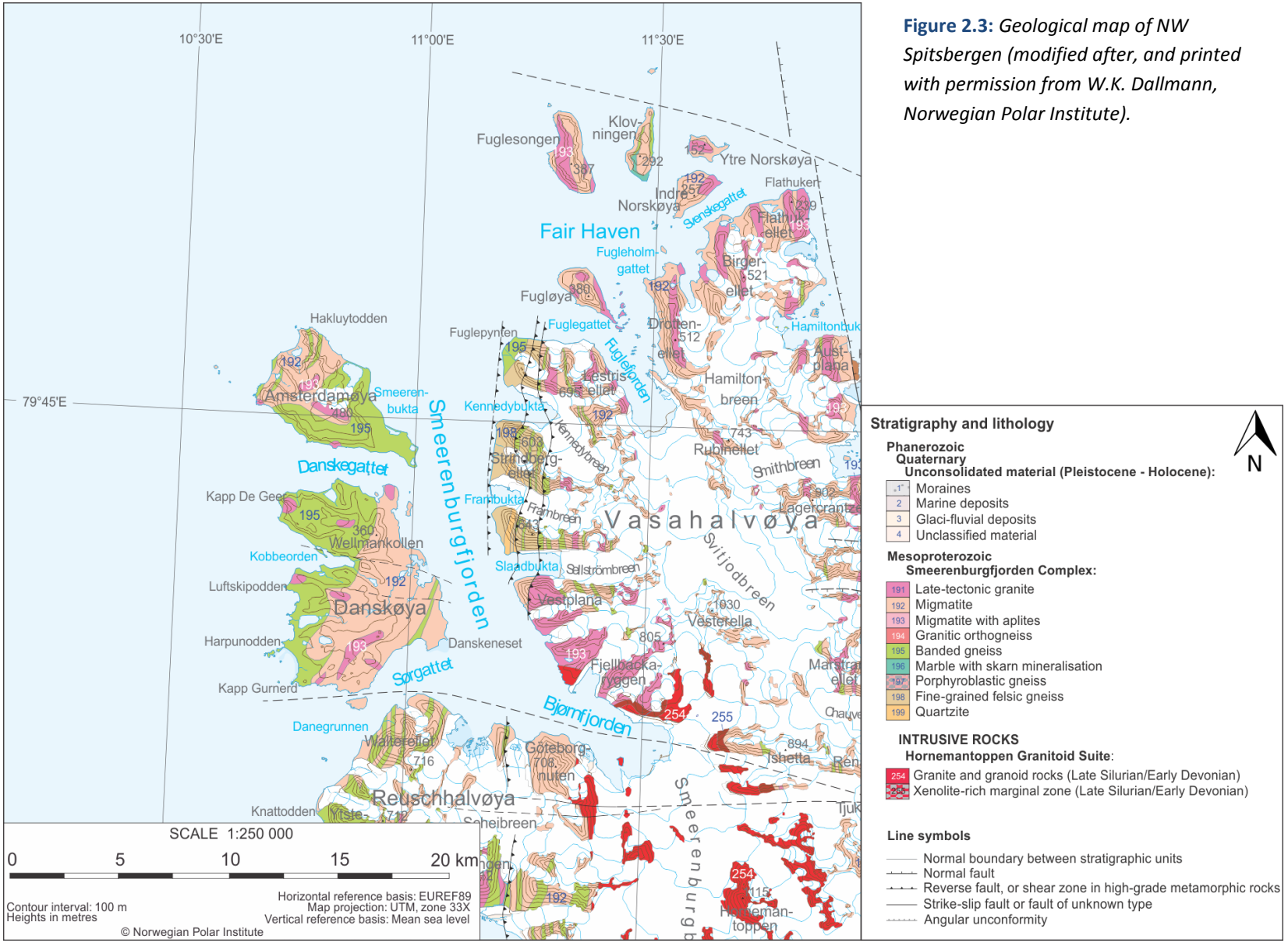

Figure 2.3: *Geological map of NW Spitsbergen (modified after, and printed with permission from W.K. Dallmann, Norwegian Polar Institute).*

2.3 Geomorphology

The term "fjord" has several definitions, but is in general a product of glacial erosion; a steep-sided coastal trough or marine basin (Howe et al., 2010). Fjords typically occur along the coast in regions such as Alaska, Canada, Greenland, Norway, Chile, New Zealand and Antarctica (e.g. Syvitski et al., 1987). The geographical setting of a fjord is influenced by a combination of long periods of glacial activity and erosion, structural fractures and weakness zones of the regional bedrock, and fluvial action (Holtedahl, 1967; Nesje & Whillans, 1994; Kessler et al., 2008). Fjords can be classified based on several different parameters, such as climate regime (polar to temperate climates; Domack & McClennen, 1996), physical regime (e.g. high- or low sedimentation rate; Syvitski et al., 1987) and glacier regime (Hambrey, 1994).

Hambrey (1994) proposed a classification based on glacier regime and influence, including Alaskan, Svalbard, Greenland and Antarctic regimes. Smeerenburgfjorden is a part of the Svalbard regime which is characterised by slightly cold, but very dynamic grounded glaciers and relatively shallow fjords with depths up to 200 meters. Also characteristic for this fjord type are the large amounts of meltwater released during the summer season which are thought to have a large effect on the sedimentation in the fjord (Hambrey, 1994).

The morphology of fjord floors usually comprises an outer sill at the fjord mouth and one or several basins separated by sills (Syvitski et al., 1987). This is also the case in Smeerenburgfjorden where large, arcuate ridges occur on the inner shelf area and the outermost part of the fjord. Within the fjord, there are three basins with smooth seafloors (< 200 m deep) separated by large ridges (Ottesen & Dowdeswell, 2009). The ridges were interpreted to represent longer stillstands in the recessional stages of the glaciation. The smooth seafloor and flat basins are the results of fine-grained sediment rain-out from turbid meltwater plumes draping the fjord floor bathymetry. The steep-sided walls of Smeerenburgfjorden display abundant slide-scars as a result of relatively recent submarine mass wasting activity. In the innermost part of the fjord (within ~2 km of the present day Smeerenburgbreen terminus), there is a 30 m high ridge extending across the fjord interpreted to mark the Little Ice Age glacier maximum extent. Inshore of the LIA moraine, the fjord floor is characterised by a series of smaller ridges, approximately 100 meters apart and with amplitudes of a few meters. These ridges are thought to be formed regularly, and sometimes annually, during smaller glacial re-advances (Figure 1.4; Ottesen & Dowdeswell, 2006, 2009).

2.4 Glaciology

Approximately 60% of Svalbard's land areas are covered by glaciers; large ice caps and smaller valley and cirque glaciers are present today. Tidewater glaciers are common in Svalbard and are characterised by the fact that they terminate in the sea. However, their margin is grounded at a cliff at the grounding line, and not a floating ice shelf. In Smeerenburgfjorden, most of the larger glaciers along the fjord sides are of tidewater type; the largest one being Smeerenburgbreen which terminates in the innermost part of the fjord (Figure 2.2; Hagen et al., 1993; Benn & Evans, 2010).

Smeerenburgfjorden has a drainage basin of 407 km^2 where 232 km^2 is covered by glaciers; a total glacial coverage of 57% (Hagen et al., 1993). The catchment area of Smeerenburgfjorden is relatively small and is constrained by the much larger drainage basins of the neighbouring fjord systems Kongsfjorden-Krossfjorden (2200 km^2) and Woodfjorden-Wijdefjorden (7500 km^2; Hagen et al., 1993; Ottesen & Dowdeswell, 2009; see Ottesen & Dowdeswell, 2009 for location).

Thirty glaciers drain into Smeerenburgfjorden (Figure 2.2; Table 2.1) from Albert I Land and Vasahalvøya and provide sediments to the fjord. The largest glaciers are listed in Table 2.1 whereas the rest are all < 1 km^2 and together only constitute a total area of 8.3 km^2 (Hagen et al., 1993).

Table 2.1: *Glaciers > 1 km^2 in the catchment of Smeerenburgfjorden. Glaciers terminating on land are marked with* **L,** *and tidewater glaciers with* **T** *(Hagen et al., 1993; *Błaszczyk et al., 2009).*

Glacier name	L/T	Area (km^2)	Glacier name	L/T	Area (km^2)
Borgbreen	L	1.55	Kvasspiggbreen	T	2.1*
Brattekleivbreen	L	1.05	Marstrandbreen	T	4.3*
Frambreen	T	4.7*	Scheibreen	L/T	8.1*
Gullmarbreen	L	2.00	Sellströmbreen	T	8.1*
Holmiabreen	T	2.0*	Smeerenburgbreen	T	95.0*
Jarlbreen	T	1.90	Svitjodbreen	T	40.8*
Kennedybreen	T	6.2*	Viksbreen	T	2.05

2.5 Climate

In periods of abundant sea ice, the Svalbard climate can be termed "continental" and is both cold and dry. This is due to the fact that sea ice reflects solar radiation and isolates the sensible and latent heat source of the ocean. On the other hand, in years or periods of little sea ice, the climate is humid and relatively mild; a more "maritime" climate (Førland et al., 2009). The sea-ice conditions are just one of several factors influencing the Svalbard climate and causing large inter-annual fluctuations in temperature. The years before the 1920s were cold, followed by a warm period with temperatures almost as high as the present from the late 1920s to the early 1950s. From the 1960s there has been a gradual warming until the present (Figure 2.4; Førland & Hanssen-Bauer, 2003; Førland et al., 2009).

Due to the stronger influence of drift ice and cold polar air, the northern and eastern parts of Svalbard are cooler than the western and southern regions. In the winter, the temperature gradient from south to north is approximately 2.5°C per degree of latitude, but is somewhat reduced in summer (e.g. Hisdal, 1998; Isaksson et al., 2005). In the coastal areas of central Spitsbergen, the mean annual air temperature (MAAT) at the beginning of the 21st century was around -5°C (Humlum et al., 2003).

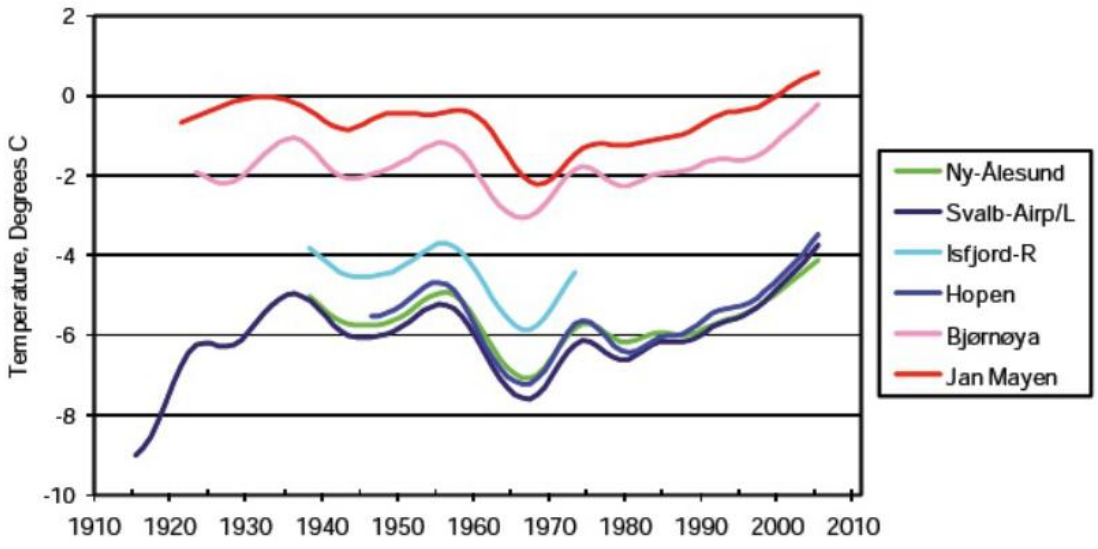

Figure 2.4: *Mean annual air temperature on Jan Mayen and in the Svalbard region (Førland et al., 2009).*

Due to stratified and stable air masses holding small amounts of water, the annual precipitation in Svalbard is relatively low and most of the precipitation occurs in association with cyclones coming in from the south-west and north-west. On Spitsbergen, there is a gradient of lower precipitation values in the north-west (~400 mm/year) to higher precipitation in the south-east (< 1200 mm/year; Hagen et al., 1993; Førland et al., 2009). At Longyearbyen Airport (see Longyearbyen in Figure 2.1 for location), the normal (1961 - 1990) annual measured precipitation is around 190 mm/year with lowest precipitation occurring in the period from April to June. The precipitation record from the same station also shows that the annual precipitation has increased by an average of 2% per decade during the last c. 100 years. Further north, Ny-Ålesund has annual precipitation ranging between ~400 – 450 mm/year (Figure 2.5; Førland & Hanssen-Bauer, 2003; Førland et al., 2009).

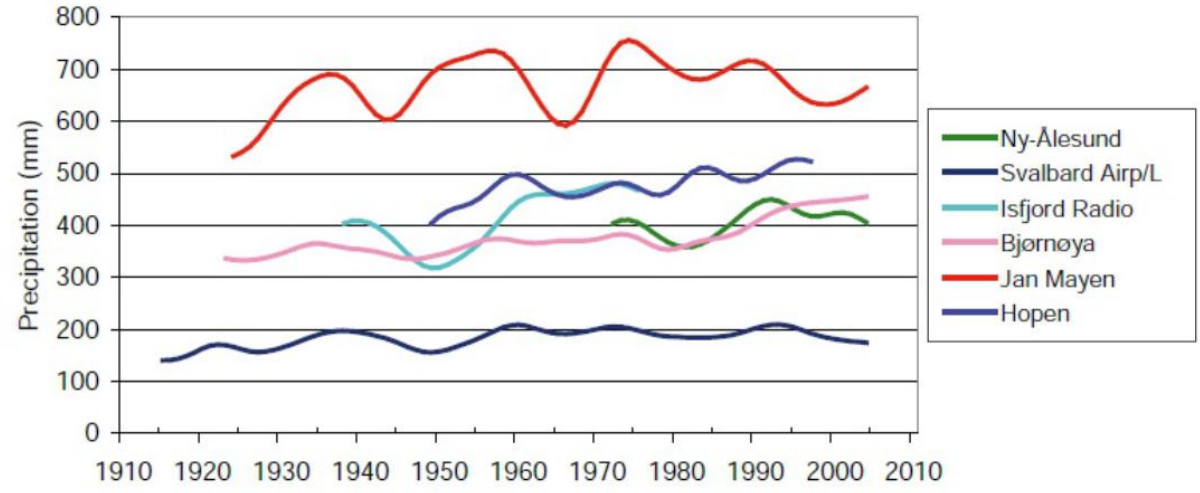

Figure 2.5: *Annual precipitation on Jan Mayen and in the Svalbard region (Førland et al., 2009).*

2.6 Oceanography

Western Spitsbergen is influenced by the relatively warm and saline Atlantic Water (AW) carried northwards in the West Spitsbergen Current (WSC). The WSC follows the continental slope along the west Spitsbergen margin before it enters the Arctic Ocean (Figure 2.6; e.g. Gammelsrød & Rudels, 1983; Saloranta & Svendsen, 2001; Rasmussen et al., 2007; Ślubowska-Woldengen et al., 2007). Arctic-type Water (ArW) originates from the East Spitsbergen Current (ESC) and is cooler and less saline than the Atlantic Water (Nilsen et al., 2008). The ArW is carried from Storfjorden and further north along western Spitsbergen on

the shelf in the Coastal Current (CC; Rasmussen et al., 2007). The boundary between the Atlantic water and Arctic water is termed the Arctic Front and can be divided into two layers; a surface layer (0 – 50 m) which is a density front, and a subsurface layer (> 50 m) which can be characterised as a temperature-salinity front (Saloranta & Svendsen, 2001).

Due to mixing processes with Arctic water on the shelf, the AW entering the fjords on western Spitsbergen differs from the original AW in the WSC. The Atlantic water entering the fjords is therefore often regarded as Transformed Atlantic Water (TAW; Svendsen et al., 2002; Nilsen et al., 2008).

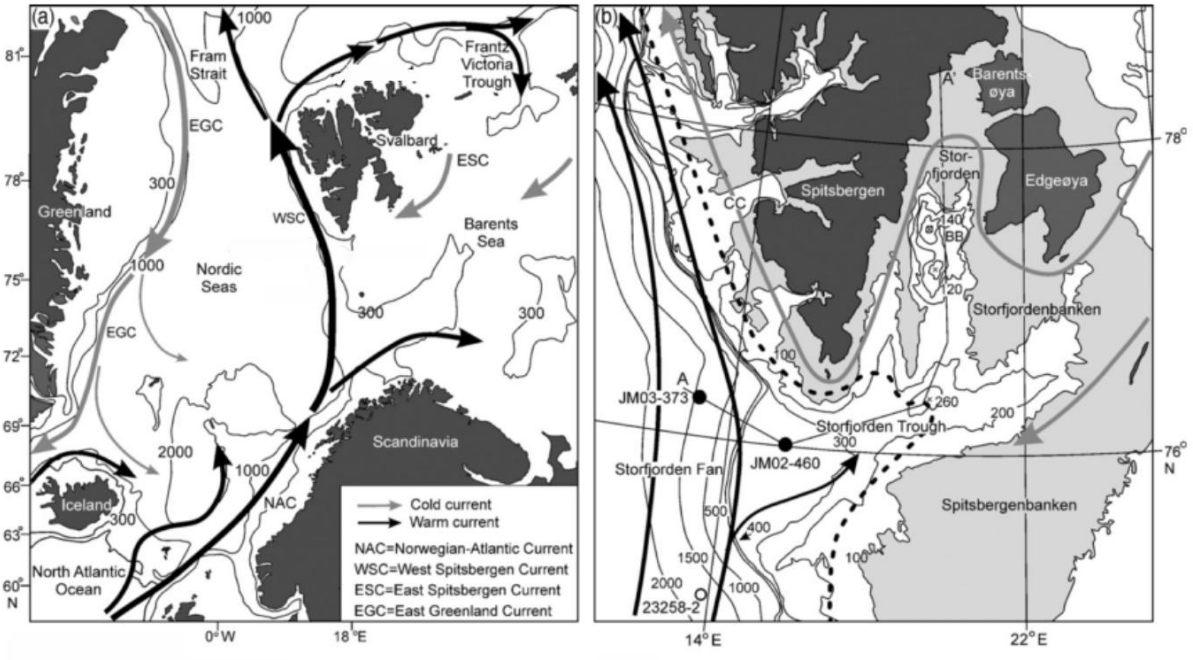

Figure 2.6: *Overview of the main currents in the Svalbard region. The dashed line in the right figure indicates the position of the Arctic Front (Rasmussen et al., 2007).*

Arctic and Svalbard fjords usually consist of three layers of water masses; a cold and fresh surface layer, an intermediate layer at the sill depth and dense deep water below (Figure 2.7; e.g. Azetsu-Scott & Syvitski, 1999; Skogseth et al., 2005; Nilsen et al., 2008, Cottier et al., 2010). The surface waters (SW) are fresh and commonly derived from glacier melt and river runoff; the surface layer is therefore usually best developed in late spring and summer (Nilsen et al., 2008). The intermediate water (IW) can be external to the fjord and formed through a mixture between the SW and the underlying TAW (Azetsu-Scott & Syvitski, 1999; Nilsen et

al., 2008, Cottier et al., 2010). The deepest and densest water masses are formed through the intense cooling of AW during winter or from brine release associated with sea-ice formation (Skogseth et al., 2005; Nilsen et al., 2008).

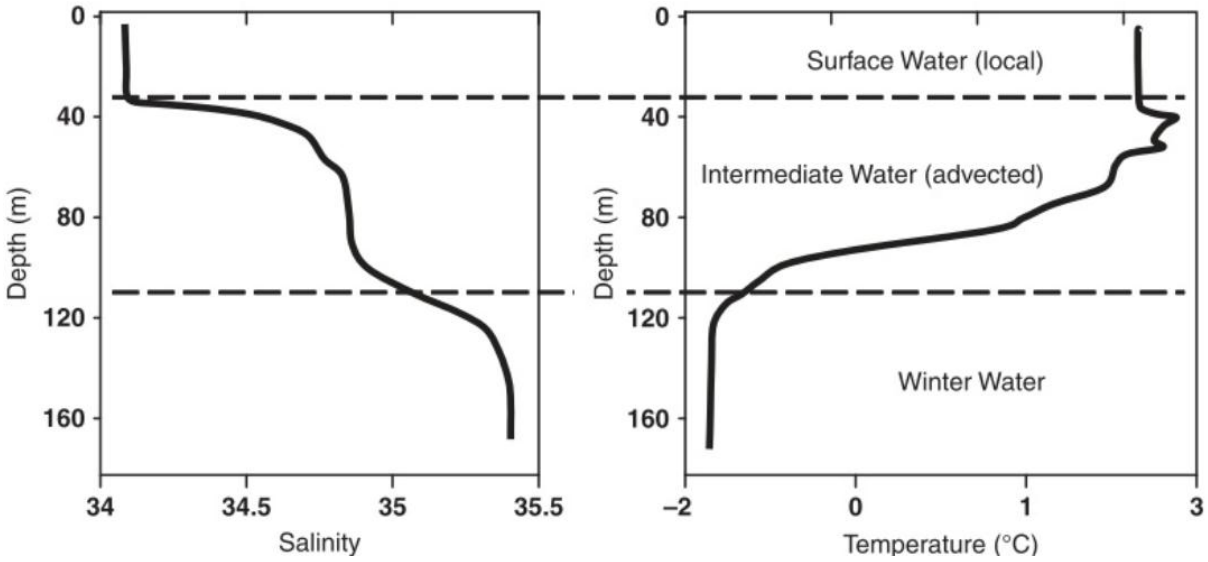

Figure 2.7: *Salinity and temperature profiles illustrating a typical three-layer water mass stratification within an Arctic fjord. The figure is based on data from Storfjorden (SE Svalbard; From Skogseth et al., 2005 in Cottier et al., 2010).*

Both the origin of the different water masses and the stratification can vary inter-annually (e.g. Cottier et al., 2007). The stratification is best developed during summer, whereas heat loss and stronger winds will cause mixing and the formation of local water in autumn. During winter, surface cooling, sea-ice formation and brine release will cause haline convection and further mixing before the spring freshwater input re-establishes the stratification (Svendsen et al., 2002; Nilsen et al., 2008; Cottier et al., 2010).

The general circulation in a fjord depends on several external factors (e.g. freshwater discharge, winds and tides) in combination with the fjord's bathymetry and the Coriolis effect (rotational dynamics; Skarðhamar & Svendsen, 2010). The Coriolis effect causes flow to the right side in the Northern Hemisphere (Syvitski et al., 1987). Due to the Coriolis force, meltwater entering the fjord at the fjord head is deflected to the right (in the out-fjord direction) and the distribution of freshwater in the fjord may therefore vary across the fjord (Svendsen et al., 2002; Cottier et al., 2010). Because the effect of the Coriolis force depends

on the stratification of the fjord's water masses, the impact of the rotation may vary within the fjord (Skarðhamar & Svendsen, 2010).

Jakubas et al. (2011) characterized Smeerenburgfjorden as an "Atlantic environment" and found that the Atlantic Water is present over the whole shelf area and in the fjord from July to August (Figure 2.8). For late August, Ślubowska-Woldengen et al. (2007) found that the Atlantic Water is restricted to the slope area and that the water masses on the shelf are mostly Surface Water and Arctic-type Water (Figure 2.9). Large inter-annual and shorter-time-scale variations in the oceanography of fjords may occur (Cottier et al., 2007; Forwick et al., 2010; Skarðhamar & Svendsen, 2010) and as August is the end of the melt season, the AW may be driven out to the slope area by the large amounts of glacial meltwater entering the fjord.

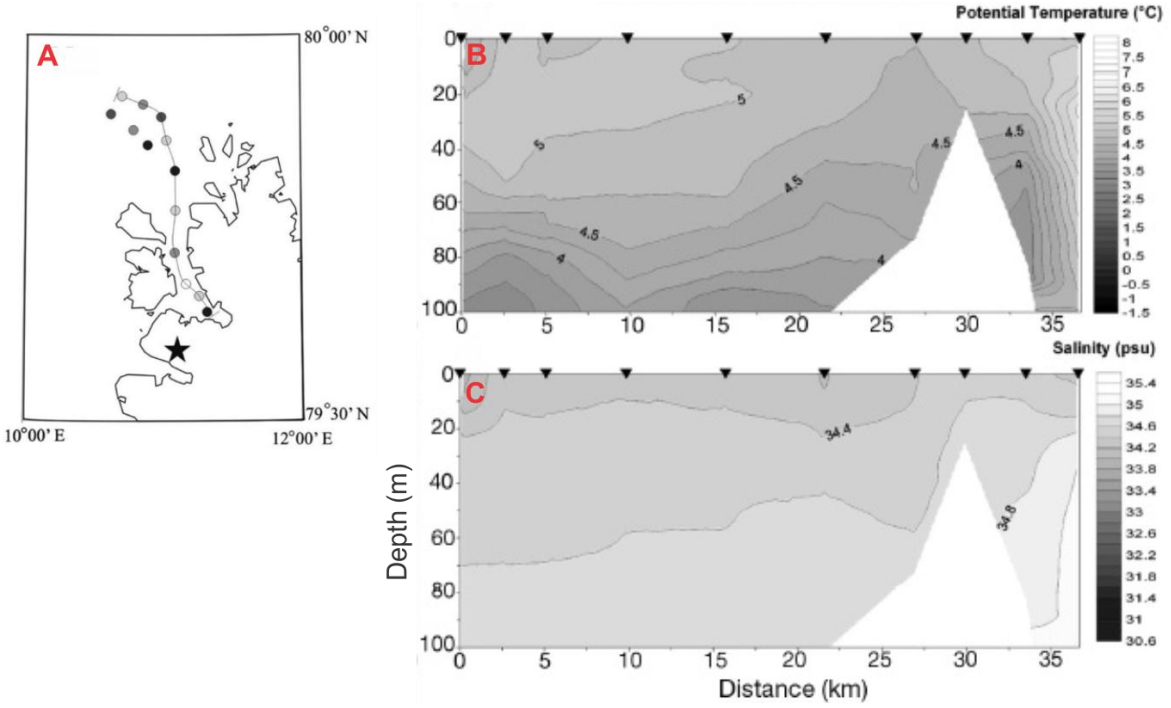

Figure 2.8: ***A:*** *Line indicating the CTD transect line.* ***B:*** *Temperature profile.* ***C:*** *Salinity profile. The triangles on top in B and C correspond to the CTD stations in A. Modified from Jakubas et al., 2011.*

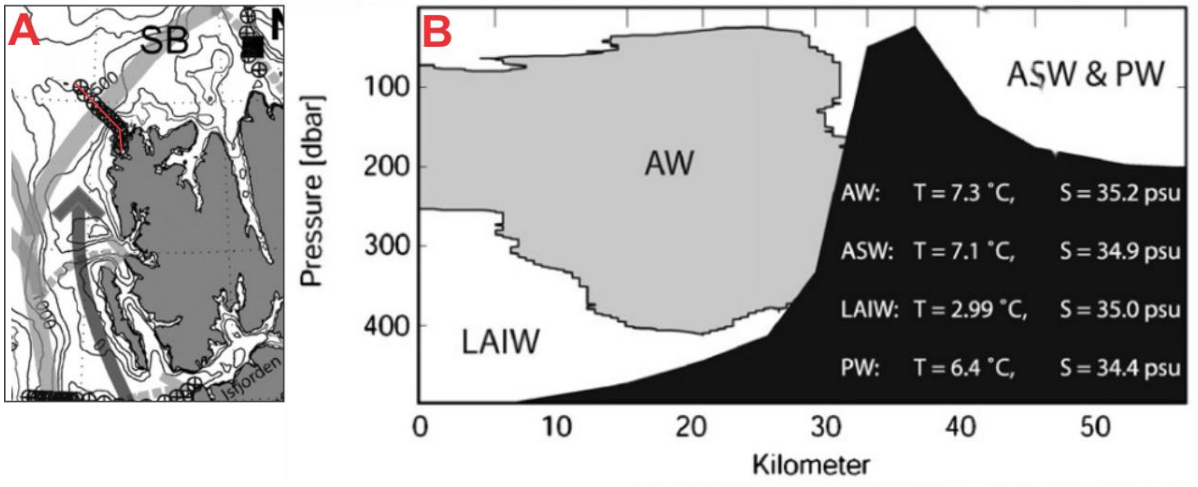

Figure 2.9: A: *The CTD transect across the slope and shelf off Smeerenburgfjorden (red line).* ***B:*** *Water masses on the slope and shelf off Smeerenburgfjorden.* ***LAIW****: Lower Arctic Intermediate Water,* ***AW****: Atlantic Water,* ***ASW****: Arctic Surface Water (compares with SW in the text),* ***PW****: Polar Water (compares with ArW in the text). The tick marks on top correspond to the CTD stations. Modified from Ślubowska-Woldengen et al., 2007.*

3. Materials and methods

3.1 Sediment cores

The sediment cores used in this study were collected with a gravity corer in the springs of 2006 and 2007. They were retrieved during educational cruises of the courses AG-202 and AG-211 ("Arctic Marine Geology") at the University Centre in Svalbard (UNIS) on board the research vessel of the University of Tromsø, R/V Jan Mayen (now R/V Helmer Hanssen). Details of the sediment cores are provided in Table 3.1, below.

Table 3.1: *Core station location and information on the cores used in this study.*

Station	Date	Time (UTC)	Long. (N)	Lat. (E)	Water depth (m)	Penetration (m)	Recovery (m)
JM06-021-GC2	06.05.06	20:02	79°38.32'	11°22,10'	169.3	N.A.	0.60
JM06-022-GC2	06.05.06	21:37	79°39.36'	11°17,32'	150	6	4.35
JM06-023-GC2	06.05.06	22:54	79°41.93'	11°07,69'	197.2	6	4.86
JM06-024-GC3	07.05.06	N.A.	79°48.26'	11°06,87'	181	6	4.10
JM07-048-GC2	04.05.07	13:15	79°43.97'	11°04.67'	214	6	2.75
JM07-049-GC1	04.05.07	14:00	79°46.28'	11°04.75'	174.4	7	3.04

The gravity corer consisted of a 6 meter long steel barrel with a 1600 kg weight attached to its top. The steel barrel contained a 6 meter long plastic liner which was secured in the bottom with a core cutter and core catcher. As the gravity corer penetrated into the seafloor sediments, the core cutter acted as a sharp knife cutting the sediment and making way for the steel barrel which was pushed into the seafloor by the overlying weight. The plastic liner was then filled with sediment secured into place by the core catcher. After retrieving the corer, the plastic liner was removed from the barrel and cut into sections of approximately 1 meter. Each section was sealed with plastic caps and tape before it was thoroughly labelled with station and section number. The cores were stored in 4 °C conditions until they were opened in 2011.

3.2 Laboratory work

The laboratory work started in July 2011 and was continued until March 2012. The work was mainly carried out at the laboratory of the Department of Geology, University of Tromsø, Norway. However, grain-size distribution analyses were performed at the geology laboratory of the Alfred Wegner Institute in List, Sylt, Germany.

3.2.1 Physical properties

Prior to opening, the cores were logged using a GEOTEK Multi Sensor Core Logger (MSCL). The core logger is used to determine physical properties of the sediment such as wet bulk density, P-wave velocity and amplitude as well as magnetic susceptibility. Core diameter and temperature is also recorded during the logging. A belt and a core pusher move the core sections along cylindrical plastic rails. The core is then traveling past the different sensors (Figure 3.1). The core logger can be set to measure at different intervals. In this study the interval was set to 1 cm and the measuring time was 10 seconds. An opening diameter of 5 mm was chosen to collimate the γ-rays.

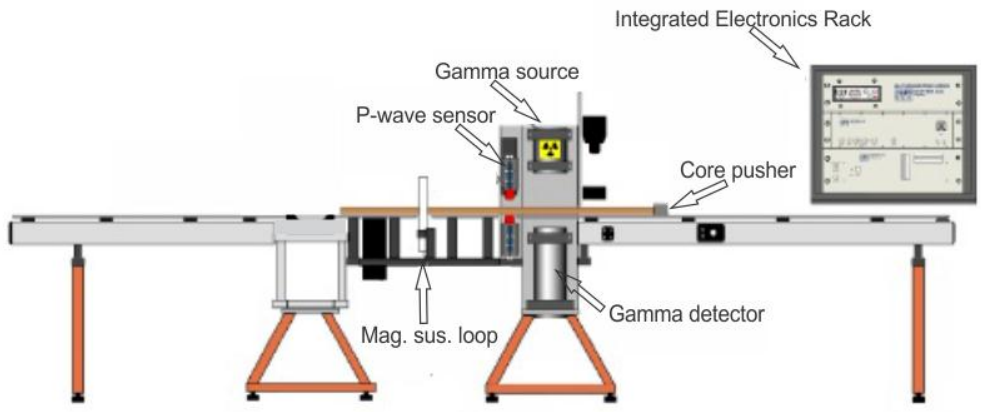

Figure 3.1 *Figure showing the GEOTEK Multi Sensor Core Logger with its main features (Modified from GEOTEK, 2000).*

3.2.1.1 γ-ray attenuation (wet-bulk density)

The wet-bulk density is obtained by measuring unscattered photons that have travelled through the core from a ^{137}Cs source on one side to a detector mounted on the other side. A beam of γ-rays is emitted from the source, and the photons in the beam are scattered as they are blocked by electrons in the sediments. As the density of electrons is related to the density of a material, the bulk density of the core sediments can be calculated (GEOTEK, 2000).

As the ^{137}Cs source is radioactive, its intensity decays over time and to account for these intensity changes, the gamma counts are calibrated before measurement. For the calibration, a short, sealed plastic liner filled with a cylindrical aluminium piece of varying thickness surrounded by water is sent through the core logger. Gamma rays are then sent through the sample piece for long count times (50 seconds) at the different aluminium thicknesses. The information obtained during these measurements is then transferred into the gamma density processing panel, and all essential empirical adjustments are carried out. In addition, different factors can influence the attenuation coefficient of the sediment; e.g. beam spreading and water in the sediment (GEOTEK, 2000).

3.2.1.2 P-wave velocity

One P-wave Transducer (PWT) is attached to each side of the MSCL rail. One transducer acts as a transmitter and the other as a receiver. In the transmitter, a short P-wave pulse is created and sent through the core before it is detected by the receiver. Both the travel time and distance of the pulse is recorded and can be used to calculate the P-wave velocity with a 1.5 ms^{-1} resolution (GEOTEK, 2000).

The P-wave amplitude is also recorded. The amplitude is the intensity of the received pulse which reflects the transducer-liner and liner-sediment contacts. The acoustic coupling between these contacts is of importance as a bad contact will decrease the P-wave amplitude. If the P-wave amplitude is low, the P-wave velocity measurements may not be accurate. The amplitude measurements can also be used for porosity estimates where a low P-wave amplitude may reflect a higher porosity of the sediment (GEOTEK, 2000).

The distance between the two transducers provides information on the core thickness. The core diameter is measured between the active faces of the PWTs with a reference to a known thickness and it is the difference between this reference thickness and the actual core diameter that is recorded (GEOTEK, 2000).

3.2.1.3 Magnetic susceptibility

For magnetic susceptibility measurements, a loop sensor with a given magnetic field is mounted on the core logger. The sensor measures the sediment's ability to become magnetic when exposed to a magnetic field. All materials with magnetic susceptibility will cause a change in the frequency of the magnetic field. The recorded changes in frequency are then converted to magnetic susceptibility values expressed as either mass or volume specific (GEOTEK, 2000).

3.2.1.4 Temperature measurements

During logging, the room temperature is recorded by a thermometer and it is assumed that the cores are of the same temperature. All cores were therefore stored in the same room as the logger for at least one day before the logging started. The temperature is of importance as some of the physical properties (e.g. velocity measurements) are temperature dependent (Weber et al., 1997; GEOTEK, 2000).

3.2.2 Opening cores

The cores were opened in July 2011 using a circular saw and an osmotic knife. One core half was kept for further analysis and lab work while the other half was wrapped in plastic and archived in a cool-storage room at approximately 4 °C.

3.2.3 Sedimentological description and logging

After opening, the surfaces of the sediment cores were studied and described systematically. Visible variations of grain-size, clast content, sedimentary structures, fossils, bioturbation and colour were noted. The latter was decided and named according to the Munsell Soil Color Charts. The results are presented in lithological logs together with colour images (see 5. *Lithostratigraphy*).

3.2.4 X-ray photography

X-ray photographs were taken of half-core sections using a Philips Macrotank. The X-ray photos are basically shadow images where differences in density are shown as lighter or darker areas. Higher density regions are lighter (brighter) whereas lower density areas are darker. This makes it possible to identify internal structures and features of the sediment core that might otherwise not be visible to the eye. The X-ray photographs were described for features such as clasts, fossils, bioturbation and sedimentary structures.

3.2.5 Element geochemistry

Half-sections of the cores were scanned with X-ray fluorescence for determining the geochemical composition, using an Avaatech XRF core scanner. The core scanner has a

Rhodium (Rh) target X-ray tube that gives off primary radiation and the atomic mass range from Mg to U can be measured (Richter et al., 2006; www.avaatech.com).

The electrons of an atom have different characteristic energies, depending on their host element and shell. Electrons of the outer shells have higher energies than the electrons of the inner shells. When the different elements in a sediment sample are hit by primary radiation from an X-ray source, the X-rays are able to expel electrons from their atom, leaving a vacancy in the host shell. The atom is then in an unstable position and replaces the expelled electron with one from an adjacent, outer shell. The new electron (being from an outer orbit) has a higher energy level, and this additional energy is emitted as a secondary X-ray. The detector of the XRF core scanner measures the emitted energies and determines the element composition of the core (Brouwer, 2003).

When using the Avaatech XRF core scanner, the area of measurement can be adjusted in down- and cross-core direction by adjusting slits between the X-ray source and the sediment surface, as well as the sediment surface and the detector. For this study, 10 mm down-core and 12 mm cross-core slits were chosen. The measurements were performed at 10 mm steps using the following settings: 1) 10kV, 1000 µA, 10 sec. counting time, no filter, for measuring the elements Al, Si, S, Cl, K, Ca, Ti, Mn, Fe and Rh, and 2) 30 kV, 2000 µA, 10 sec. counting time, Pd-thick filter, for measuring the elements Rb, Sr and Zr. Other elements were identified, but not included as they did not show any values of interest.

In order to avoid measuring through air, the system measures through a He-flushed chamber. This is also a way of improving the detection of light elements (www.avaatech.com), because the energy of the secondary radiation emitted from these elements would not be sufficiently high to reach the detector when travelling through air. As the He-chamber is located directly on the sediment surface while measuring, the surface of the sediment was smoothened and covered in ultralene foil (4 µm) to prevent contamination of the device. In addition, in order to avoid too much water collecting and forming a water film underneath the ultralene foil, the cores were left in room temperature for some time before the foil was applied (see Tjallingii et al., 2007).

In an attempt to eliminate possible sources of error, the XRF data are given in element ratios rather than intensities. The ratios have earlier shown to be useful for correlations as they are not sensitive to dilution effects caused by, for example, air bubbles or water pools between the sediment surface and the foil. These factors may influence the results in some part as they

might reduce the element intensities of lighter elements such as Al and Si (Tjallingii et al., 2007; Weltje & Tjallingii, 2008). However, they are assumed to be more reliable than exclusively presenting results of single elements.

3.2.6 Colour imaging

The Avaatech core scanner is also equipped with a Jai L-107CC 3 CCD RGB Line Scan Camera (70 µm resolution) which was used to photograph all the core sections. Prior to image acquisition, the sediment surface was cleaned thoroughly using a plastic card. After cleaning, the core surfaces were exposed to air for some time to allow the water to evaporate in order to avoid reflections during acquisition.

3.2.7 Grain-size analysis

3.2.7.1 Sampling

The cores were sub-sampled in volumes of approximately 0.125 cm^3 at intervals of 2 cm (JM06-022-GC2 and JM06-024-GC3), 10 cm (JM06-021-GC2) and 15 cm (JM06-023-GC2, JM07-048-GC2 and JM07-049-GC1). The samples were covered with tap water and kept in closed containers and shipped to the Alfred Wegner Institute of Polar and Marine Research (AWI) in List, Sylt, Germany.

3.2.7.2 Preparation

At the AWI, the samples were treated with acetic acid (CH_3COOH) in order to eliminate carbonates, and with hydrogen peroxide (H_2O_2) to remove organic matter. The chemicals were left to react overnight and then flushed with water two times after each treatment. Finally, sodium polyphosphate (Graham's salt/Calgon) was added to avoid aggregates forming in the samples. They were left on a shaker for approximately 48 hours before measuring (compare with Hass et al., 2010).

Samples from the cores JM06-021-GC2 and JM07-048-GC2 had dried up during shipping and were therefore left in the ultrasonic bath for 5 minutes before measuring. The concentration of the sample was measured at the beginning and end of the ultrasonic bath, but did not differ significantly. The fact that these samples were dried up is therefore not regarded as a significant source of error.

3.2.7.3 Measurements and statistics

The grain-size analysis was carried out with the CILAS 1180L laser-diffraction particle size analyser which has a measurement range of 0.04 – 2500 µm (www.particle-size-analyser.com). Statistical calculations of the data were performed using the software GRADISTAT v. 8.0 (Blott & Pye, 2001). Grain-size distribution percentages given in the following text relate to volume percent as the particle size analyser measures grain volume (cf. Hass et al., 2010).

The grain-size divisions and associated terminology used in the following text is based on the division used in the GRADISTAT program (Table 3.2). Subdivisions of the grain-sizes (e.g. very fine, fine, medium, etc.) are not used; the text refers only to clay, silt and sand.

Table 3.2: *Overview of grain-sizes and descriptive terminology. The GRADISTAT terminology is used in this study. From Blott & Pye, 2001.*

Grain size		Descriptive terminology			
phi	mm/µm	Udden (1914) and Wentworth (1922)	Friedman and Sanders (1978)	GRADISTAT program	
			Very large boulders		
−11	2048 mm		Large boulders	Very large	
−10	1024		Medium boulders	Large	
−9	512	Cobbles	Small boulders	Medium	Boulders
−8	256		Large cobbles	Small	
−7	128		Small cobbles	Very small	
−6	64		Very coarse pebbles	Very coarse	
−5	32		Coarse pebbles	Coarse	
−4	16	Pebbles	Medium pebbles	Medium	Gravel
−3	8		Fine pebbles	Fine	
−2	4	Granules	Very fine pebbles	Very fine	
−1	2	Very coarse sand	Very coarse sand	Very coarse	
0	1	Coarse sand	Coarse sand	Coarse	
1	500 µm	Medium sand	Medium sand	Medium	Sand
2	250	Fine sand	Fine sand	Fine	
3	125	Very fine sand	Very fine sand	Very fine	
4	63		Very coarse silt	Very coarse	
5	31		Coarse silt	Coarse	
6	16	Silt	Medium silt	Medium	Silt
7	8		Fine silt	Fine	
8	4		Very fine silt	Very fine	
9	2	Clay	Clay	Clay	

3.2.8 Radiocarbon dating

Macrofossils were observed both on the sediment surface as well as in the x-radiographs and these observations were used to select the intervals containing material suitable for dating. The macrofossils were collected from the core, thoroughly cleaned and weighed. Moreover, the species were determined before given a lab reference and shipped to the ^{14}CHRONO Centre at Queens University, Belfast, Northern Ireland, for AMS dating. A total of twelve shells and shell fragments were selected (Table 3.3). Of these, *Macoma calcarea* and *Nuculana pernula* were the most frequently occurring species.

Table 3.3: *The shells and shell fragments collected for radiocarbon dating.*

Lab reference	Core	Sampling depth (cm)	Species
UBA-19498	JM06-022-GC2	381 - 383	*Macoma calcarea*
UBA-19499	JM06-022-GC2	318.5 – 319	*Hiatella arctica*
UBA-19500	JM06-022-GC2	201.5 - 202	*Nuculana pernula*
UBA-19501	JM06-022-GC2	111.5 - 112	*Hiatella arctica*
UBA-19502	JM06-022-GC2	8	*Nuculana pernula*
UBA-19503	JM06-023-GC2	432 - 436	*Gastropod (columella) fragments*
UBA-19504	JM07-049-GC1	288	*Macoma calcarea*
UBA-19505	JM06-024-GC3	402.5	*Nucula sp.*
UBA-19506	JM06-024-GC3	303.5 – 304.5	*Yoldiella lenticula*
UBA-19507	JM06-024-GC3	204 – 205.5	*Nuculana pernula*
UBA-19508	JM06-024-GC3	100.5 - 101	*Macoma calcarea*
UBA-19509	JM06-024-GC3	2.5 - 3	*Cardium sp.*

3.2.8.1 Principle

^{14}C is a natural and radioactive carbon isotope formed in the upper atmosphere through the collision of nitrogen (^{14}N) and neutrons. When ^{14}C is formed it rapidly chains to oxygen and creates CO_2. The carbon dioxide is further mixed throughout the atmosphere and into the oceans. It also enters plant materials through photosynthesis and becomes a part of calcareous ($CaCO_3$) marine organisms. This way, ^{14}C is included in the carbon cycle. When organisms die, they stop being a part of this exchange, and the unstable ^{14}C isotope starts decaying with a half-life of 5730 years (Bowman, 1990).

3.2.8.2 Accelerator Mass Spectrometry (AMS)

The samples were prepared and measured at the ^{14}CHRONO Centre at Queens University, Belfast, Northern Ireland (http://chrono.qub.ac.uk/) using Accelerator Mass Spectrometry (AMS). AMS is performed by accelerating the sample particles to high speeds and subjecting them to a magnetic field. If the particles have the same velocity, but different atomic weights, the heaviest particle will deflect the least toward the magnetic field. On the basis of the angle at which the particles are deflected, it is possible to identify them and directly measure the number of ^{14}C atoms present in the sample (Bowman, 1990)

3.2.8.3 Calibration and marine reservoir effects

Different factors, such as variations in the Earth's magnetic field and sunspot activity, have caused the production rate of ^{14}C to vary through time (Bowman, 1990; Hughen et al., 2004). Thus, the concentration of ^{14}C in the atmosphere and in living organisms is not constant. Radiocarbon ages therefore need to be calibrated in order to be given in calendar years.

Samples from marine environments also have to be corrected for the marine reservoir effect. ^{14}C is mixed into the ocean waters at the ocean-atmosphere interface. As a consequence, the reduction of the ^{14}C in the surface waters is compensated by ^{14}C from the atmosphere. This results in more or less similar ^{14}C concentrations in the surface waters and the atmosphere. However, as the water sinks downward, the decaying ^{14}C is no longer compensated through the mixing with the incoming, fresh ^{14}C from the atmosphere. This results in an apparent age increase of the water masses. This is called the marine reservoir effect. In addition, there is a local marine effect (ΔR) which can vary greatly over short distances (Bowman, 1990; Reimer & Reimer, 2001; Mangerud et al., 2006). These factors need to be taken into account when marine organisms are dated, because they will obtain an apparent age which is older than their true age when they incorporate the ^{14}C from the older surrounding water masses into their shells/tests.

The CALIB 6.1.0 software (Stuiver & Reimer, 1993; http://calib.qub.ac.uk/calib) was used in order to calibrate the radiocarbon ages. The program uses the Marine09 calibration curve (Reimer et al., 2009) with an average marine reservoir age of 400 years. The Marine09 dataset represents the global ocean, and an additional regional difference (ΔR) has to be accounted for. In this study, a ΔR of 105 ± 24 was applied (Mangerud et al., 2006).

The dates presented in this study are given in cal. years BP (calibrated years before present). "Before present" refers to before 1950 which is the zero point in the radiocarbon timescale. This is due to the increasing burning of fossil fuel in the early twentieth century and the testing of nuclear weapons from 1945 and onwards which diluted the natural ^{14}C concentrations in the atmosphere (Bowman, 1990).

3.3 Swath bathymetry

In contrast to normal echo-sounders, which use one single beam emitted directly below the vessel, multi-beam echo-sounders send out a fan consisting of multiple sound beams. As the width of the swath increases with water depth, several million depth soundings can be collected for each kilometre the vessel travels. This makes it possible to scan a wider area in high detail. Multi-beam echosounding makes it possible to investigate the seafloor for different purposes, e.g. the distribution and types of sediment or rock or slope angles and properties for stability assessment (Carter, 2009).

The swath bathymetry data used in this study was collected in the spring of 2006 using the Kongsberg Maritime Simrad EM 300 Multibeam echo sounder on board the R/V Jan Mayen (now R/V Helmer Hanssen). It is a hull-mounted system with a nominal operational frequency of 30 kHz. The system consists of 135 beams with an angular coverage sector of 150° and a depth range from 10 to 5000 metres. The beam angle and the angular coverage sector are variable with depth in order to maximize the use of the beams (Kongsberg Maritime, 2003).

3.4. Chirp sonar

The Chirp sonar is an acoustic system which provides high-resolution, artefact-free and real-time measurements of the acoustic attenuation in marine sediments (Schock et al., 1989). The difference between a Chirp sonar and normal pingers and boomers is the Chirp source signature; rather than transmitting a short pulse of a single frequency, it sends out a computer-generated, phase- and amplitude-compensated sweep of frequencies between 400 Hz and 20 kHz (Quinn et al., 1998; Mosher & Simpkin, 1999). The amplitude- and phase-compensation correct for the sonar system response and the precise waveform of the Chirp pulses help reducing correlation noise and source-ringing which influences the vertical resolution (Schock et al., 1989; Quinn et al., 1998).

The Chirp profile used in this study was collected in June 2012 using the EdgeTech 3300-HM hull-mounted sub-bottom profiler on board the R/V Helmer Hanssen of the University in Tromsø. The pulse frequency was 2 – 10 kHz and a 20 ms pulse length was used. The ship travelled at a speed between 8 and 8.5 knots and the ping rate was 2 Hz.

4. Acoustic data

4.1 Swath bathymetry

Based on swath bathymetry data (Figure 4.1), the large-scale submarine landforms were identified, described and interpreted. This was done as a supplement to the chirp and sedimentary data in order to provide a more complete picture of the sedimentary processes and products in Smeerenburgfjorden. As the sediment cores are the main focus of this study and because the bathymetry of the fjord is studied in detail in Ottesen & Dowdeswell (2009), only the main bathymetric features are considered here. For more details and specific dimensions concerning the submarine landforms, see Ottesen & Dowdeswell (2009).

4.1.1 Description

There are three basins within the dataset; one at the fjord mouth, one in the middle fjord and one in the inner fjord (Figure 4.2 A; 1, 3 and 5 in Figure 4.3). The basins have relatively flat seafloors with a smooth appearance. The basin in the middle fjord is both the largest and the deepest (Figure 4.2 A), stretching over ~7 km with a maximum water depth of approximately 250 m. The two other basins have water depths of ~175 meters and are smaller. Two large ridges separate the three basins. The outermost ridge stretches towards NW from Fuglepynten (Figure 4.2 B; 2 in Figure 4.3). The ridge covers the eastern half of the fjord and ends approximately 500 meters from the western fjord side. The gap between the western fjord side and the ridge has a water depth of ~160 m whereas the crest of the ridge is situated at approximately 50-100 meters below sea level. The ridge is relatively narrow and has a gentle slope towards the fjord mouth, whereas the slope facing the fjord head is relatively steep (Figure 4.2 B). The innermost ridge separates the inner basin from the mid-fjord basin. It crosses the fjord from Marstrandbukta towards Danskeneset (4.2 C; 4 in Figure 4.3). The ridge is comparatively wide (~500 m) with a somewhat unclear outline and an undulating surface character. The slope facing the fjord head is steep while the out-fjord facing slope has a more gentle gradient. The ridge is found at water depths of approximately 100 – 150 m.

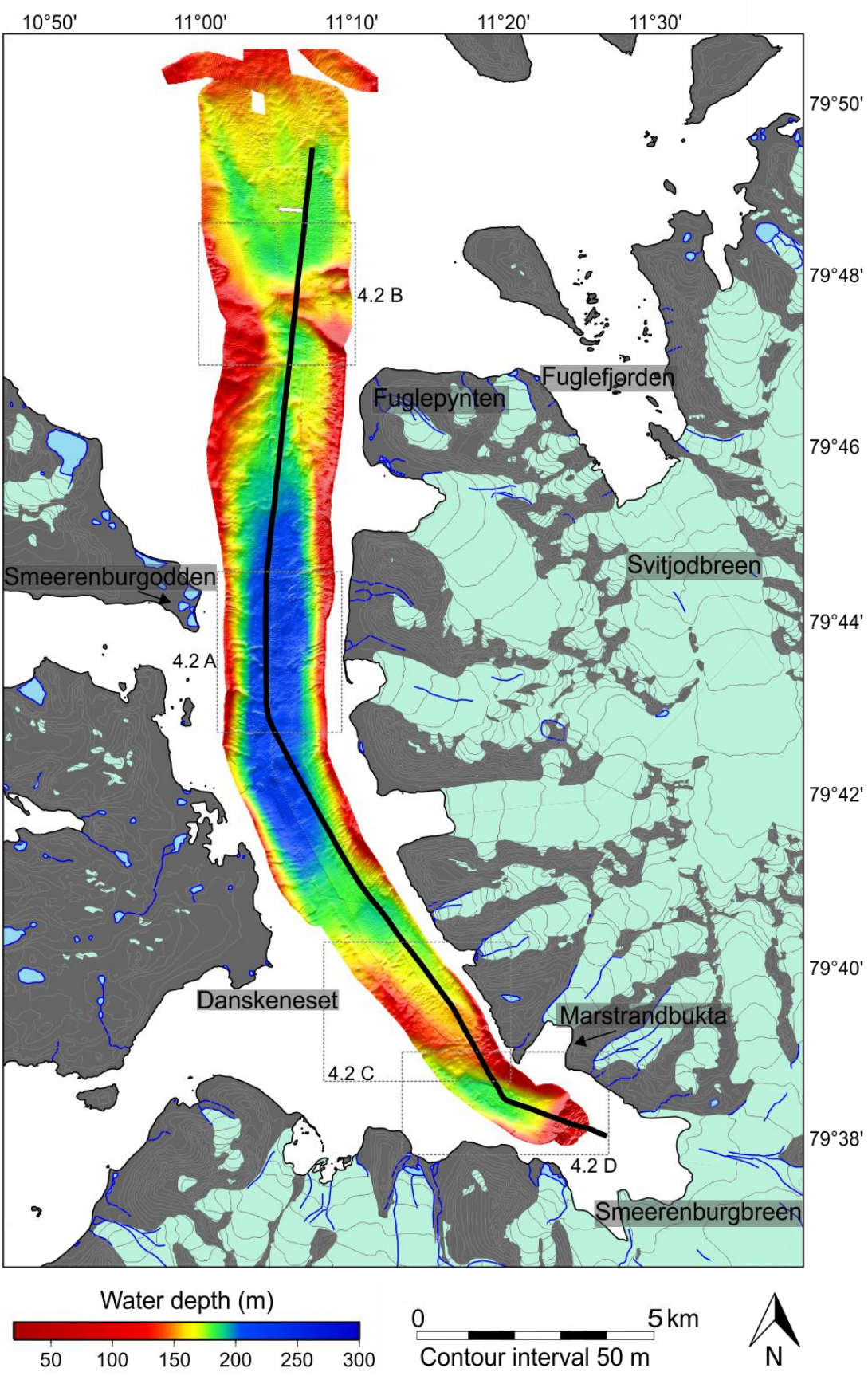

Figure 4.1: *The swath bathymetry of Smeerenburgfjorden. The black line is the chirp profile. Place names mentioned in the text are indicated. Glaciers are marked in light green and rivers/lakes in dark blue/blue, respectively.*

Smaller ridges with lower heights and semi-regular spacing are also observed in the fjord. They are most apparent in the northern part and across the shallow areas off Marstrandbukta where they seem superimposed on the large ridge crossing the fjord (Figure 4.2 C; 4 in Figure 4.3). The ridges are irregular in shape with an orientation transverse to the fjord. Some of the transverse ridges are seen in the mid-fjord basin and just in-fjord of the outer ridge where they are not as evident on the fjord floor but are seen more towards the fjord sides. In this area it may look as if the ridges have a more arcuate shape. In the innermost part of the fjord, in-fjord of the innermost basin, there is a rapid decrease in water depth in the form of a ridge running across the fjord at c. 100 m water depth (Figure 4.2 D). The slope from the ridge down towards the basin is relatively gentle and displays several gullies and channels. From the ridge towards the limit of the data set (towards Smeerenburgbreen; 6 in Figure 4.3), several small sub-parallel, transverse and irregular ridges occur (Figure 4.2 D).

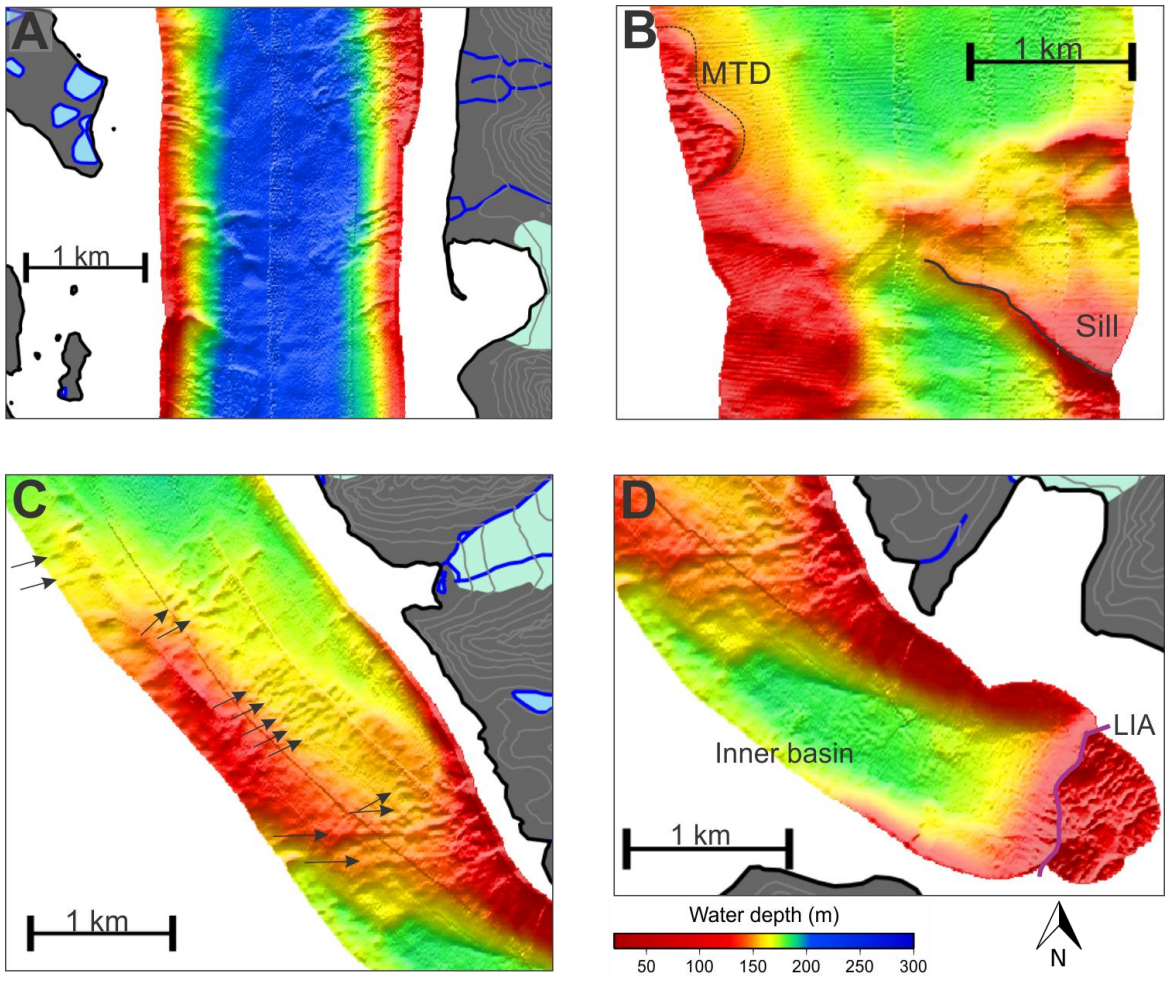

Figure 4.2: ***A)*** *Mid-fjord basin with slide scars and -deposits;* ***B)*** *Outer-fjord with fjord mouth sill and MTD;* ***C)*** *Bedrock ridge in the inner parts of the fjord. Superimposed recessional moraines are indicated with arrows;* ***D)*** *Innermost part of the fjord with inner basin, LIA moraine and recessional moraines within the LIA moraine.*

Gullies, or channels, occur as incisions in the upper parts of the slopes along the fjord sides (Figures 4.1 and 4.2 A). The gullies are especially evident in the mid-fjord region where the fjord sides are steepest. Directly downslope of these features, lobe shaped deposits occur. The lobate structures vary in shape and size; some are elongated while others have wider cross-sections. The surfaces of the lobes vary as well; some have smooth surfaces whereas others have a more rugged and rough appearance.

4.1.2 Interpretation

The general smoothness of the fjord floor, especially in the basins, may indicate that suspension fallout and deposition of fine-grained sediments from glacial meltwater plumes is an important process in the fjord (e.g. Elverhøi et al., 1980, 1983; Ottesen & Dowdeswell, 2009). The bedrock boundary (seen in Figure 2.3) has approximately the same orientation as the inner large ridge (4 in Figure 4.3) and this ridge may therefore be a bedrock sill. The outer large ridge may be a moraine deposited during a longer stillstand of the glacier (Ottesen & Dowdeswell, 2009).

The smaller transverse ridges are interpreted as recessional moraines deposited during stillstands in overall retreat. They may also be formed due to push and squeeze as the glacier front re-advances slightly during winter. Such wintertime re-advances are caused by sea ice suppressing iceberg calving and they may therefore be annual (Ottesen & Dowdeswell, 2006, 2009). However, this is difficult to estimate based only on the bathymetry (see *Chapter 6.2*). The moraine in the inner fjord (6 in Figure 4.3) was interpreted by Ottesen & Dowdeswell (2009) to represent the late Holocene maximum glacier extent, i.e. the Little Ice Age moraine. The moraine may be a result of an advance due to climatic cooling during the LIA or due to a surge (e.g. Plassen et al., 2004). As no information on the absolute age exists to confirm this, it is only a speculation. However, it is not unlikely that this moraine is the LIA extent as similar features have been described from other Spitsbergen fjords (e.g. Plassen et al., 2004; Ottesen & Dowdeswell, 2006; Baeten et al., 2010).

Figure 4.3 (next page): *Summary interpretation of the swath bathymetry. The numbers refer to* ***1)*** *The outermost basin,* ***2)*** *outermost large ridge,* ***3)*** *mid-fjord basin,* ***4)*** *large ridge with superimposed smaller transverse ridges,* ***5)*** *innermost basin, and* ***6)*** *Possible LIA moraine (purple) and recessional moraines (yellow). Place names mentioned in the text are indicated. Glaciers are marked in light green and rivers/lakes in dark blue and blue, respectively.*

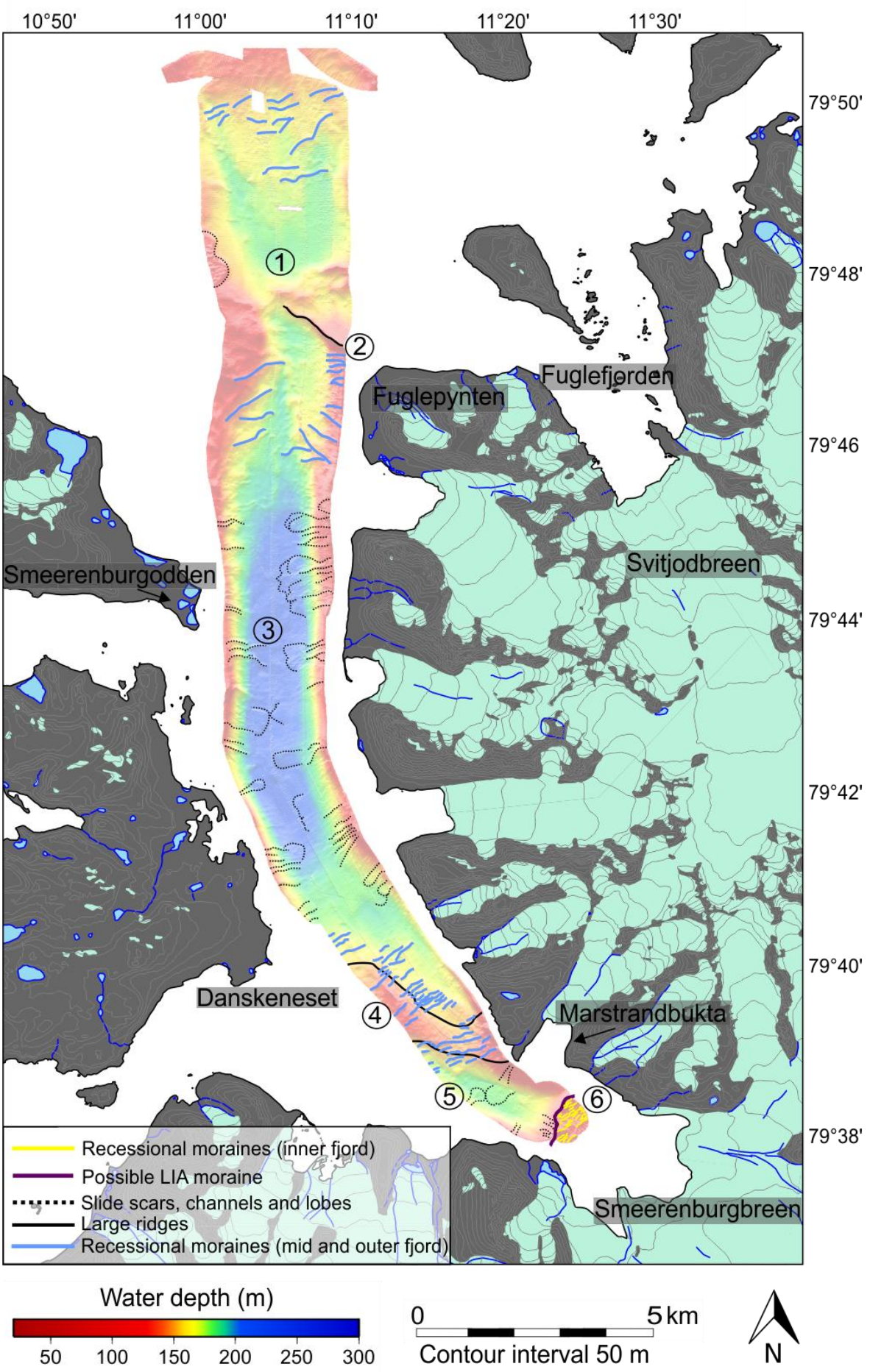
10°50'
11°00'
11°10'
11°20'
11°30'
79°50'
79°48'
79°46
79°44'
79°42'
79°40'
79°38'
①
②
③
④
⑤
⑥
Fuglefjorden
Fuglepynten
Svitjodbreen
Smeerenburgodden
Danskeneset
Marstrandbukta
Smeerenburgbreen
Recessional moraines (inner fjord)
Possible LIA moraine
Slide scars, channels and lobes
Large ridges
Recessional moraines (mid and outer fjord)
Water depth (m)
50
100
150
200
250
300
0
5 km
Contour interval 50 m
N

The gullies and the lobe-shaped deposits are interpreted to be slide scars/channels and slide deposits (mass transport deposits; MTD's). The difference in the surface appearance of the lobes (smooth and rugged) may represent different materials in the lobes. The smooth surfaced lobes may contain mostly fine-grained muds whereas the rugged deposits may contain more blocky sediments. It is also a possibility that the smooth lobes are older and that they have been covered by fine-grained sediments over time. Such slide scars and mass transport deposits have been described from the study area (Ottesen & Dowdeswell, 2009), but they are also found in several other Spitsbergen fjords (e.g. Plassen et al., 2004; Ottesen & Dowdeswell, 2006; Forwick & Vorren, 2007; Baeten et al., 2010).

4.2 Chirp

The chirp line (Figure 4.1) was divided into two regional reflections; R1 and R2 (seafloor), and one unit. The line is described as a whole focusing on the large-scale basin stratigraphy.

4.2.1 Description

The lowermost reflection, R1, is irregular and rugged and acoustically impenetrable. In some areas, the horizon is diffuse and relatively difficult to follow, e.g. in the innermost part of the fjord. Small "mounds" of approximately the same height and spacing can be found all along the reflection (see Figure 4.4).

Generally, the unit U1 is semi-transparent. However, there is a slight decrease in transparency from the base to the top of the unit which is especially evident in the inner and middle parts of the fjord. Diffuse, discontinuous internal reflections occur within the basins and where the unit is thickest (Figure 4.4). Towards the fjord mouth, smaller bodies of stacked internal reflections occur more frequently. These reflections are discontinuous with chaotic seismic patterns. The unit generally creates a drape over the underlying R1 reflection. However, localised sediment infill occurs in depressions and basins. The unit is thicker in the basins than on ridges and slopes and is generally thinning from the inner fjord towards the fjord mouth.

The seafloor reflection is undulating and generally mirrors the reflection R1. However, in the basins where the underlying unit U1 is thicker, the R2 horizon is relatively smooth and only gently undulating.

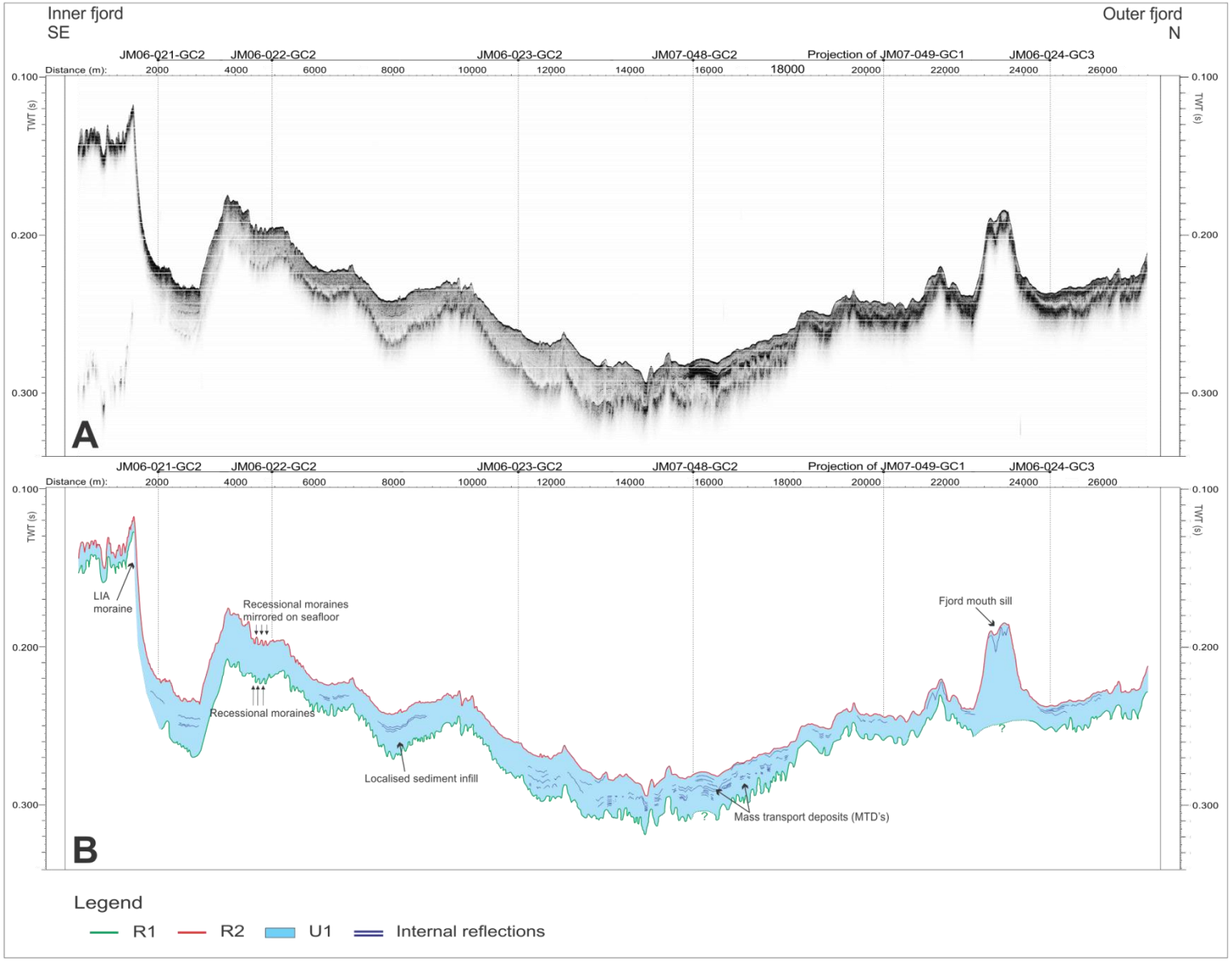

Figure 4.4: ***A:*** *Chirp line with core locations indicated.* ***B:*** *Interpretation of the chirp line.*

4.2.2 Interpretation

The fact that the reflection R1 is acoustically impenetrable by the chirp implies that the underlying material is either consolidated subglacial till or bedrock (e.g. Hjelstuen et al., 2009; Batchelor et al., 2011). Based on the appearance of the reflection, with its undulating and rugged surface, the R1 is interpreted to reflect the sub-surface of a subglacial till. The small "mounds" that can be seen along this reflection may be recessional moraines deposited at the glacier front either during stillstands or smaller re-advances in overall glacial retreat throughout the deglaciation (Ottesen & Dowdeswell, 2006, 2009). Such moraines have been observed in several Spitsbergen fjords, e.g. in Billefjorden (Baeten et al., 2010), Tempelfjorden (Forwick et al., 2010) and Borebukta (Ottesen & Dowdeswell, 2006).

The semi-transparency of the unit is interpreted to reflect relatively uniform glacimarine sedimentation by rain-out of suspended sediment from turbid meltwater plumes (e.g. Elverhøi et al., 1980, 1983; Hjelstuen et al., 2009; Batchelor et al., 2011). The diffuse and discontinuous internal reflections observed in the basin areas may represent changes in grain-size resulting from periods of more IRD input compared to the concentration of suspended sediment (e.g. Batchelor et al., 2011). The chaotic and stacked smaller bodies of internal reflections may be mass transport deposits originating from the fjord sides (e.g. Hjelstuen et al., 2009). In the innermost basin there are also some chaotic reflections in the upper part of the unit as well as a more transparent sediment body in the lower part of the unit. These may also be mass transport deposits initiated upslope on the larger inner fjord moraine (e.g. Forwick & Vorren, 2007, 2011a).

The sediment drape in U1 makes the palaeorelief from R1 visible on the seafloor (R2). However, the localised sediment infill in the basins and smaller depressions gives the seafloor horizon a relatively smooth and flat appearance in some areas.

5. Lithostratigraphy

In this chapter, the results from the various methods described in chapter 3 are compiled for correlation purposes and to interpret the depositional environment of the cores.

The lithological logs (Figure 5.2) were created based on the study of the sediment surface, the X-ray photographs and, to some extent, the grain-size analysis data. In this study, all grains and clasts > 63 µm (sand and coarser) are regarded as ice rafted, either by icebergs or sea ice (e.g. Dowdeswell & Dowdeswell, 1989; Elverhøi et al., 1995; Hebbeln, 2000; Hass, 2002). As the CILAS laser particle counter only measures particles up to 2.5 mm (see Table 3.2), the gravel fraction is not included in the lithological logs. However, grains exceeding the sand fraction (> 2 mm) are referred to as "clasts" and are marked in the lithological logs as individual features.

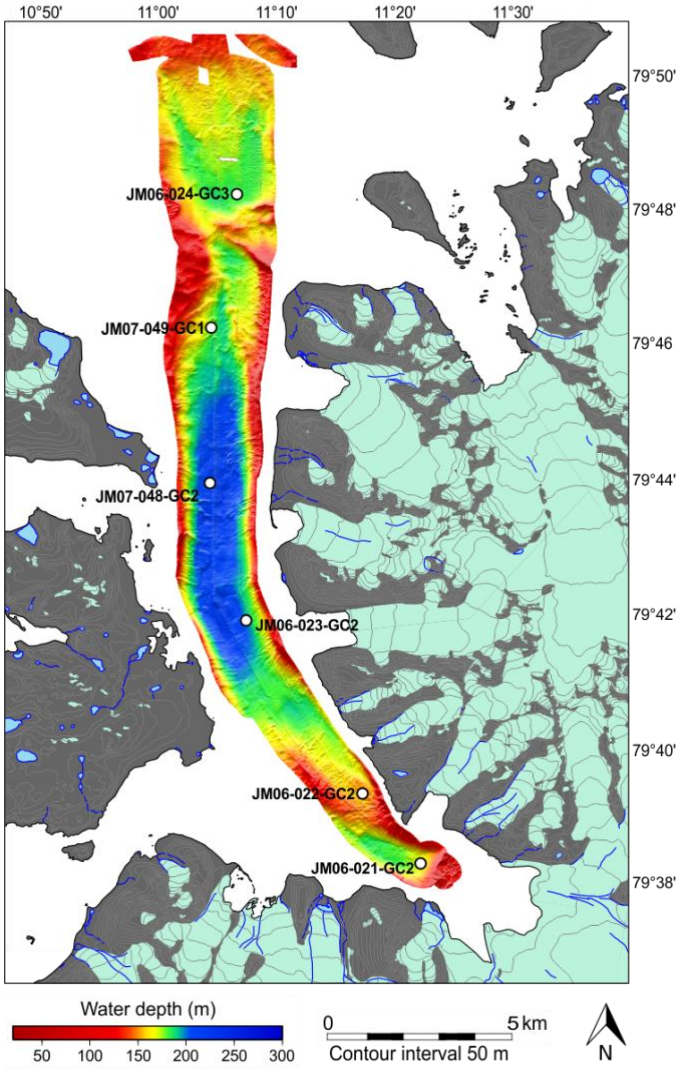

Figure 5.1: *The cores (circles) used in this study (cf. Table 3.1).*

None of the sediment cores have been subdivided into units. This is due to the relatively homogenous character of the sediment. None of the observed sedimentological structures, colour changes or grain-size variations were regarded as significant enough to provide a natural unit boundary in the lithological logs. The cores are therefore described as a whole (from bottom to top) with references only to depths where interesting features were observed. As there are no lithological units to refer to, the physical properties, grain-size distribution and geochemical data are described in relation to the specific graph's mean value and general trends for each core. The mean values can be found in Table 5.1 below.

Table 5.1: *Mean values for the measured physical properties, the sedimentation rate and the element geochemistry.*

	Inner fjord					Fjord mouth
	JM06-021-GC2	**JM06-022-GC2**	**JM06-023-GC2**	**JM07-048-GC2**	**JM07-049-GC1**	**JM06-024-GC3**
Wet bulk density (g/cm^3)						
Min	1.49	1.44	1.42	1.40	1.07	1.41
Max	1.99	1.83	1.76	1.76	1.76	1.72
Mean	1.72	1.70	1.58	1.53	1.59	1.57
Magnetic susceptibility (10^{-5} SI)						
Min	93.5	86.8	6.1	4.7	2.6	2.0
Max	185.8	162.0	79.0	27.6	27.5	25.5
Mean	139.8	116.0	47.8	12.3	7.6	5.6
Sedimentation rate (mm/yr)						
Mean	No data	4.08	2.82	No data	0.32	0.37
Fe/Ca ratio						
Mean	2.2	2.2	2.2	1.8	1.5	2.0
Fe/S ratio						
Mean	18.1	40.7	32.8	22.6	24.1	27.8
Ca/S ratio						
Mean	7.9	18.2	15.5	11.4	17.7	17.6
Ca/Zr ratio						
Mean	10.2	16.9	24.0	27.7	32.2	32.1
Ca/Sr ratio						
Mean	11.7	16.3	19.8	21.9	23.0	22.9

As mentioned in *3.2.1.2 P-wave velocity*, the recorded P-wave amplitude may be used as a guide to whether or not the P-wave velocity measurements are reliable. For most of the cores, the P-wave amplitude was 0 and the P-wave velocity values were therefore excluded from the correlations and interpretations of the cores.

The results from the AMS radiocarbon dating and the calibrated ages are given in Table 5.2 below. The calibrated ages are based on a mean of the 1σ range. Linear sedimentation rate was calculated by assuming a constant accumulation rate between the calibrated ages. These rates were in turn used to estimate ages in between the dated levels.

Table 5.2: *Results from the radiocarbon dating and the calibration.*

Lab reference	Core	Sampling depth (cm)	Species	^{14}C age BP	Cal. yr BP Calib 6.1.0 1σ range	Cal. yr BP Calib 6.1.0 1σ mean	Cal. yr BP Calib 6.1.0 2σ range
UBA-19498	JM06-022-GC2	381 - 383	*Macoma calcarea*	1494 ± 28	895 - 975	935	844 - 1041
UBA-19499	JM06-022-GC2	318.5 – 319	*Hiatella arctica*	1157 ± 31	567 - 580 595 – 659	627	539 - 680
UBA-19500	JM06-022-GC2	201.5 - 202	*Nuculana pernula*	923 ± 27	430 – 491	460	366 – 517
UBA-19501	JM06-022-GC2	111.5 - 112	*Hiatella arctica*	505 ± 20	Invalid age	Invalid age	Invalid age
UBA-19502	JM06-022-GC2	8	*Nuculana pernula*	410 ± 20	Invalid age	Invalid age	Invalid age
UBA-19503	JM06-023-GC2	432 - 436	*Gastropod (columella) fragments*	2080 ± 23	1486 - 1588	1537	1409 – 1631
UBA-19504	JM07-049-GC1	288	*Macoma calcarea*	8441 ± 40	8843 - 8995	8919	8719 – 9031
UBA-19505	JM06-024-GC3	402.5	*Nucula sp.*	10044 ± 46	10779 - 11031	10905	10684 - 11094
UBA-19506	JM06-024-GC3	303.5 – 304.5	*Yoldiella lenticula*	8311 ± 41	8602 - 8789	8695	8572 – 8919
UBA-19507	JM06-024-GC3	204 – 205.5	*Nuculana pernula*	6916 ± 44	7290 - 7394	7342	7238 – 7424
UBA-19508	JM06-024-GC3	100.5 - 101	*Macoma calcarea*	4654 ± 31	4708 - 4820	4764	4620 – 4843
UBA-19509	JM06-024-GC3	2.5 - 3	*Cardium sp.*	Modern	-	-	-

Based primarily on their locations (see Figure 5.1), two key cores were selected for a more detailed study. Core JM06-022-GC2 (Core 22) in the inner part of the fjord was chosen due to its vicinity to the major tidewater glacier Smeerenburgbreen. Core JM06-024-GC3 (Core 24) is the outermost core retrieved beyond the fjord mouth sill and has the longest sediment record, i.e. the oldest sediments. In addition to a grain-size distribution sample interval of 2 cm, material for radiocarbon dating was selected every ~100 cm for these two cores. They will therefore be given more attention than the remaining four cores: JM06-021-GC2, JM06-023GC2, JM07-048-GC2 and JM07-049-GC1. It was decided to exclude the XRF data for the remaining cores as the pre-defined timeframe for this thesis was not sufficient for a detailed study of all six sediment cores.

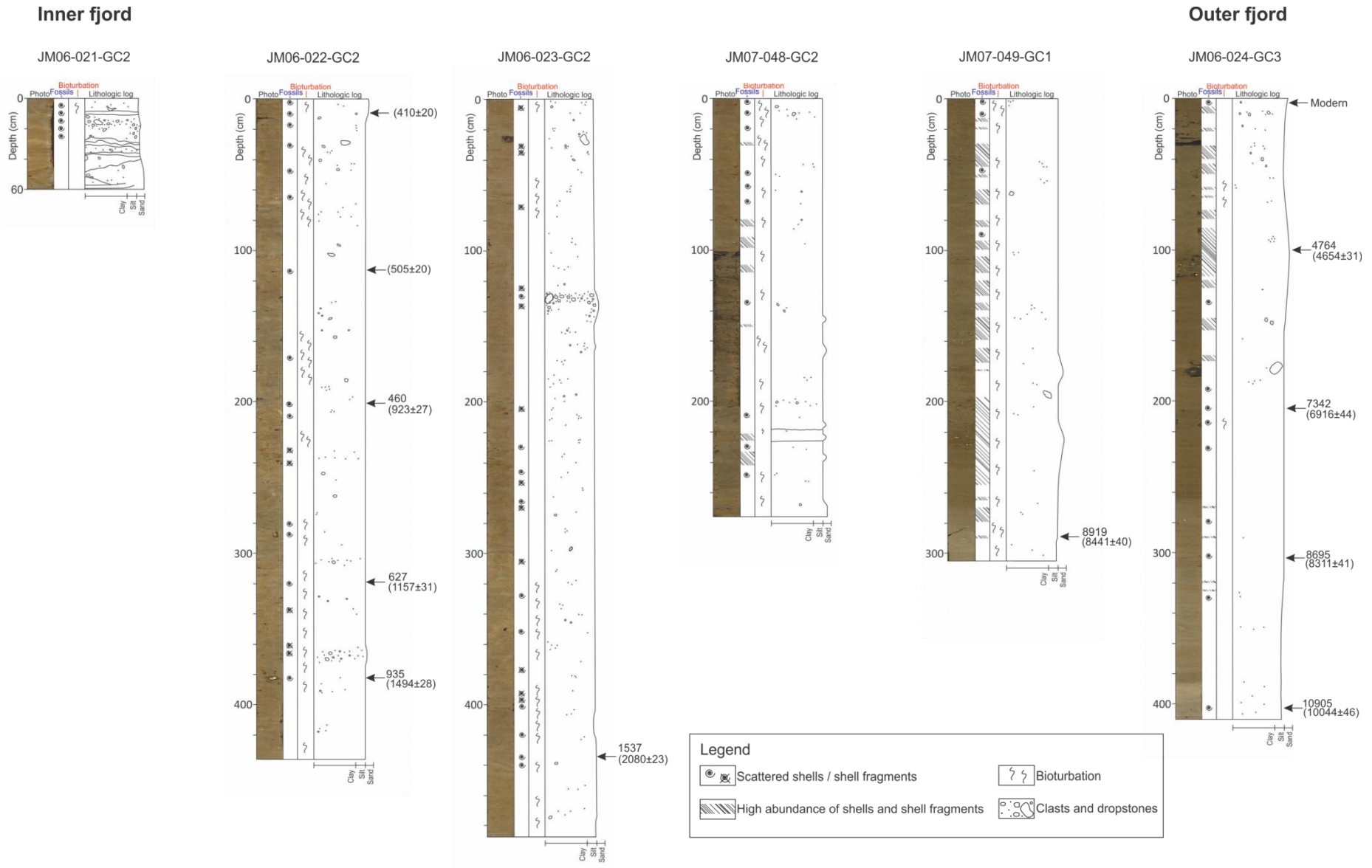

Figure 5.2: *Lithological logs from all sediment cores investigated in this study in a transect from the inner fjord (left) to the fjord mouth (right). Dated intervals are indicated by arrows. Bracketed ages are given in ^{14}C years while ages without brackets are given in calibrated years BP.*

5.1 Core JM06-021-GC2

Core JM06-021-GC2 was retrieved just downslope of the Little Ice Age moraine in the innermost part of the fjord and lies approximately 2.5 – 3 km from the termini of Smeerenburgbreen (Figure 5.1). The core length is 60 cm (Table 3.1).

5.1.1 Lithology and stratigraphy

The surface of the sediment was black when the core was opened. When the core was revisited some months later, the black colour had disappeared and the sediment surface had some spots and areas of rust. The general colour of the sediment is dark grey (Munsell Code 5Y4/1). However, thin (1-2 cm), irregular and sub-horizontal bands of grey (5Y5/1), olive grey (5Y4/2) and dark greyish brown (2.5Y4/2) occur (Figure 5.3). The boundaries between the different bands may be described as undulating (see photo detail in Figure 5.3). The lighter coloured bands (grey, 5Y4/1) seem to be rustier than the rest of the core.

The grain-size distribution shows sand and silt being the dominating fractions in the lowermost part of the core (60 - 40 cm). Towards the core top, the sand content decreases to ~10 % whereas the silt and clay contents increase to approx. 80 % and 10 %, respectively.

Clasts occur frequently throughout the core, but are found in larger accumulations in the intervals 33-31, 20-10 and 5-0 cm. A few shells (single) and shell fragments are found in the uppermost 20 cm of the core. Traces of bioturbation occur only between 5-0 cm depths.

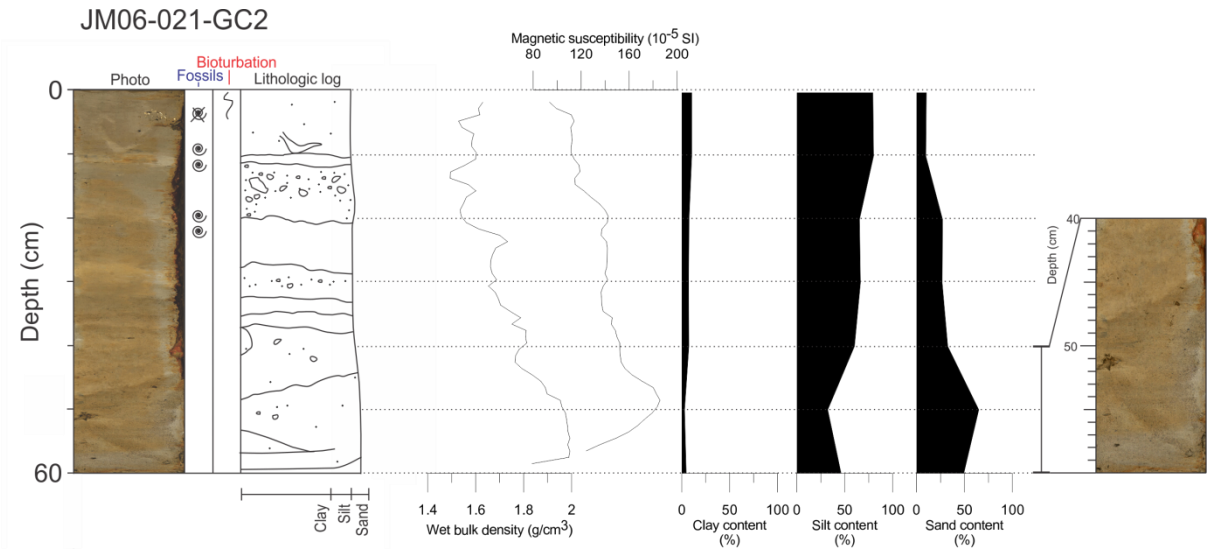

Figure 5.3: *Colour photo, shells and fragments, bioturbation, lithologic log, physical properties and grain-size distribution, for the core JM06-021-GC2. Detail: colour photo close-up of the colour changes in the lower part of the core 60- 40 cm). Legend for the lithological log is found in Figure 5.2.*

5.1.2 Physical properties

The wet-bulk density is gradually decreasing towards the top of the core; from ~1.9 g/cm^3 close to the base to ~1.6 g/cm^3 in the top (Figure 5.3). The magnetic susceptibility is generally high (mean ~139 x 10^{-5} SI) and increase from the core bottom towards 49 cm. At 49 cm, the magnetic susceptibility is 185.8 which is the highest value recorded in the core. From 49 cm towards the top, the magnetic susceptibility decreases.

5.1.3 Interpretation and correlation

The up-core decreasing wet bulk density correlates to the general grain-size distribution which is fining upward. As the core was retrieved from the foot of a slope proximal to the LIA moraine (Figure 4.1 and 5.1), it is possible that the core location has been subject to mass transport activity. The observed sub-horizontal bands of different colours may either reflect multiple smaller mass transport events such as turbidity or debris flows, or the core may have been retrieved from a slump where the original sediment structure was partly preserved (e.g. Nardin et al., 1979; Mulder & Cochonat, 1996; Mulder, 2011). Potential individual events or pulses are difficult to identify. However, the high sand content at c. 50 cm (Figure 5.3) can be correlated to the peaks in both wet bulk density and magnetic susceptibility as well as a colour change in the sediment and it is possible that this interval represents one such pulse. Another possibility is that the core contains a sequence that was deposited in one event. In summary, the core is interpreted to comprise predominantly reworked sediments. The fact that bioturbation only occurs in the uppermost 5 cm supports the interpretation that the rest of the core comprise reworked sediments (e.g. Forwick & Vorren, 2007). See further discussion in chapter *6.2 Correlation of acoustic and sedimentary data*.

5.2 Core JM06-022-GC2

Core JM06-022-GC2 was retrieved close to the eastern fjord side on the inner fjord moraine, approximately 6 km from Smeerenburgbreen (Figure 5.1). The core has a total length of 435.5 cm (Table 3.1).

5.2.1 Lithology and stratigraphy

At the time when the core was opened, the sediment surface was partly black. However, the black colour disappeared after the surface had been exposed to air for some hours. From the bottom of the core to approximately 303 cm depth, the colour of the sediment is olive grey (5Y4/2) whereas the sediment in the interval 303-0 cm is dark grey (5Y4/1).

The matrix of the core is silty mud. Between the base of the core and 50 cm, the mean sand content is 5.8%, the silt content 83.1% and the clay content 11.1% (Figure 5.4). From 50 cm and up to the core top, the sand content increases slightly to a mean of 9.6%, whereas the silt and clay contents decrease to 79.9% and 10.5%, respectively. Several peaks in the sand content occur throughout the core with the most distinctive being 11.2% at 416 cm, 10.4% at 280 cm, 19.8% at 24 cm and 15.9% at 8 cm.

Clasts are frequently found in the core and occur in somewhat larger accumulations at the approximate depths of 375, 305, 250 and 80 cm. Small (~1 - 2 cm diameter) clusters, or pockets, of grains coarser than the matrix occur at the depths of 339, 230, 198 and 169 cm. Shells (both single and paired) and shell fragments are found scattered throughout the entire core. Bioturbation occurs throughout the core, but is intensified in the intervals from 190 - 150 and 80 - 30 cm (Figure 5.5). Sub-horizontal and irregular structures with lengths of 1 - 2 cm occur in the intervals 435.5 - 407, 345 - 320 and 303 - 260 cm (Figure 5.6).

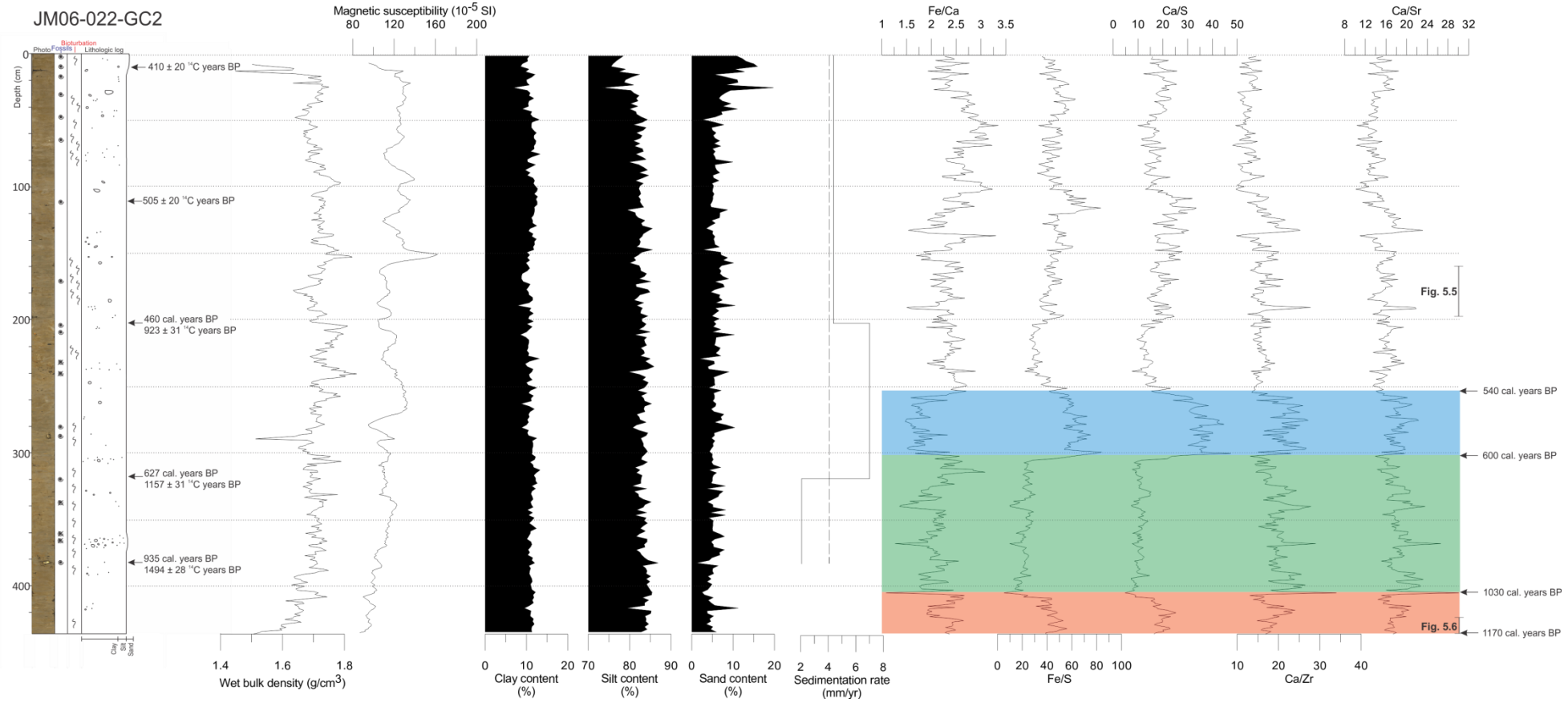

Figure 5.4: *Colour photo, shells and fragments, bioturbation, lithologic log, physical properties, grain-size distribution, linear sedimentation rate (dashed line: mean sedimentation rate) and selected element ratios for the core JM06-022-GC2. Legend for the lithological log is found in Figure 5.2. The coloured lines illustrate intervals mentioned in the text. The calibrated ages given at the correlation interval boundaries are estimated based the linear sedimentation rate. Details from x-ray photographs are found in figures 5.5 and 5.6, respectively.*

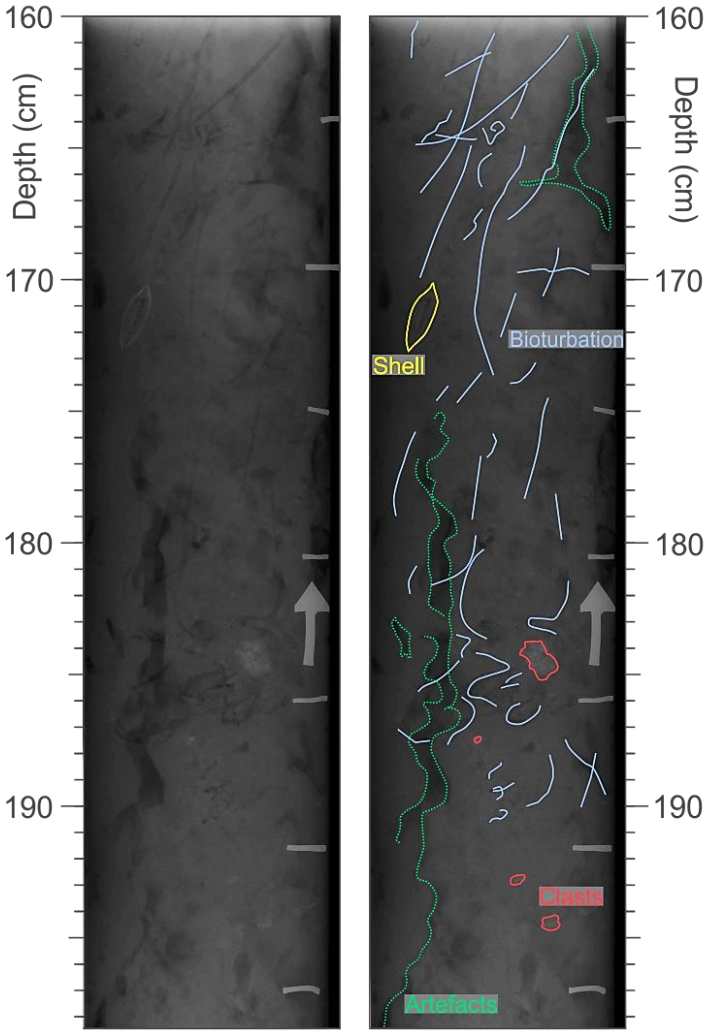

Figure 5.5: *X-ray photographs illustrating different features such as bioturbation (blue), shells (yellow), clasts (red) and artefacts (green) in core JM06-022-GC2.*

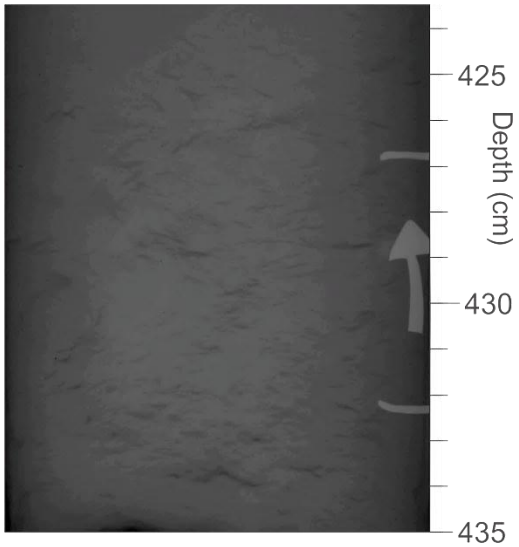

Figure 5.6: *Detail of x-ray photograph showing the sub-horizontal structures interpreted as extension cracks in core JM06-022-GC2.*

5.2.2 Physical properties

The wet bulk density increases slightly in the lowermost 30 centimetres of the core (Figure 5.4). Throughout the core, the density fluctuates around the core mean of 1.72 g/cm^3 before a minor decrease in density occurs in the uppermost c. 20 cm. The magnetic susceptibility of the core varies between ~90 (x 10^{-5} SI) and 160 with a mean of 116. Generally, the magnetic susceptibility increases up-core with small fluctuations and singular peaks.

5.2.3 Element geochemistry

Values slightly higher than the mean are observed for the ratios Fe/S, Ca/S, Ca/Zr and Ca/Sr in the interval from 435.5 cm (core bottom) to 405 cm (red interval in Figure 5.4). From 405 – 300 cm (green interval in Figure 5.4) the Fe/Ca ratio slightly decreases, whereas more prominent drops in the Fe/S and Ca/S ratios occur. The Ca/Zr and Ca/Sr ratios increase slightly compared to the mean. All ratios, except of the Fe/Ca ratio, increase from 300 – 255 cm (blue interval in Figure 5.4). This increase is especially prominent in the Ca/S and Fe/S ratios. Towards the core top, all the ratios are frequently fluctuating around the mean. However, minor general increases occur for the Fe/Ca and Fe/S ratios, whereas slight decreases occur for the remaining ratios.

5.2.4 Chronology and sedimentation rates

A total of five shells were selected for radiocarbon dating from this core (Table 5.2). The lowermost date was collected at ~382 cm and has an age of 935 cal. years BP. Assuming a constant sedimentation rate; this indicates that the bottom of the core has an age of approximately 1100 cal. years BP. The rest of the dated material is younger, i.e. there are no age reversals. The two uppermost dates in core 22 provided "invalid ages" after calibration. This may be due to the fact that a general marine reservoir age of 400 years and a regional reservoir age of 105 ± 24 were used in calibration (Mangerud et al., 2006; Reimer et al., 2009; see *3.2.8 Radiocarbon dating*). Therefore, ages of 505 and 410 ^{14}C years would be calibrated to be younger than the radiocarbon age range (AD 1950; see *Chapter 3.2.8.3*).

Between 935 – 627 cal. years BP (382- 318.75 cm), the sedimentation rate was estimated to 2.05 mm/year. It increased to 7.00 mm/year between 627 – 460 cal. years BP (318.75 – 201.75 cm). The sedimentation rate for the uppermost interval is calculated based on the

dating at 201.75 cm (460 cal. years BP) as the shell samples taken at 111.75 cm and 8 cm had "invalid" cal. ages. The uppermost ~200 cm of the core therefore have a sedimentation rate of 4.39 mm/year. The average sedimentation rate throughout the core is 4.08 mm/year (dashed line in Figure 5.4).

5.2.5 Interpretation and correlation

The clast-rich and massive silty mud of this core is interpreted to represent a glacimarine environment. The clasts and the sand content are suggested to be IRD deposited by either icebergs or sea ice. Accumulations of coarser grains and the mentioned sand pockets may also be related to ice rafting and may be dumped by overturning icebergs (e.g. Vorren et al., 1983). The relatively frequent occurrence of paired shells and the intervals of preserved intense bioturbation may indicate that the sediments have not been reworked or disturbed by mass transport activity (compare with Forwick & Vorren, 2007).

The sub-horizontal structures observed on the x-ray photographs are suggested to be extension cracks and/or gas expansions formed by pressure release during the retrieval of the core (cf. Forwick & Vorren, 2007).

The wet bulk density and magnetic susceptibility do not seem to correlate with any of the other properties of the core. The wet bulk density may reflect changes in grain-size (Forwick et al., 2010), but no clear relationship between these properties is observed. This may be due to the fact that the wet bulk density is measured across the entire core diameter, whereas the grain-size distribution sample is only 0.125 cm^3 of the sediment surface (Figure 5.7). Individual peaks in the magnetic susceptibility may result from more magnetic clasts that were located neither along the measuring path of the gamma rays for the wet-bulk density measurements, nor that they were subsampled (Figure 5.7). The absence of correlation with the element ratios could be explained in the way that the results for the XRF-scanner measurements are obtained only from the uppermost 1-2 mm below the sediment surface (e.g. Richter et al., 2006; Figure 5.7). The decrease in both density and magnetic susceptibility toward the core top may be caused by disturbances of the sediment as the core was retrieved. As the water content and fractional porosity typically increase towards the core top, it is also possible that this has an influence on the wet bulk density.

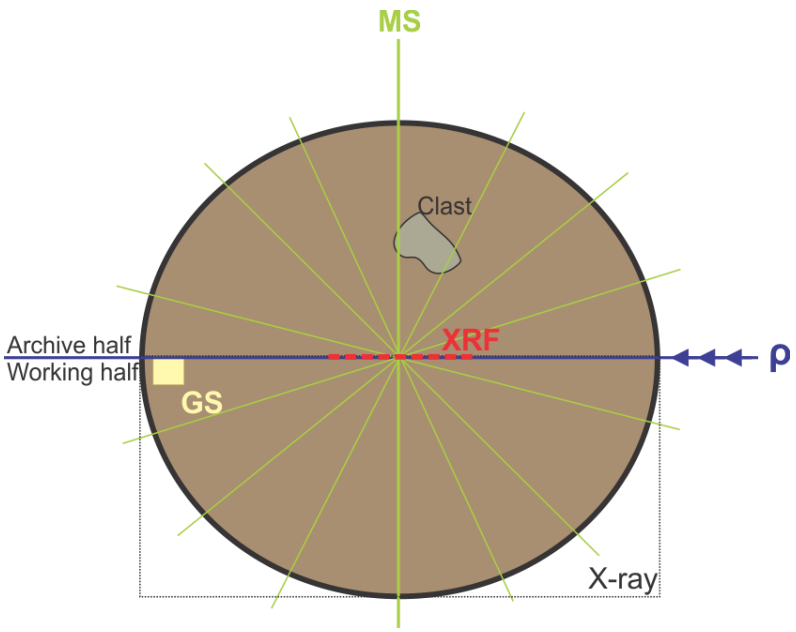

Figure 5.7: *Sketch illustrating how the magnetic susceptibility (MS; green), wet bulk density (ρ; blue) and element geochemistry (XRF; red) is measured in the sediment core. The yellow square illustrates the grain-size (GS) sample and the x-radiograph is indicated by the black stippled line. The clast in the archived half will influence the magnetic susceptibility but not the wet bulk density or the element geochemistry. In addition, it will not be visible on the sediment surface nor the x-radiographs.*

In the XRF data there are two intervals with relatively marked changes; 405 – 300 cm (green interval in Figure 5.4) and 300 – 255 cm (blue interval in Figure 5.4). The former interval has a marked decrease in both the Fe/S and Ca/S ratios which means that there is either an increase in sulphur compared to iron and calcium, or a decrease in iron and calcium compared to sulphur. However, as both mentioned ratios show a possible increase in the sulphur content and no evident decreases in either iron or calcium occur in the other ratios, it is most likely the sulphur content that is increasing in the green interval. In the following interval, from 300 – 255 cm (blue interval in Figure 5.4), all ratios concerning Ca show a relative increase in calcium compared to other elements. The Fe/Ca ratio also shows a relative increase in Ca compared to Fe, whereas the Fe/S ratio shows an increase in Fe compared to S. These opposing signals for iron may be the result of Ca overrunning the Fe signal in the Fe/Ca ratio as this Ca increase is seen in other ratios as well. The Fe/S ratio shows a large increase in the iron content, but it may also reflect a decrease in the sulphur content. As the ratios concerning sulphur (Fe/S and Ca/S) show the strongest increase, it may point to a decrease in the sulphur content, especially in relation to the underlying interval. The implications of the XRF signals are further discussed in *Chapter 6*.

5.3 Core JM06-023-GC2

Core JM06-023-GC2 was retrieved in the mid-fjord basin (Figure 5.1), close to the eastern fjord side. The core site is located approximately 3 km from the tidewater glacier Sellströmbreen (Figure 2.2). The core length is 486 cm (Table 3.1).

5.3.1 Lithology and stratigraphy

At the time when the core was opened, the sediment surface from the core bottom and up to 299 cm was described as completely black, whereas the surface from 299 - 0 cm was only partly black. After the sediment surface had been exposed to air for some hours, the black colour disappeared. The colour of the interval from 486 - 400 cm, is olive grey (5Y4/2), while the rest of the core (400 - 0 cm) has a dark greyish brown (2.5Y4/2) colour. Scattered rust spots occur throughout the core.

The grain-size distribution is relatively stable throughout the core with a mean sand content of 4%, silt content of 85% and clay content of 11%, i.e. the matrix consists of a silty mud. Only minor deviations from these average values occur, e.g. in the lowermost part of the core (480 cm) where the sand content is as low as 0.2% and the clay content is 16.4% (Figure 5.8).

Clasts occur frequently in the core, especially in the interval 140 - 130 cm (Figure 5.8). Small pockets of sediment softer than the surrounding matrix were found at the intervals 268 - 267 and 237 - 236 cm. A large, angular (granite) clast was found at 27 - 23 cm depth. Mostly shell fragments occur in this core and there are relatively few whole shells (only single, no paired) present. Polychaetes were found at the depths of 388, 282 and 186 cm. Bioturbation was observed in the interval from 486 - 320 cm and in the upper 100 cm of the core. The bioturbation is most intense between 486 - 300 cm.

5.3.2 Physical properties

From the core bottom to approximately 300 cm, the wet bulk density is slightly lower than the core mean (1.58 g/cm^3). The density is increasing up-core only interrupted by a drop between 435 – 405 cm (Figure 5.8). From 300-100 cm, the wet bulk density is generally somewhat higher than the mean, before a marked drop occurs around 97 cm. The magnetic susceptibility increases up-core; from ~10 (x 10^{-5} SI) in the bottom to ~70 in the top. There is a slight decrease in magnetic susceptibility in the uppermost part of the core. However, the susceptibility is still above the core average of 47.8.

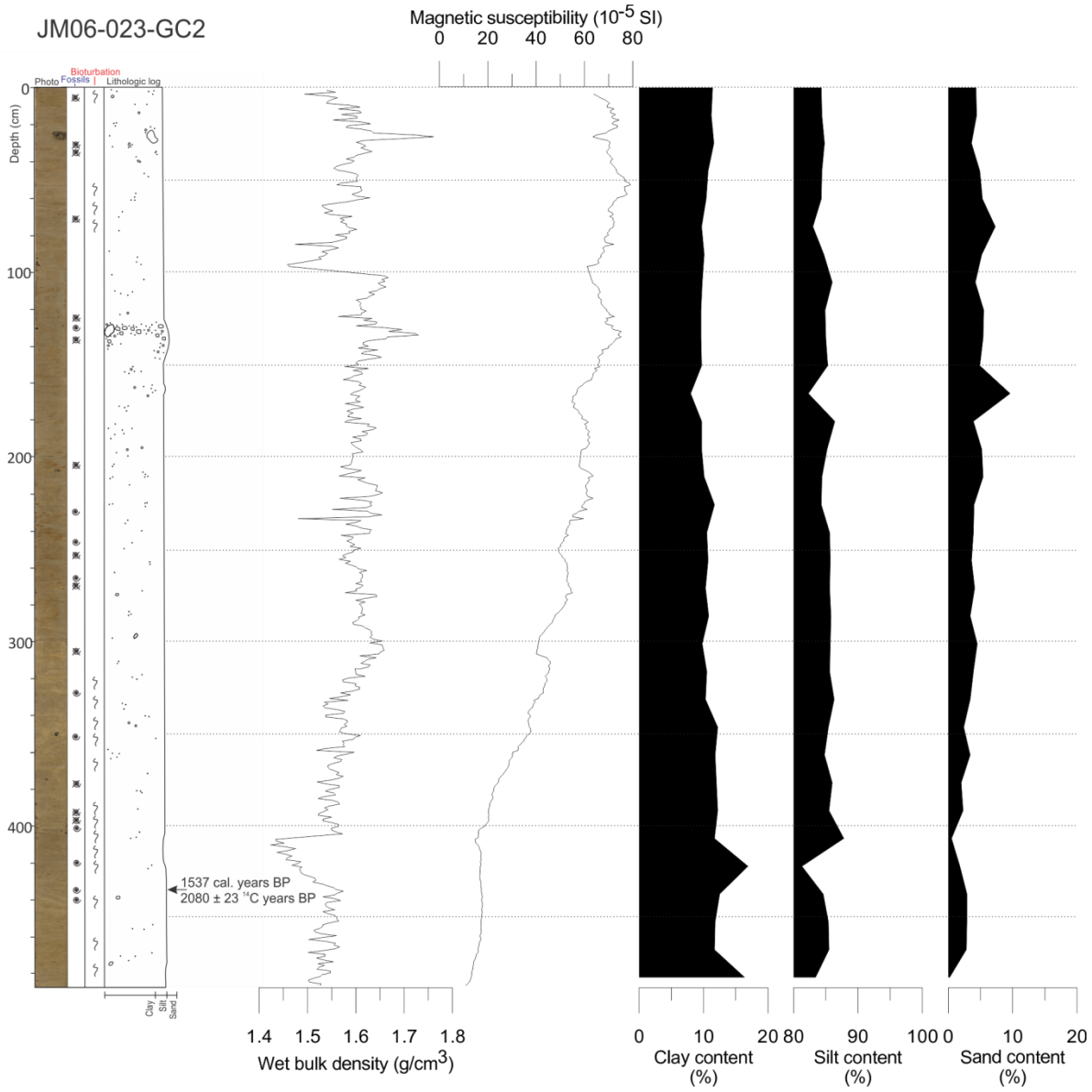

Figure 5.8: *Colour photo, shells and fragments, bioturbation, lithologic log, physical properties and grain-size distribution for the core JM06-023-GC2.Legend for the lithological log is found in Figure 5.2.*

5.3.3 Chronology and sedimentation rates

One shell fragment was collected for radiocarbon dating from this core. The shell was taken from the lowest possible level containing shells (~434 cm) in order to obtain a maximum age for the sediments. The age of the shell fragment is 1537 cal. years BP. This indicates that the base of the core has an age of approximately 1700 cal. years BP, if assuming a constant sedimentation rate. Based on this one date, the linear sedimentation rate of the core is 2.82 mm/year. The obtained date is be found in Table 5.2.

5.3.4 Interpretation and correlation

Bioturbation occurs throughout the core, and it is, therefore, not likely that the sediments are reworked (e.g. Forwick & Vorren, 2007). Thus, the high clay and silt content of the core are interpreted to be deposited through rain-out from sediment laden glacial meltwater plumes and represent a typical glacimarine environment (e.g. Powell, 2003; Forwick & Vorren, 2009; Baeten et al., 2010). The clast content in this core is very high compared to the other cores investigated in this study and it is suggested that the clasts originate from ice rafting by icebergs and/or sea ice. The core location is relatively close to the termini of the tidewater glacier Sellströmbreen (Figure 2.2) which may be a significant source of icebergs and, thus, IRD to the location. The small pockets of softer sediment may also be IRD which has been dumped off an overturning iceberg (e.g. Vorren et al., 1983). As the core is intensely bioturbated, it is also possible that the pockets are hollows or burrows made by the Polychaeta that have been filled in with sediment. The clast found at ~25 cm is most likely also ice rafted and, due to the angular shape of the clast, it may originate from supraglacial debris that has fallen onto the glacier from the surrounding steep mountain sides, e.g. around Sellströmbreen (cf. Forwick & Vorren, 2009; Figure 2.2).

There is no direct correlation between the wet bulk density, magnetic susceptibility and lithology for this core. However, there seems to be a decrease in density at ~420 cm where the silt and clay content peaks. Further up-core, in the interval between 140 – 130 cm, there is a small peak in both density and magnetic susceptibility at the same level as the large accumulation of clasts. The increase in magnetic susceptibility may be caused by the lithologies of the clasts in this accumulation. A more apparent relation between wet bulk density and grain-size distribution should not be excluded as the sampling interval for grain-size is 15 cm in this core. Fluctuations and details of the distribution may therefore not be visible.

5.4 Core JM07-048-GC2

Core JM07-049-GC2 was retrieved from the mid-fjord basin (Figure 4.3), relatively close to the western fjord side (Figure 5.1). The core is 275 cm long (Table 3.1).

5.4.1 Lithology and stratigraphy

The plastic lid on section 2 (99 - 202 cm) had not been completely sealed and the sediment in the section had therefore dried out. The dry sediment made it more difficult to perform a visual description of the sediment surface. At the time of opening the core, the sediment surface from 99 - 0 cm was black and smelled of H_2S. However, after the sediment surface had been exposed to air for some hours, the black colour and the smell disappeared. From the bottom of the core and up to 202 cm the colour of the sediment is olive grey (5Y4/2). A very vague colour change is found between c. 226 – 219 cm (Figure 5.9 and 5.11). The lower contact of this interval is described as sharp, whereas the upper is erosional (compare with Benn & Evans, 2010). The interval from 202 - 0 has a dark greyish brown (2.5Y4/2) colour.

The matrix of the core consists of a silty mud where the mean silt and clay contents are 83.8% and 10.7%, respectively. The mean sand content is 5.5%. The lowermost sample in this core was taken at 270 cm, and there the sand content is relatively high with 13.9%. At 165 cm, the sand content peaks again with 22.5%. The clay content is more or less stable throughout the core.

Clasts are scattered throughout the core. However, they are more frequent in the upper 20 cm. Pockets of grains coarser than the matrix occur at the depths of 212, 168, 145 and 110 cm, respectively. Brighter reflections (higher densities) on the X-radiographs occurred at the depths of 239 - 235, 226 - 222, 219 - 214 and 146 - 144 cm (Figure 5.10). Shells (single and paired) and shell fragments are scattered throughout the core, but some clusters of shells occur as well. Bioturbation is found throughout the core; it is most abundant in the uppermost ~30 cm.

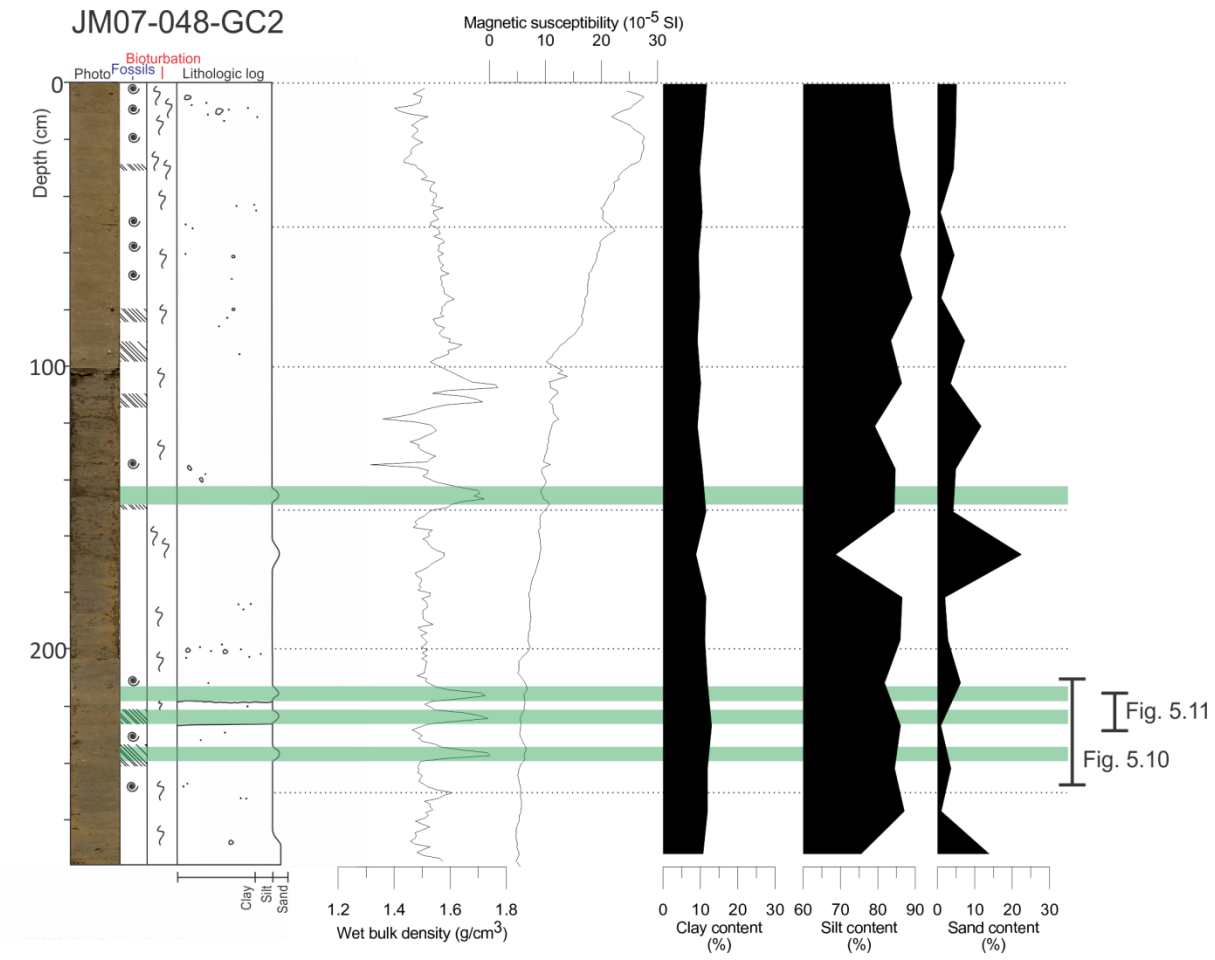

Figure 5.9: *Colour photo, shells and fragments, bioturbation, lithologic log, physical properties and grain-size distribution for the core JM07-048-GC2.The legend for the lithological log is found in Figure 5.2. The green lines illustrate the intervals of mass transport deposits mentioned in the text. Details from the X-ray photographs and colour images are displayed in figures 5.9 and 5.10, respectively.*

5.4.2 Physical properties

The mean wet bulk density for this core is ~1.53 g/cm^3. Distinct peaks occur at ~238 cm, 224 cm, 216 cm, 146 cm, 112 cm and 107 cm (Figure 5.9). From c. 100 cm, the density is slightly higher than the mean until it decreases in the uppermost 30 cm of the core. The mean magnetic susceptibility for this core is 12.3 (x 10^{-5} SI). The susceptibility is increasing from the core bottom towards the top. The up-core increase is gradual and relatively small from the core bottom (275 cm) and up to c. 100 cm depth. In the uppermost 100 cm the values increase more rapidly.

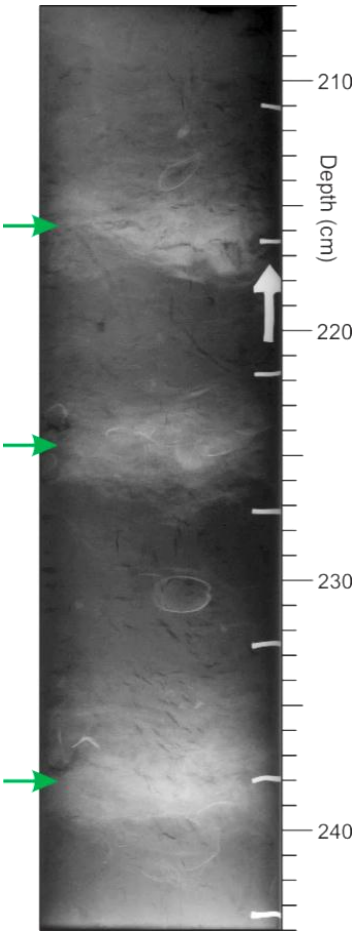

Figure 5.10: *Detail from an x-ray photograph from core JM07-048-GC2. The arrows indicate the mass transport deposits. The location of this figure in relation to the physical properties of the core is seen in Figure 5.9.*

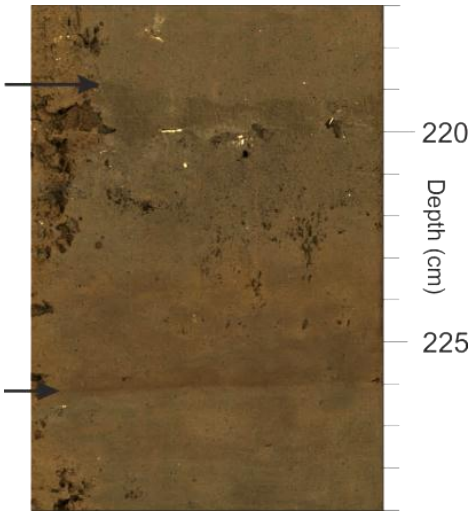

Figure 5.11: *Detail from colour image of core JM07-048-GC2. The arrows indicate the erosional (upper arrow) and sharp (lower arrow) boundaries. The location of this figure in relation to the physical properties of the core is seen in Figure 5.9.*

5.4.3 Interpretation and correlation

The core is interpreted to represent a glacimarine environment where the generally fine-grained sediment is deposited through suspension fall-out and the clasts are IRD. The intervals of higher density sediments observed in the x-rays (239 - 235, 226 - 222, 219 - 214 and 146 - 144 cm; Figure 5.10) correlate with some of the measured peaks in the wet bulk density (green intervals in Figure 5.9). Such density fluctuations may indicate either enhanced compaction or a coarser granulometric composition within the mentioned intervals compared to the rest of the core (e.g. Forwick & Vorren, 2007). As no apparent increase in coarser grains is observed in the grain-size distribution, the density peaks are probably related to compaction. The core is located relatively close to the western fjord side where gullies and slide scars are observed (Figure 5.1). The basin floor in the area displays lobes previously interpreted to be mass transport deposits (see Ottesen & Dowdeswell, 2009; *4.1 Swath bathymetry*; Figures 4.3 and 4.4). Based on the density changes and the core location, it is suggested that the above mentioned intervals consist of reworked sediments deposited by mass transport processes such as submarine debris flows and/or turbidity flows. The absence of whole shells and bioturbation in the intervals support the interpretation. As both shells and bioturbation are found between the intervals, it is most likely that they are four individual episodes rather than one or two. The sharp and erosional boundaries found at 226 and 219 cm, respectively, may also be correlated to the mass transport events (Forwick & Vorren, 2007, 2011b; Benn & Evans, 2010; Forwick et al., 2010; Figure 5.11). The lack of any visible erosional boundaries or other deformations in the other mass transport deposits (MTD's) may be because they are more distal turbidites or because they were deposited by non-eroding turbidity flows or hydroplaning debris flows (Elverhøi et al., 2000; Mulder & Alexander, 2001; Forwick & Vorren, 2007; Baeten, 2007). The magnetic susceptibility does not correlate to the other properties of the core. As the magnetic susceptibility does not fluctuate in the MTD intervals, it is suggested that the re-deposited sediment is of the same source as the rest of the sediment in the core.

5.5 Core JM07-049-GC1

Core JM07-049-GC1 was retrieved in the outer part of the fjord (Figure 5.1) and has a length of 304 cm (Table 3.1).

5.5.1 Lithology and stratigraphy

The sediment surface in the interval from 101 - 0 cm was black shortly after the core was opened. After having been exposed to air, the colour of the sediment surface is greyish brown (2.5Y5/2) from the core bottom to 270 cm, olive grey (5Y4/2) from 270 - 101 cm and dark greyish brown (2.5Y4/2) from 101 - 0 cm.

The matrix in this core comprises a silty mud. The lowermost sample in this core was taken at 285 cm and showed a grain-size distribution of 0.5% sand, 85.8% silt and 13.7% clay. From 285 cm and up to 210 cm, the sand content increases, whereas the silt and clay contents decrease. A peak in the silt content (79.8%) occurs at 195 cm with a related decrease in the sand content (11.8%). The sand content peaks again at 180 cm with 22% before it decreases up-core towards ~100 cm. From 90 cm, the sand content increases again before it decreases in the upper 75 cm of the core.

A few clasts occur scattered in the core, with a larger clast (3 - 5 cm) occurring at ~195 cm depth (Figure 5.12). Throughout the core, there is a very high abundance of shells (single and paired) and shell fragments occurring both alone, in clusters and in layers (Figure 5.13). A Polychaeta occurs at 14 cm depth. Bioturbation occurs throughout the core.

5.5.2 Physical properties

From the bottom of the core and up to 230 cm, the wet bulk density generally increases (Figure 5.12). From 230 cm, it is relatively stable around the core mean of 1.59 g/cm^3 and in the uppermost 40 centimetres it decreases to approx. 1.47 g/cm^3. The mean magnetic susceptibility for the whole core is 7.6 (x 10^{-5} SI). From the core bottom and up to ~200 cm, the values decrease somewhat. Around 200 cm, a slight increase starts and continues up-core towards the core top where the magnetic susceptibility is approximately 26.

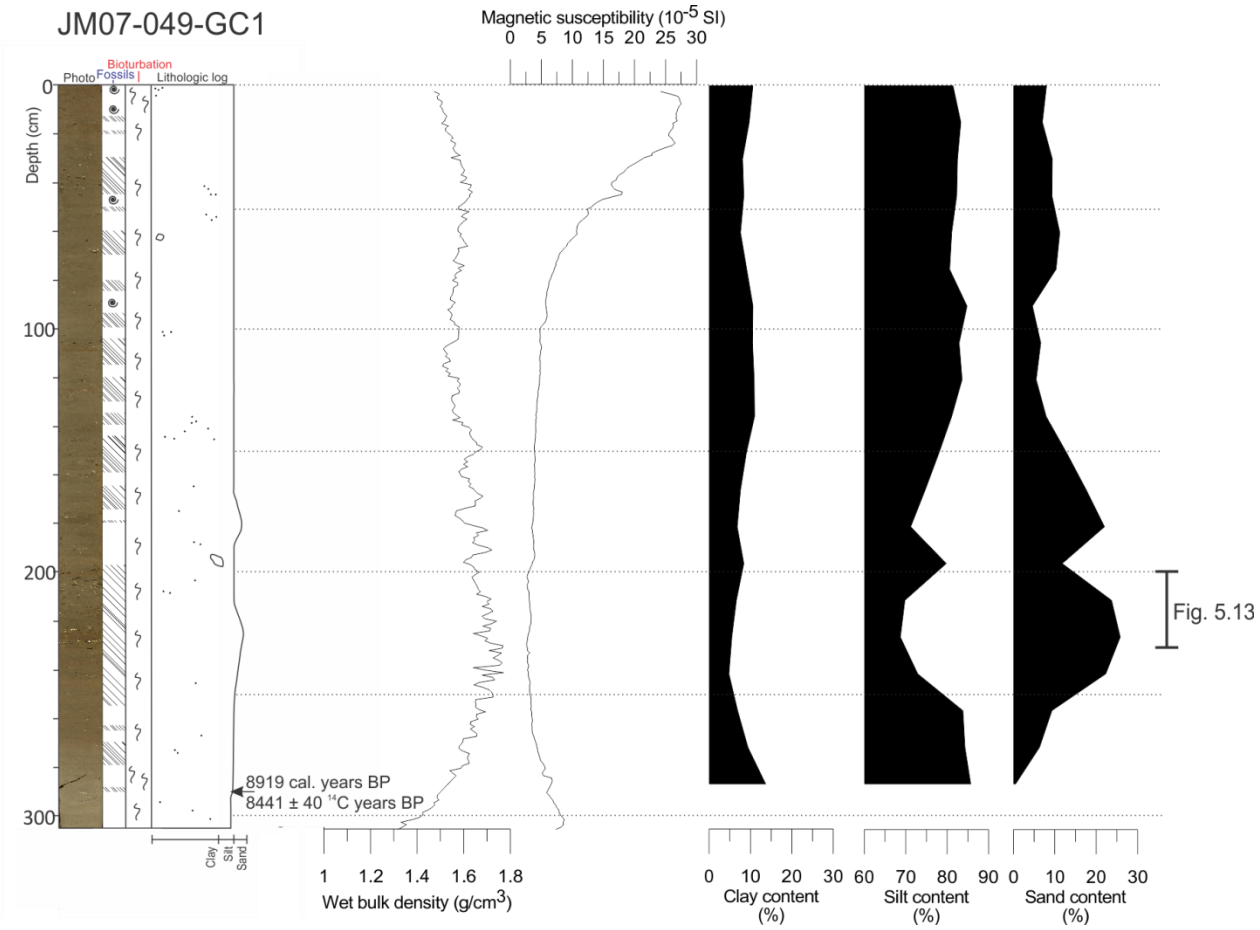

Figure 5.12: *Colour photo, shells and fragments, bioturbation, lithologic log, physical properties and grain-size distribution for the core JM07-049-GC1. Legend for the lithological log is found in Figure 5.2. A detail from the X-ray photographs and colour images is displayed in figure 5.12.*

5.5.3 Chronology and sedimentation rates

One shell was radiocarbon dated. The shell was collected at the lowest possible level containing shells (288 cm) in the core in order to obtain a maximum age for the sediments. The age of the shell is 8919 cal. years BP (Table 5.2). The linear sedimentation rate was calculated as an average from 288 – 0 cm and is estimated to 0.32 mm/year.

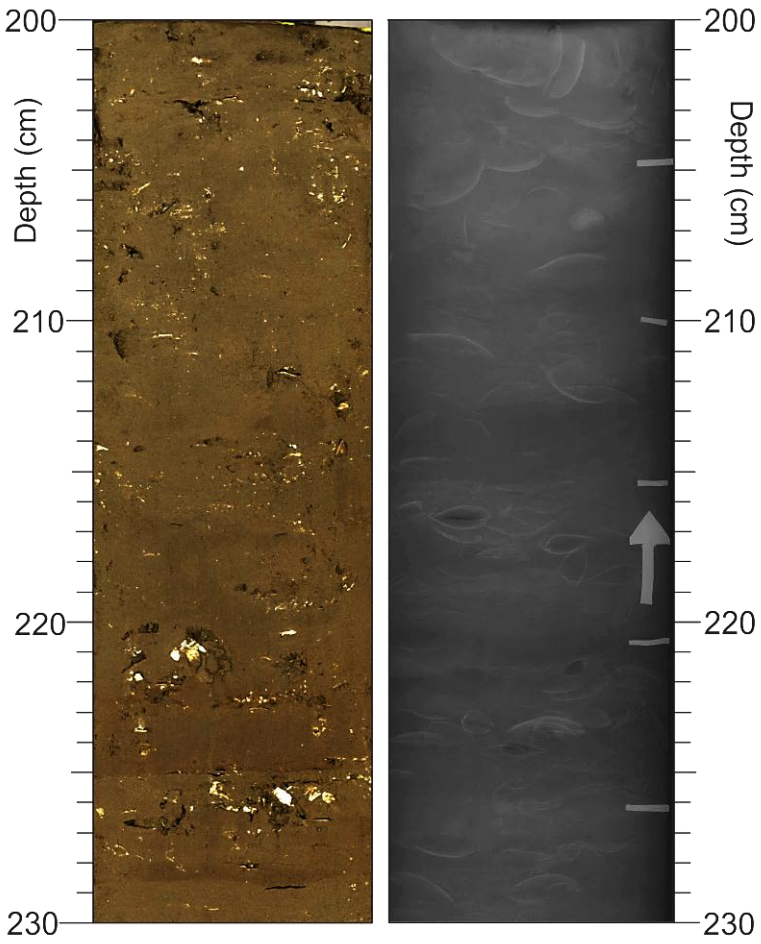

Figure 5.13: *Detail from colour and x-ray photographs showing one of the intervals with a high abundance of shells and shell fragments. The location of this figure in relation to the physical properties of the core is indicated in Figure 5.12.*

5.5.4 Interpretation and correlation

The core is interpreted to reflect a glacimarine environment where the clasts are ice rafted either by icebergs or sea ice (Forwick & Vorren, 2009; Baeten et al., 2010; Forwick et al., 2010). The great amount of single and paired shells as well as shell fragments (Figure 5.13) point towards favourable environmental living conditions for molluscs. Preserved bioturbation throughout the core indicates that the sediments have not been reworked (Forwick & Vorren, 2007). As the sampling interval for the grain-size distribution is 15 cm, it is not possible to relate the small fluctuations in density to the grain-size fractions. However, the large-scale trend of the wet bulk density correlates well with the sand content of the core. There is no evident correlation between the magnetic susceptibility and the core lithology or wet bulk density.

5.6 Core JM06-024-GC3

Core JM06-024-GC3 was retrieved from the outer fjord basin beyond the fjord mouth sill (Figure 5.1) and the core total length is 410 cm (Table 3.1).

5.6.1 Lithology and stratigraphy

The sediment surface of the upper ~20 cm was black shortly after the core was opened. After the sediment had been exposed to air for some hours, the black colour disappeared. The colour of the sediment from the core bottom to 385 cm is described as greyish brown (2.5Y5/2). A gradual change into dark greyish brown (2.5Y4/2) occurs around 385 cm and continues until 260 cm. In the interval from ~260 - 0 cm, the colour is slightly darker (olive grey, 5Y4/2).

The matrix of the core consists of a silty mud (Figure 5.14). From the bottom of the core and up to 312 cm, the clay content is on average 20.2% and the silt content 79.3%. For the same interval, the sand content is on average 0.5% although there are several 2 - 8 cm large intervals with no sand present whatsoever. From 312 cm there is an increase in the silt content which remains stable around 85% until 126 cm. For the same interval, the clay content decreases slightly up-core whereas the sand content increases. The sand content rises further and reaches 31.9% at 102 cm and is followed by a slight decrease. Another increase occurs in the uppermost few centimetres of the core. Both the clay and silt contents generally increase somewhat from around 100 cm.

Scattered clasts occur in the lowermost 30 cm and in the upper 200 cm of the core. In the interval between, i.e. from ~380 – 200 cm, hardly any clasts occur. A large, rounded clast (diorite) was found between 178 and 172 cm depth. Scattered shells and shell fragments occur throughout the entire core, but their abundance increases above 200 cm where clusters, or layers, of shells occur frequently. Polychaetes (annelid worms) occur at the depths of 47 and 38 cm. Some bioturbation is observed in the core.

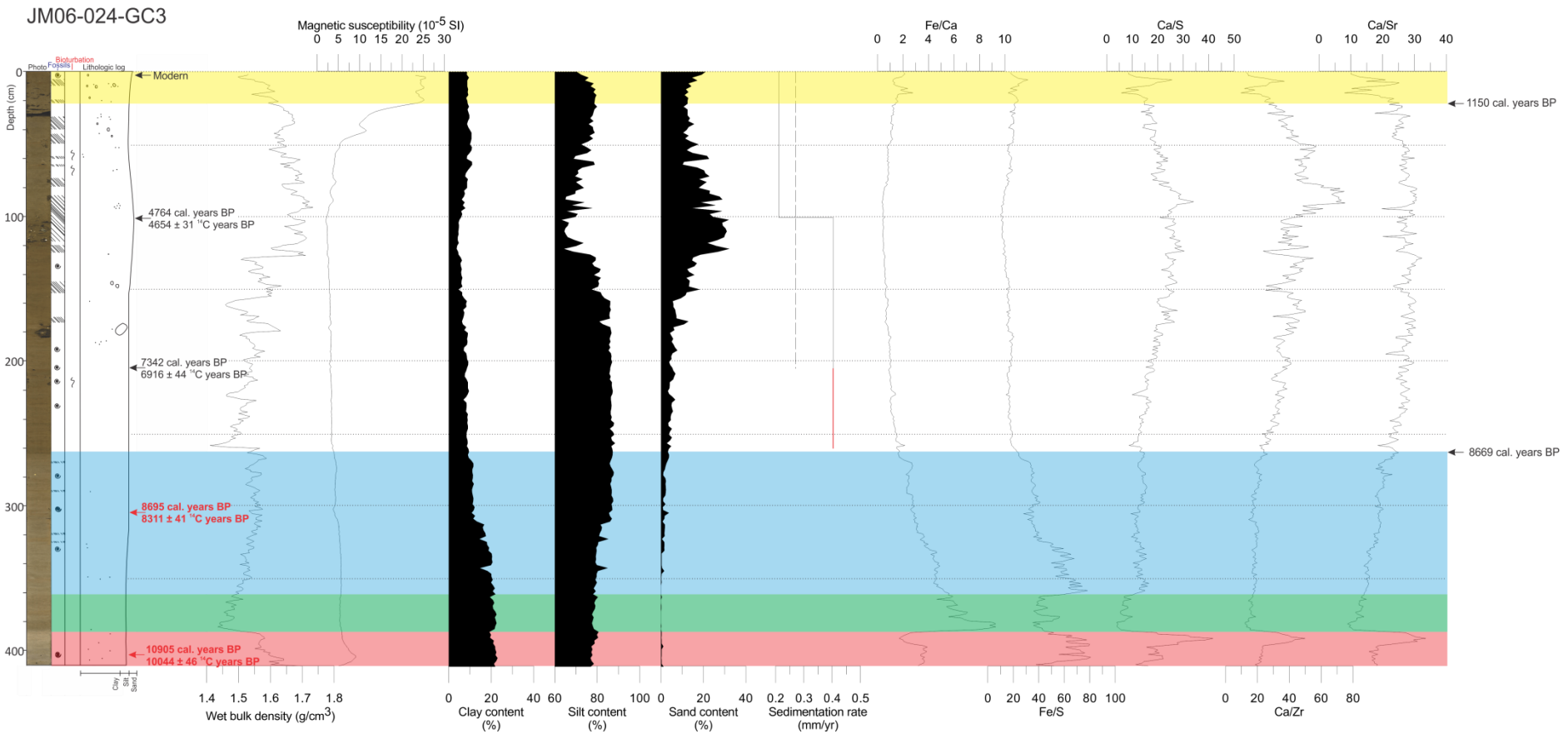

Figure 5.14: *Colour photo, shells and fragments, bioturbation, lithologic log, physical properties, grain-size distribution, linear sedimentation rate (dashed line: mean sedimentation rate; red line: extrapolated sedimentation rate) and selected element ratios for the core JM06-024-GC3. Legend for the lithological log is found in Figure 5.2. The coloured lines illustrate correlated intervals mentioned in the text. The calibrated ages given at the correlation interval boundaries are estimated based the linear sedimentation rate. The ages given in red colour are retrieved from sediments that have been interpreted as reworked. They are therefore excluded and sedimentation rates for the lowermost ~150 cm are not estimated.*

5.6.2 Physical properties

The mean wet bulk density of the core is 1.57 g/cm^3. The interval between the core bottom and ~383 cm has a relatively high wet bulk density (red interval in Figure 5.14). After a drop at 383 cm, the density generally increases up-core only interrupted by another drop at ~260 cm. The wet bulk density continues to increase up-core with values higher than the core mean in the interval from 135 – 40 cm. A small decrease occurs in the uppermost 40 cm of the core. The mean magnetic susceptibility of this core is 5.6 (x 10^{-5} SI). Apart from a slight peak in the susceptibility around 404 cm, it is generally low from the core base to approximately 50 cm depth where a rapid increase occurs. The uppermost ~25 cm of the core has a relatively high magnetic susceptibility of approximately 25 (yellow interval in Figure 5.14).

5.6.3 Element geochemistry

In the interval between 410 – 387 cm (red interval in Figure 5.14), the Fe/S ratio is quite high compared to the mean, whereas the Fe/Ca ratio is only slightly higher. A pronounced peak in the Ca/S, Ca/Zr and Ca/S ratios and a drop in the Fe/Ca ratio occurs at 391 cm. At ~387 cm there is a marked drop in all the element ratios which is most apparent in the Fe/S and Ca/S ratios. The Fe/Ca ratio increases in the same interval. From ~362 cm and up to ~263 cm (blue interval in Figure 5.14), the Fe/Ca and Fe/S ratios are higher than the mean and decrease up-core, whereas the opposite trend (low ratios; increasing up-core) is observed for the element ratios Ca/S, Ca/Zr and Ca/Sr. From 265 cm the Ca/S, Ca/Zr and Ca/Sr ratios are generally higher than the mean with more frequent peaks. In the same interval, the Fe/Ca and Fe/S ratios are low. In the uppermost ~25 cm of the core there is a slight shift in the trend where the Fe/Ca and Fe/S ratios increase (yellow interval in Figure 5.14).

5.6.4 Chronology and sedimentation rates

A total of five shells were collected for radiocarbon dating from this core (Table 5.2). The lowermost shell was collected from 402.5 cm and is dated to 10905 cal. years BP. This indicates that the bottom of the core has an age of approximately 11000 cal. years BP if a constant sedimentation rate is assumed. The other datings are younger which means that there are no age reversals of the samples. The uppermost sample, collected from 2.5 – 3 cm, came back as “modern” from the radiocarbon laboratory. However, the sample dated at ~100.75 cm is dated to 4764 cal. years BP.

In the interval from 10905 – 8695 cal. years BP (402.5 – 304 cm) the sedimentation rate is 0.45 mm/year. The rate increases to 0.73 mm/year in the interval from 8695 – 7342 cal. years BP (304 – 204 cm). From 7342 – 4764 (204 – 100.75 cm), the sedimentation rate is 0.40 mm/year whereas the uppermost interval from 4764 cal years BP (100.75 – 0 cm) has a rate of 0.21 mm/year. The mean sedimentation rate for the core is 0.37 mm/year (dashed line in Figure 5.14).

5.6.5 Interpretation and correlation

The core is interpreted to represent a glacimarine environment where the clast and sand content relate to IRD. As the content of both sand and larger clasts increase up-core, it is suggested that the uppermost ~150 cm of the core represent a period of enhanced glacial activity (compared to the underlying sediments) and more iceberg calving and rafting (e.g. Forwick & Vorren, 2009; Baeten et al., 2010; Jessen et al., 2010). The very high frequency of paired shells in the core points to a depositional environment with favourable living conditions for molluscs. The two apparent colour changes at ~385 cm and 260 cm may also be related to changes in the sedimentary environment or provenance.

The two most evident changes in the wet bulk density (~380 cm and 260 cm) coincide with the two changes in sediment colour and thereby support the interpretation of a change in the sedimentary environment. Although there is no direct correlation, the high wet bulk density of the uppermost ~130 cm of the core may be related to the grain-size distribution and the increase in sand content at this point (e.g. Forwick et al., 2010). The decrease in wet bulk density observed in the uppermost 40 cm of the core does not correlate to the increasing sand content at the same interval. It is possible that the wet bulk density is influenced by the increase in water content and fractional porosity that typically occur towards the core top. The magnetic susceptibility is generally very low for this core (mean 5.6), however, it increases up-core to reach ~25 in the upper 20 cm (yellow interval in Figure 5.14). Such a marked increase in otherwise relatively stable values may be related to a shift in lithology and/or provenance of the sediments.

The peak in the ratios Ca/S, Ca/Zr and Ca/Sr and the drop in Fe/Ca observed around 390 cm (red interval in Figure 5.14) all point to an increase in the calcium content compared to other elements. At ~387 cm, there is a drop in all ratios apart from Fe/Ca which increases to values well above the mean (green interval in Figure 5.14). This most probably indicates a drop in

the calcium content. The strongest changes are reflected in the Fe/S and Ca/S ratios which are presumably related to an increase in sulphur. The opposing signals for Fe in this interval may be due to the relative decrease in Ca (seen in the other ratios) which allows the Fe signal to increase in the Fe/Ca ratio, whereas in the Fe/S ratio the S overruns the Fe signal causing a relative decrease in Fe. The decrease in the Ca/S ratio may support this as that signal also points to an increase in the sulphur content. From 362 cm (blue interval in Figure 5.14), the up-core decreasing trend of the Fe/Ca and Fe/S ratios together with the up-core increasing trend of the other ratios (Ca/S, Ca/Zr and Ca/Sr), indicate a general decrease of the iron content at the same time as the calcium content increases. This may relate to the increasing occurrence of shells and shell fragments in the core, especially up-core from ~230 cm. The slightly shifting trends in Fe/Ca and Fe/S at the core top indicate a somewhat higher iron content which possibly can be correlated to the observed increase in magnetic susceptibility (yellow interval in Figure 5.14).

Generally, it seems that the geochemical properties of the core can be correlated to the colour changes of the sediment and, to some extent, the wet bulk density and magnetic susceptibility (see coloured intervals in Figure 5.14).As the changes in wet bulk density as well as geochemistry are relatively abrupt, it is suggested that the sediments are reworked and that the colour changes represent the boundaries between these events (see further discussion in *6.2 Correlation of acoustic and sedimentary data*). The two dates retrieved from this interval are therefore excluded (Figure 5.14).

6. Discussion

In this chapter, the results from the previous chapters are compiled and compared. Firstly, the acoustic data (i.e. the swath bathymetry and the chirp profile) will be integrated in order to discuss the origin of the submarine landforms observed. As mentioned earlier, Ottesen & Dowdeswell (2009) studied the seafloor morphology in the NW Spitsbergen fjords, including Smeerenburgfjorden. The seafloor morphology will therefore not be discussed in great detail here.

Secondly, the acoustic and the lithological data are correlated. This is done for the two key cores JM06-022-GC2 and JM026-024-GC3. In addition, the cores JM06-021-GC2 and JM07-048-GC2 are correlated to improve the interpretation of sedimentary environments and processes. In order to compare the cores, both within this study and to other studies, a P-wave velocity of 1600 m/s was used to project the cores onto the chirp profile and to estimate sediment thickness (e.g. Elverhøi et al., 1995; Plassen et al., 2004; Forwick & Vorren 2007, 2011a; Forwick et al., 2010).

Next, the sedimentation rates will be discussed with regards to both spatial and temporal changes. The different rates found within the fjord are compared to each other as well as to accumulation rates found in other Spitsbergen fjords before they are discussed in relation to time and changes through the Holocene. As the cores 22 (JM06-022-GC2) and 24 (JM06-024-GC3) have several dated intervals, they show more details of the sedimentation rate, and will therefore be the main focus of this discussion.

The sediment provenance and the main depositional processes acting in Smeerenburgfjorden will be clarified. This discussion addresses the sedimentary processes in the “internal system” of the fjord (Figure 6.1, below) and the relative importance of the processes at the individual core locations.

The last part of the discussion will summarise the internal processes and products and relate them to the external forces (Figure 6.1) and their changes through the Holocene. This discussion will be based on a compilation of all the different results, but mainly centre around the sedimentary data.

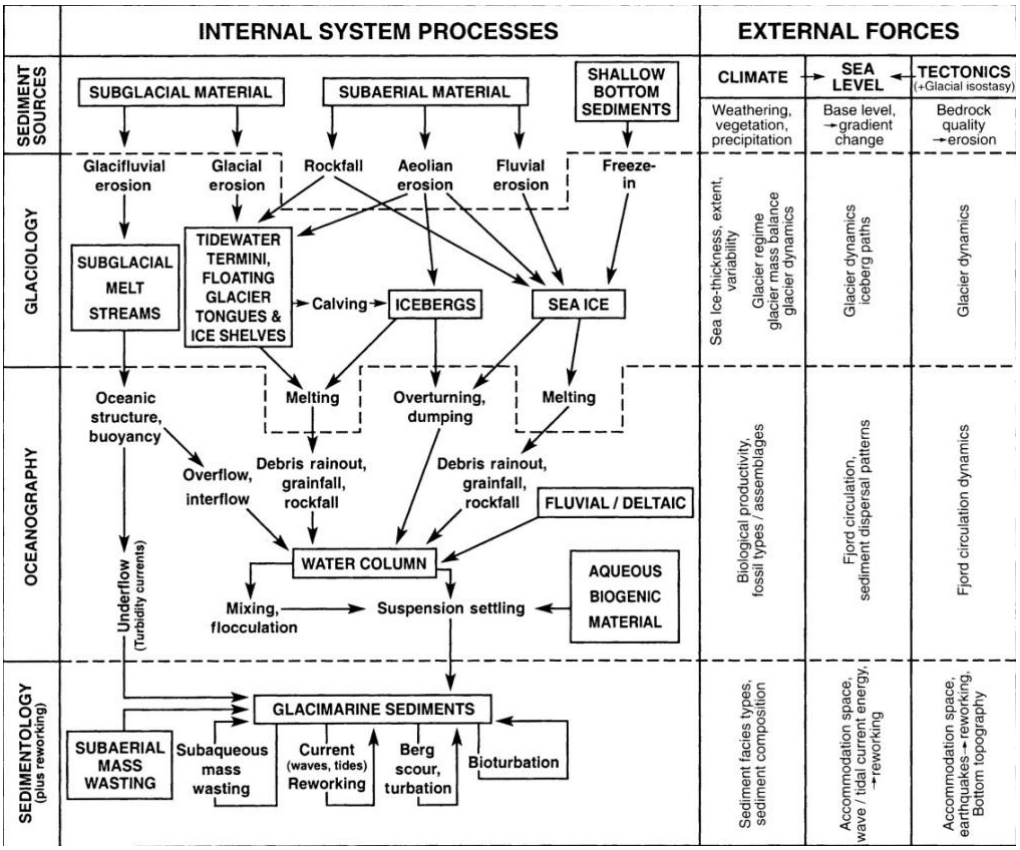

Figure 6.1: *Schematic figure of internal system processes and the external forces acting in a glaciated fjord (Dowdeswell, 1987).*

6.1 Morphology and origin of the submarine landforms

Amongst the submarine landforms observed on the swath bathymetry and chirp data, the recessional moraines are the most striking features. Recessional moraines are formed by small winter re-advances of the tidewater glacier front during overall glacial retreat. The sea-ice cover at the glacier termini in winter suppresses iceberg calving and causes the glacier to grow. During the advance, sediment at the grounded glacier front is pushed, folded and thrusted and forms the recessional moraine (Boulton, 1986; Ottesen & Dowdeswell, 2006, 2009; Ottesen et al., 2007). The fact that they are the result of such short-lived re-advances is also the reason for the comparatively small amount of sediment they are made up of (Ottesen et al., 2007).

On the bathymetry data, the recessional moraines are most apparent in the northern part of the dataset and in the more shallow (< 200 m water depth) areas. However, the chirp profile reveals that they occur along the entire fjord axis (Figure 4.4). As the moraines occur on the

lowermost reflection (R1), below the sediment succession of Unit 1 (U1; Figure 4.4), they are most likely formed during the last deglaciation (see below). The moraines are of approximately the same heights (3 - 4 m) and have a semi-regular spacing of 120 – 160 m (mean ~140 m; Figure 6.2). Similar moraines have been found in other fjords (e.g. Ottesen & Dowdeswell, 2009; Baeten et al., 2010; Forwick et al., 2010; Forwick & Vorren, 2011a; Kempf et al., in prep) and it is therefore reasonable to assume that the small transverse ridges in Smeerenburgfjorden are recessional moraines as well. As recessional moraines are formed by winter-summer oscillations of the glacier front, they may be produced annually. If the moraines in Smeerenburgfjorden were formed annually during deglaciation, the average retreat rate of the glacier was ~140 m/year. Similar rates have been observed in other Spitsbergen fjords, e.g. ~170 m/year in Billefjorden (Baeten et al., 2010) and between 80 – 190 m/year in Van Keulenfjorden (Kempf et al., in prep.).

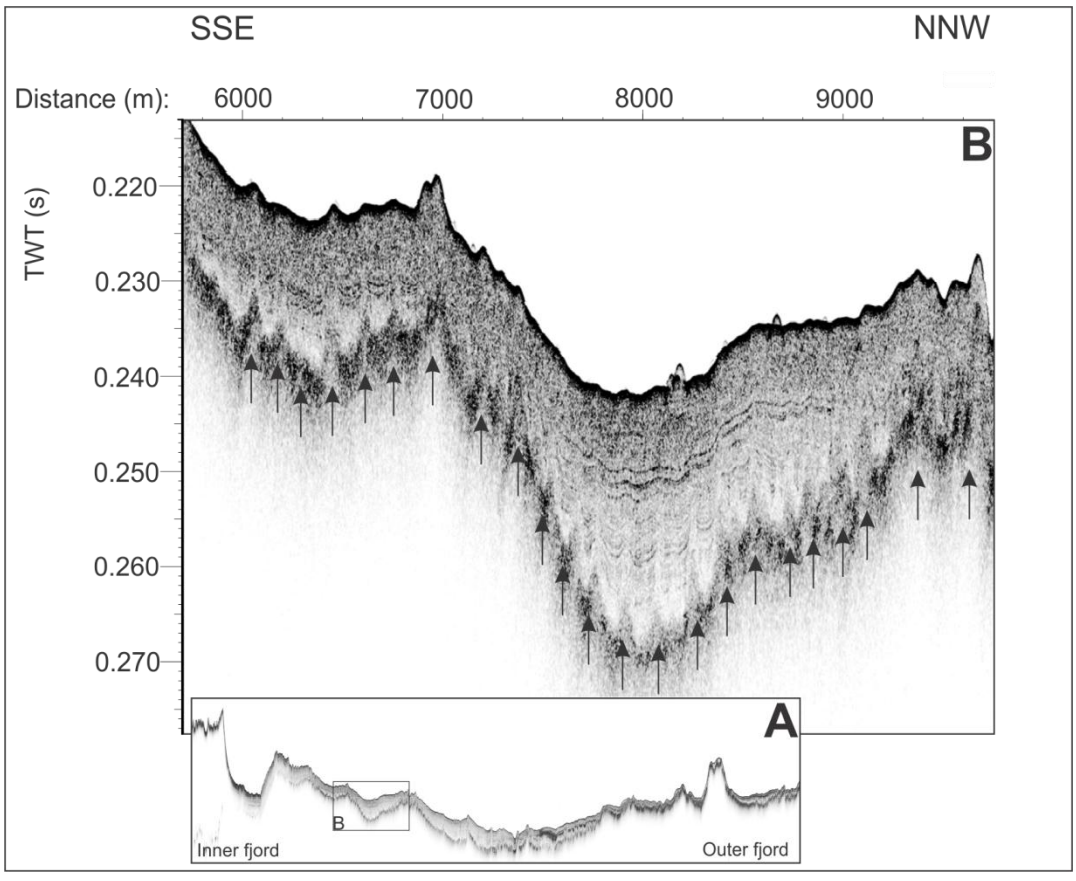

Figure 6.2: *Section of the chirp profile with arrows indicating the recessional moraines.*

As mentioned earlier, only some of the recessional moraines beyond the LIA moraine are seen on the present day seafloor. This is most probably the result of high sediment supply that has both draped and smoothened the morphological expression of the moraines. Generally, the sediment succession is thinning towards the fjord mouth (Figure 4.4). The innermost basin has a sediment thickness of ~30 meters, whereas the mid-fjord basin has a thickness of approximately 20 meters. Topographic highs generally have sediment thicknesses of ~11 meters. In the outermost part of the fjord, the sediment thickness is 10 meters. The thinner sediment cover on topographic highs and the general thinning towards the fjord mouth is most likely the reason for the well-preserved recessional moraines in these areas (on the large inner fjord moraine, 4 in Figure 4.3; the outermost basin, 1 in Figure 4.3).

The moraines observed between Smeerenburgbreen and the Little Ice Age moraine (Figures 4.4 and 6.3) are also interpreted to be recessional moraines. They may have been formed as Smeerenburgbreen retreated from the LIA moraine to its present day position. The moraines can therefore be regarded as a modern analogue to the recessional moraines formed during the early Holocene deglaciation. Such relatively recent moraines are also reported from other Spitsbergen fjords; e.g. Rindersbukta (Inner Van Mijenfjorden; Ottesen et al., 2008), Van Keulenfjorden (Liestøl, 1977; Ottesen et al., 2008), Magdalenefjorden (Ottesen & Dowdeswell, 2009), and in Borebukta and Yoldiabukta (Ottesen & Dowdeswell, 2006).

In the chirp profile, 16 recessional moraines occur within the LIA moraine over a distance of 1400 meters. If these moraines were deposited annually, it would indicate a retreat rate of 87.5 m/year for the front of Smeerenburgbreen. This rate is similar to the 90 m/year retreat rate found in the inner basin of Van Keulenfjorden (Ottesen et al., 2008). It is evident from both the chirp profile as well as the swath bathymetry data that some of the moraines in the innermost part of the fjord are overlapping. It is therefore possible that there are more moraines in this area and that the average retreat rate is somewhat lower. In addition, the data coverage towards Smeerenburgbreen is limited and there are most probably more moraines towards the glacier front that are not possible to include in the estimate.

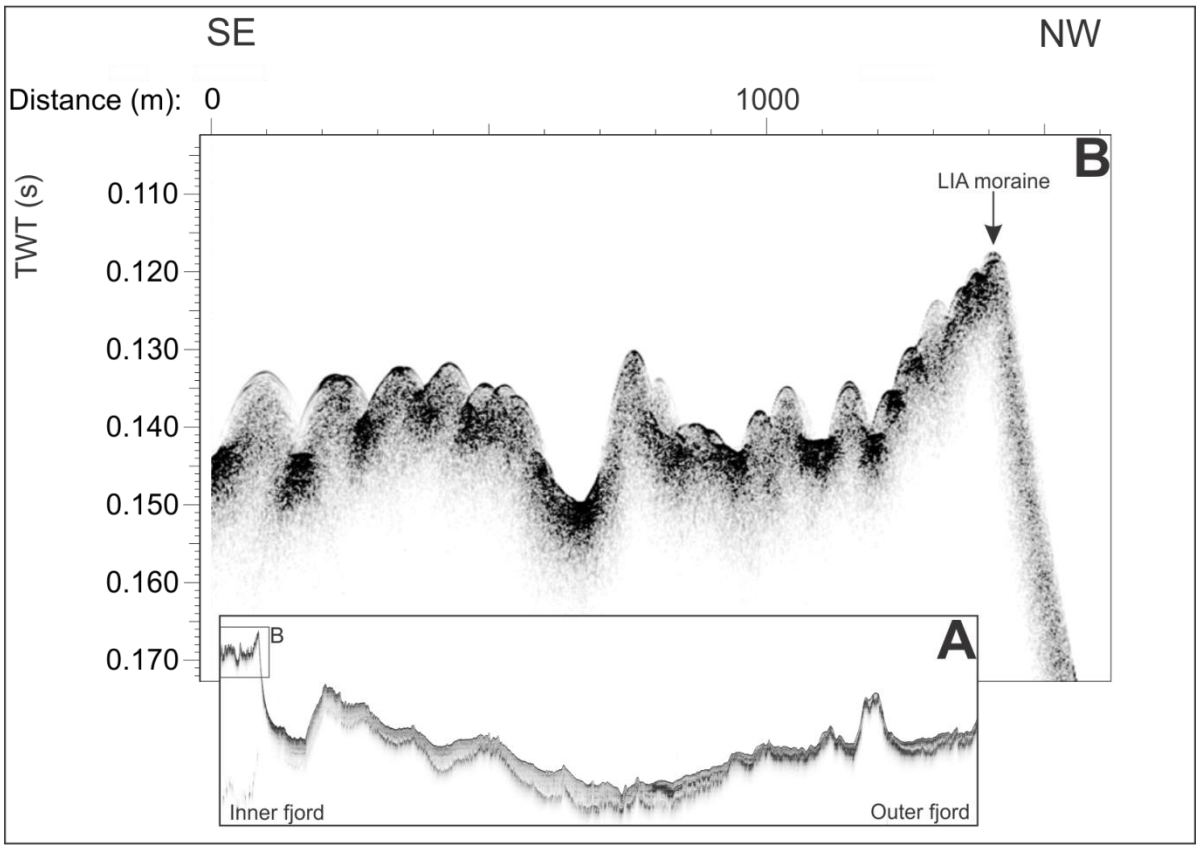

Figure 6.3: *Section of the chirp profile showing the recessional moraines in the innermost part of Smeerenburgfjorden.*

In summary, the recessional moraines in Smeerenburgfjorden are the most interesting features that have been observed from the acoustic data. If the recessional moraines are assumed to be produced annually, the retreat rate of the glacier during the deglaciation is estimated to 140 m/year. The post LIA-retreat rate is estimated to 87.5 m/year. Both the recessional moraines themselves and the retreat rates are similar to those found in other Spitsbergen fjords.

6.2 Correlation of acoustic and sedimentary data

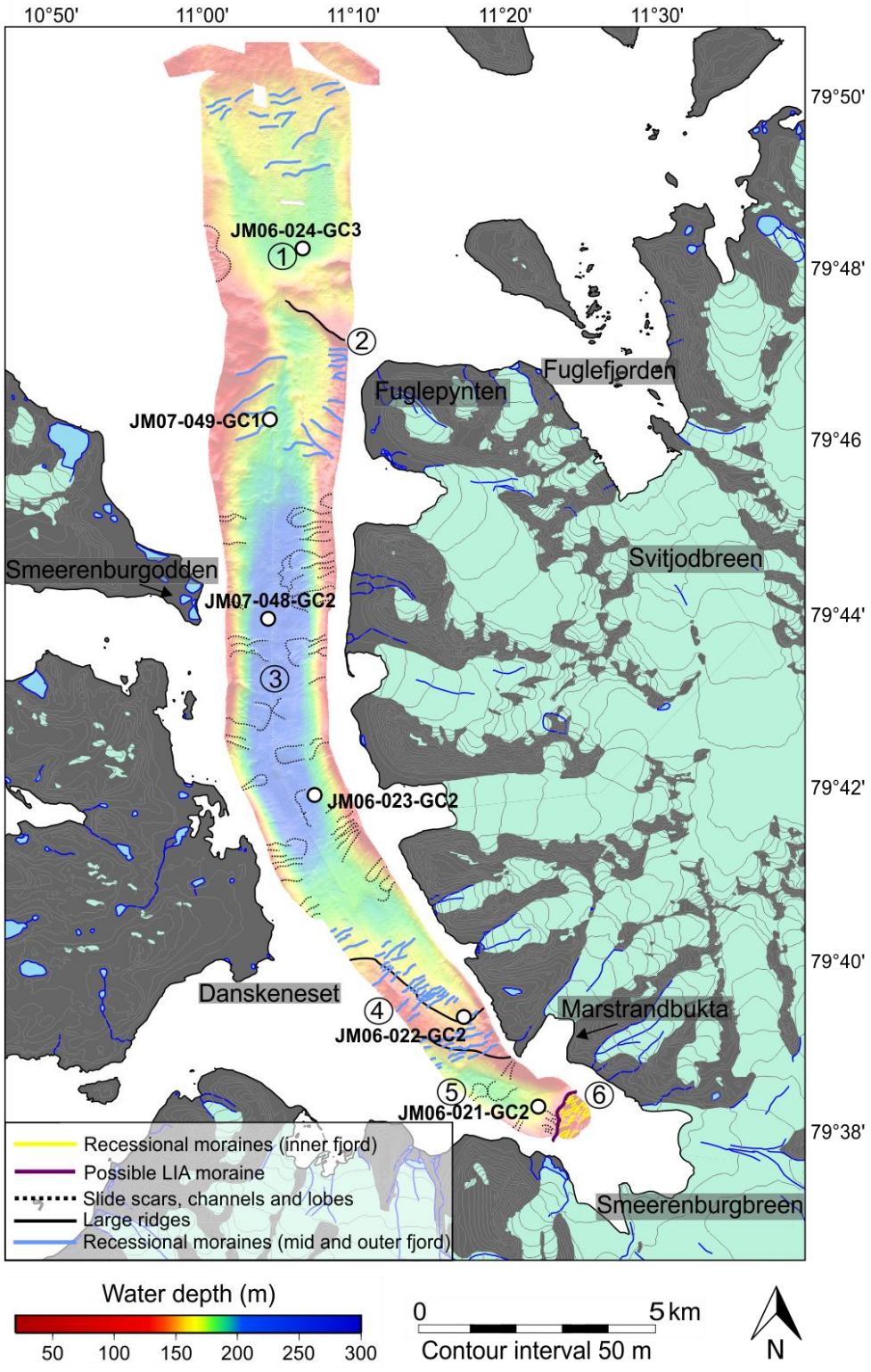

Figure 6.4: *Summary interpretation of the swath bathymetry and the core locations (white circles). The numbers refer to 1) The outermost basin, 2) outermost large ridge, 3) mid-fjord basin, 4) large ridge with superimposed smaller transverse ridges, 5) innermost basin, and 6) Possible LIA moraine (purple) and recessional moraines (yellow). Place names mentioned in the text are indicated. Glaciers are marked in light green and rivers/lakes in dark blue and blue, respectively.*

Core 21. Based on the colour changes of the sediment and the chaotic/transparent character of the acoustic data, core 21 is interpreted to contain reworked sediments. From the swath bathymetry data, it is evident that slope failures occur on the distal slope of the Little Ice Age moraine. On the chirp profile the slightly irregular and hyperbolae surface of reflection R2 (Figure 4.4) in the inner fjord basin (5 in Figure 6.4) indicate that the deposits are slumps and slides (e.g. Mulder & Cochonat, 1996; Mulder, 2011). The processes of slope failure will be further discussed in *6.4.4 Provenance and post-glacial sedimentary processes*. The inner fjord basin holds a sediment succession of 25 – 35 meters. As core 21 is only 60 cm long, it does not reveal the characteristics of the underlying sediments (Figure 6.5).

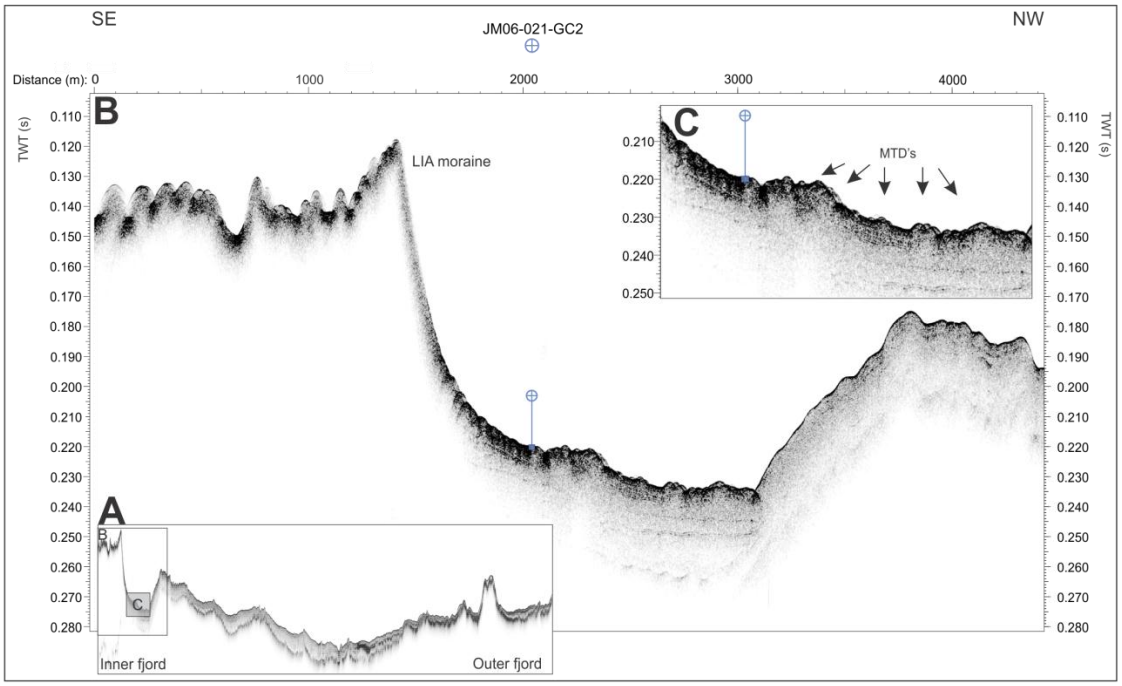

Figure 6.5: *Section of the chirp profile showing the inner fjord basin with the location of core JM06-021-GC2 indicated in blue. The Little Ice Age moraine is indicated in B, and mass transport deposits are indicated in C.*

Core 22. This core is retrieved just outside the transverse bedrock sill in the inner fjord (4 in Figure 6.4). The core has been interpreted to consist of glacimarine sediments. The chirp profile shows that the sediment succession at the core location is ~17 meters thick and relatively transparent. This points towards relatively fine-grained material typical of a glacimarine environment (e.g. Elverhøi et al., 1980, 1983; Hjelstuen et al., 2009; Forwick &

Vorren, 2011a). A few internal reflections are observed and these are interpreted to represent changes in grain-size (e.g. more IRD compared to rain-out of suspended sediment) and/or changes in compaction (e.g. Plassen et al., 2004; Batchelor et al., 2011). As seen in Figure 6.6, core 22 penetrates some of these internal reflections. However, no intervals of higher or lower IRD concentrations were observed. The measured physical and geochemical properties do not seem to correlate to the internal reflections either. Internal reflections are caused by a change in acoustic impedance which is a product of density and P-wave velocity. As no apparent changes in density are observed, the internal reflections may represent changes in P-wave velocity. However, as previously mentioned, the P-wave velocity measurements were disregarded due to inaccuracies (cf. *5. Lithostratigraphy*).

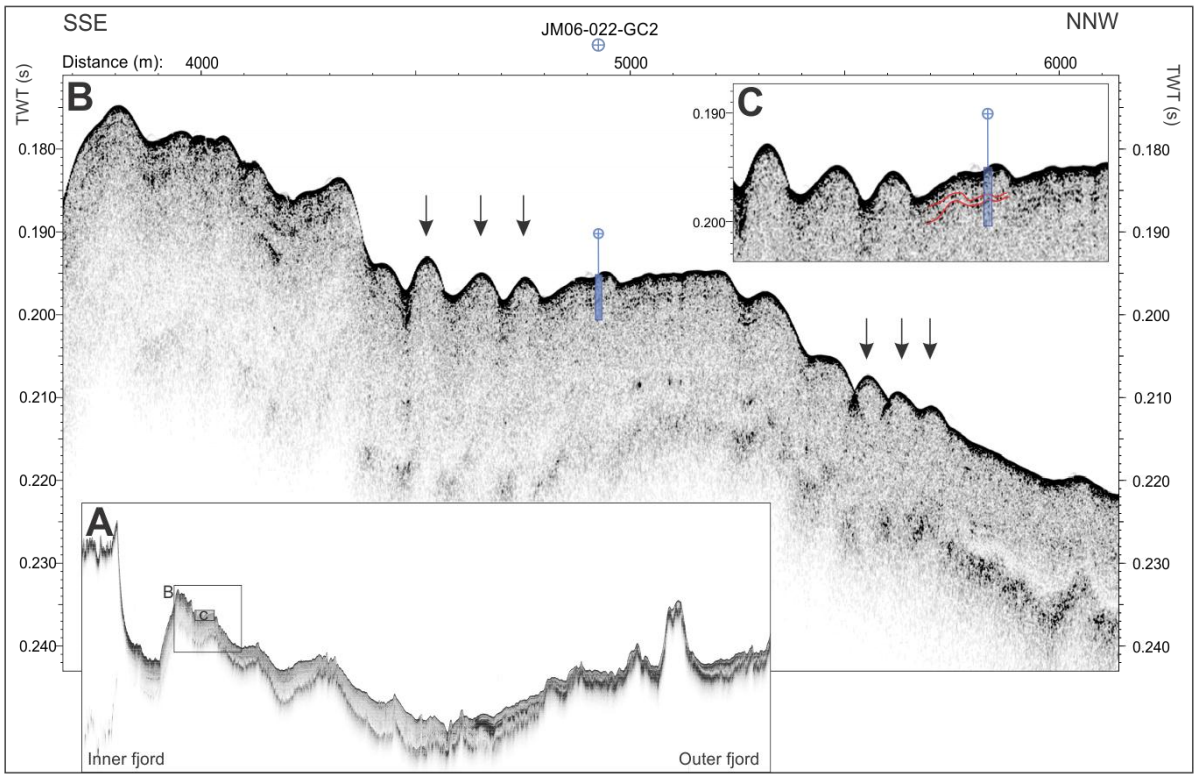

Figure 6.6: *Section of the chirp profile with the location of core JM06-022-GC2 indicated in blue. The arrows indicate recessional moraines expressed on the seafloor. The red lines in C show the internal reflections penetrated by core JM06-022-GC2.*

Core 48. This core is retrieved from the mid fjord basin, close to the western fjord side (Figure 6.4). Based on changes in wet bulk density as well as in the x-radiographs, four intervals of mass transport deposits were identified. From the swath bathymetry data, it is

evident that both the western and eastern fjord sides are subject to slope failure and lobe-shaped mass transport deposits are identified downslope of the slide scars (Figure 4.3). The chirp profile further supports the theory, as several stacked, strong and irregular reflections are found in the mid-fjord basin, and especially at the location of core 48 (Figures 4.4 and 6.7).

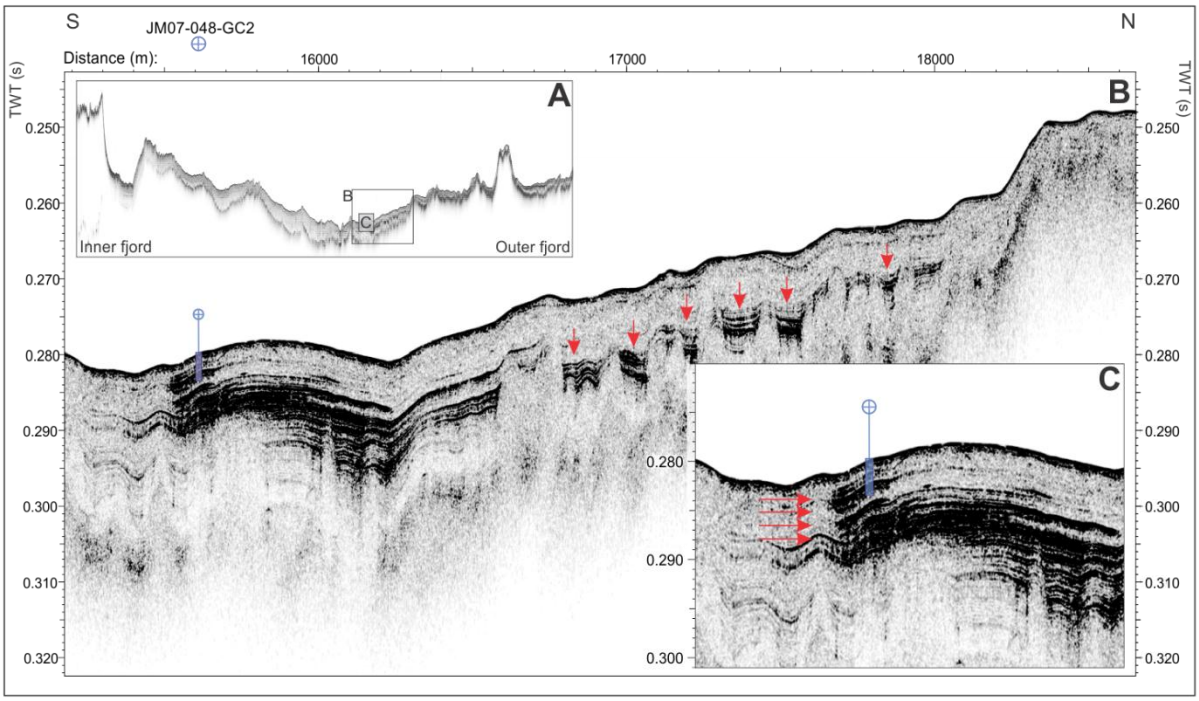

Figure 6.7: *Section of the chirp line with the location of core JM07-048-GC2 indicated in blue. The red arrows indicate the stacked internal reflections interpreted to be mass transport deposits.*

Core 24. On the chirp profile, two of the internal reflections are penetrated by core 24 (red and blue line in Figure 6.8 C). These reflections are suggested to correlate with the colour changes observed at ~385 cm (top of red interval in Figure 5.14) and 263 cm (top of blue interval in Figure 5.14). The two reflections have slightly undulating and irregular surfaces and are thinning towards the north (Figure 6.8). Based on this, it is suggested that the two intervals with different colours below 260 cm in core 24 are mass transport deposits (MTD's) that have originated either from the adjacent outer fjord moraine (2 in Figure 6.4), or from the shallow areas west of the core site where lobe shaped features occur (Figure 6.4). The very marked changes in both wet bulk density, geochemistry and, to some extent, magnetic susceptibility in this part of the core are also indicative of a different sediment composition,

and, thus, support sediment reworking. It is possible that the above mentioned changes in sediment properties are related to a change in provenance of the sediment. However, the observed changes are very abrupt and it is unlikely that there has been such a dramatic change in sediment provenance. The absence of bioturbation is also indicative of reworked sediments (e.g. Forwick & Vorren, 2007).

The two dates retrieved from 402.5 cm (10905 cal. years BP) and 304 cm (8659 cal. years BP) appeared in a normal order (i.e. with no age reversals). However, they are collected from intervals containing reworked sediments and it is therefore probable that the shells also are reworked. The two mentioned dates are therefore disregarded from further discussion. Based on this interpretation, the sedimentation rates as well as the wet bulk density, magnetic susceptibility, grain-size and geochemical composition of the sediments below 260 cm are excluded from further discussion.

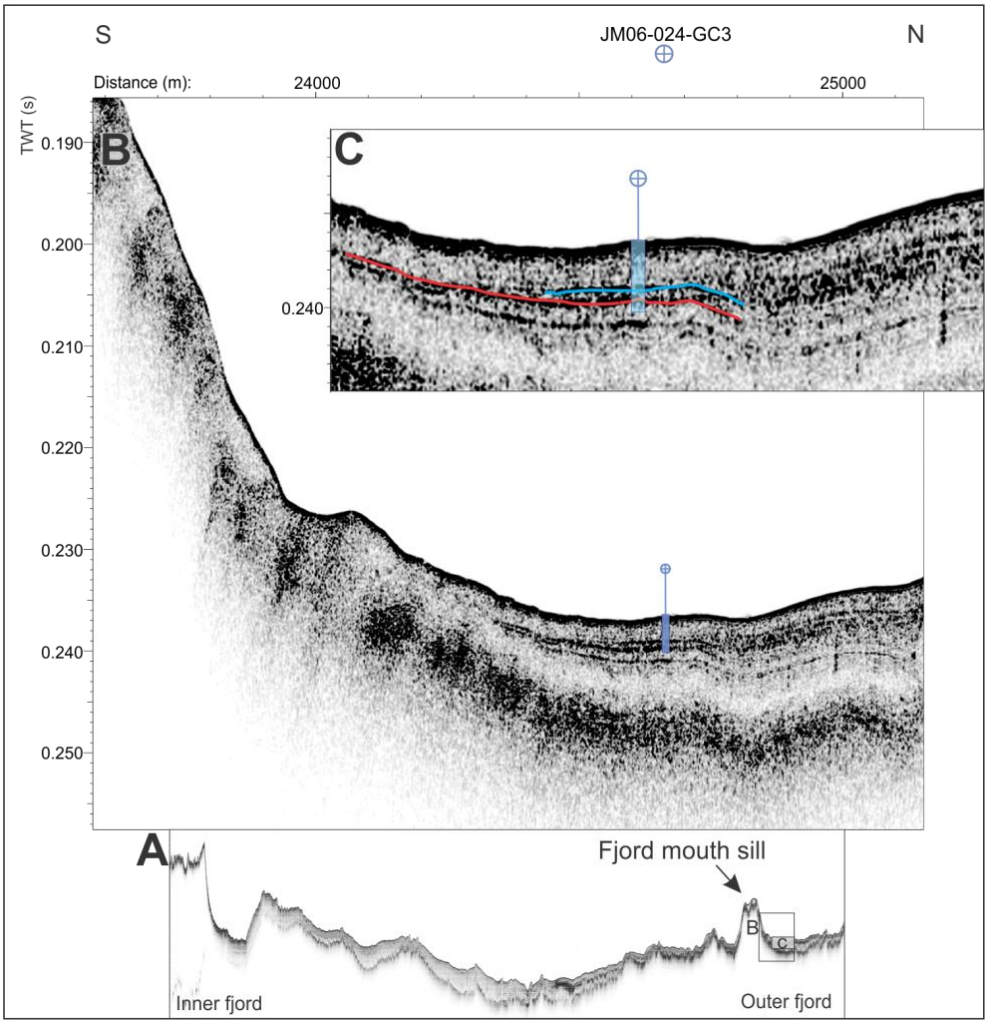

Figure 6.8: *Section of the chirp profile with the location of core JM06-024-GC3 indicated in blue. The blue and red lines in C correspond to the internal reflections and MTD-intervals mentioned in the text.*

6.3 Sedimentation rates

For the estimation of linear sedimentation rates, a constant accumulation rate of sediment between all dated intervals was assumed. In addition, the top of the core was presumed to be the modern seafloor. The estimated linear sedimentation rates (in cm/cal. ka) are presented in Table 6.1.

Core 22 was collected in 2006 which would imply that the core top contains sediment deposited in 2006. However, by applying an age model using calibrated years BP, one assumes the core top to be deposited in AD 1950 (0 cal. years BP). When sediment cores are retrieved, it is not uncommon for the core top to be somewhat disturbed and a few centimetres of sediment can be lost. However, the sedimentation rates of core 22 are relatively high, so assuming that the top of the core is AD 1950 would mean a loss of approximately 20 cm of sediment. No disturbances of the sediment are observed in the x-radiographs, and therefore it is not likely that as much as 20 cm has been removed. For these reasons and to be able to correlate core 22 to other studies addressing the latest Holocene, the top of core 22 is assumed to be AD 2006 and discussed age intervals from this core will be given in cal. years AD.

In core 24, the sedimentation rates are low and the difference between AD 2006 and AD 1950 would only represent a couple of centimetres of sediment. An age model using cal. years BP is therefore applied for core 24.

Table 6.1: *Estimated sedimentation rates for the dated intervals. Sedimentation rates in bold are the mean rates calculated for the whole core length.* ***Sedimentation rate calculated based on cal. years AD.***

Core	Depth interval (cm)	Age interval (cal. years BP)	Age interval (cal. years AD)	Sedimentation rate (cm/cal. ka)
JM06-022-GC2	382 - 318.75	935 - 627	1015 - 1323	205
	318.75 - 201.75	627 - 460	1323 - 1490	700
	201.75 - 0	460 - 0	1490 - 2006	439, *390
	382 - 0	935 - 0	1015 - 2006	**408, *385**
JM06-023-GC2	434 - 0	1537 - 0		**282**
JM07-049-GC1	288 - 0	8919 - 0		**32**
JM06-024-GC3	204 - 100.75	7342 - 4764		40
	100.75 - 0	4764 - 0		21
	204 - 0	7342 - 0		**27**

Core 22. The lowest linear sedimentation rate in core 22 (205 cm/cal. ka) occurs between 935 – 627 cal. years BP. It increased to 700 cm/cal. ka in the following interval between 627 – 460 cal. years BP; the highest rate throughout the entire record, before decreasing to 390 cm/cal. ka. The overall mean linear sedimentation rate for the core is 408 cm/cal. years BP (Table 6.1).

408 cm/cal. ka is comparatively high and is probably a result of the location of the core in the vicinity of the large inner fjord tidewater glaciers (e.g. Smeerenburgbreen, Marstrandbreen, Scheibreen and Kvasspiggbreen; Figure 2.2). Although the sedimentation rates in core 22 are the highest rates found in this particular study, they are an order of magnitude lower than rates found in other Spitsbergen fjords. Elverhøi et al. (1983) found sedimentation rates in the range from 5000 – 10000 cm/ka at a distance of up to 10 km from the glacier front in Kongsfjorden. At the grounding line fan of Kronebreen in Kongsfjorden, Trusel et al. (2010) calculated sedimentation rates of ~30000 cm/ka and rates of 6000 – 9000 cm/ka in the inner fjord basin. In Tempelfjorden, the mean sedimentation rate in the inner fjord was estimated to 1700 cm/ka for the last 130 years (Plassen et al., 2004). Forwick et al. (2010) found rates of 3800 cm/ka in the vicinity of the glacier in Tempelfjorden. The studies mentioned above may have found higher rates because their core locations and measuring points are closer to either the glacier front (Trusel et al., 2010) or close to other point sources, e.g. rivers (Plassen et al., 2004; Forwick et al., 2010; see *6.4.1 Suspension settling*).

The core site for core 22 is located approximately 6 km from the present day terminus of Smeerenburgbreen (Figure 2.2), but the sedimentation rate is still lower than the rates found within 10 km off Kronebreen in Kongsfjorden (Elverhøi et al., 1983). A reason for the large differences in sedimentation rate may be the amount of glacial meltwater entering the fjord either at the glacier front or from the fjord sides (from glaciers terminating on land). The drainage basin area in Kongsfjorden is 1428 km^2, compared to the 407 km^2 of Smeerenburgfjorden (Hagen et al., 1993). This means that the glaciers and rivers in Kongsfjorden have a larger area to erode and collect sediment from, and, thus, a larger flux of sediment enters the fjord system. Furthermore, the glaciers in Kongsfjorden are situated in sedimentary rocks which are more easily eroded compared to the gneisses and granites in Smeerenburgfjorden (Elverhøi et al., 1980; Dallmann et al., 2002; Ohta et al., 2007, 2008). In addition, the stability of the glacier front with regards to iceberg calving influence the input of IRD to the fjord (cf. *6.4.2 Ice rafting*).

Jernas et al. (in press) investigated two sediment cores from the Hinlopen and Kongsfjorden troughs (for location see Fig. 1 in Jernas et al., in press), and found a general increase in sedimentation rate for the age interval AD c. 1200 – 1500 (Figure 6.9). The interval with the highest sedimentation rates in core 22 (700 cm/cal. ka) represent the time span from AD c. 1323 – 1490 and may, therefore, correlate to the periods of higher sedimentation rates in Kongsfjorden and Hinlopen. In addition to the increased sedimentation rates, Jernas et al. (in press) found an increase in the IRD flux and attributed this to either glacier surges or general glacier growth on Svalbard during this period.

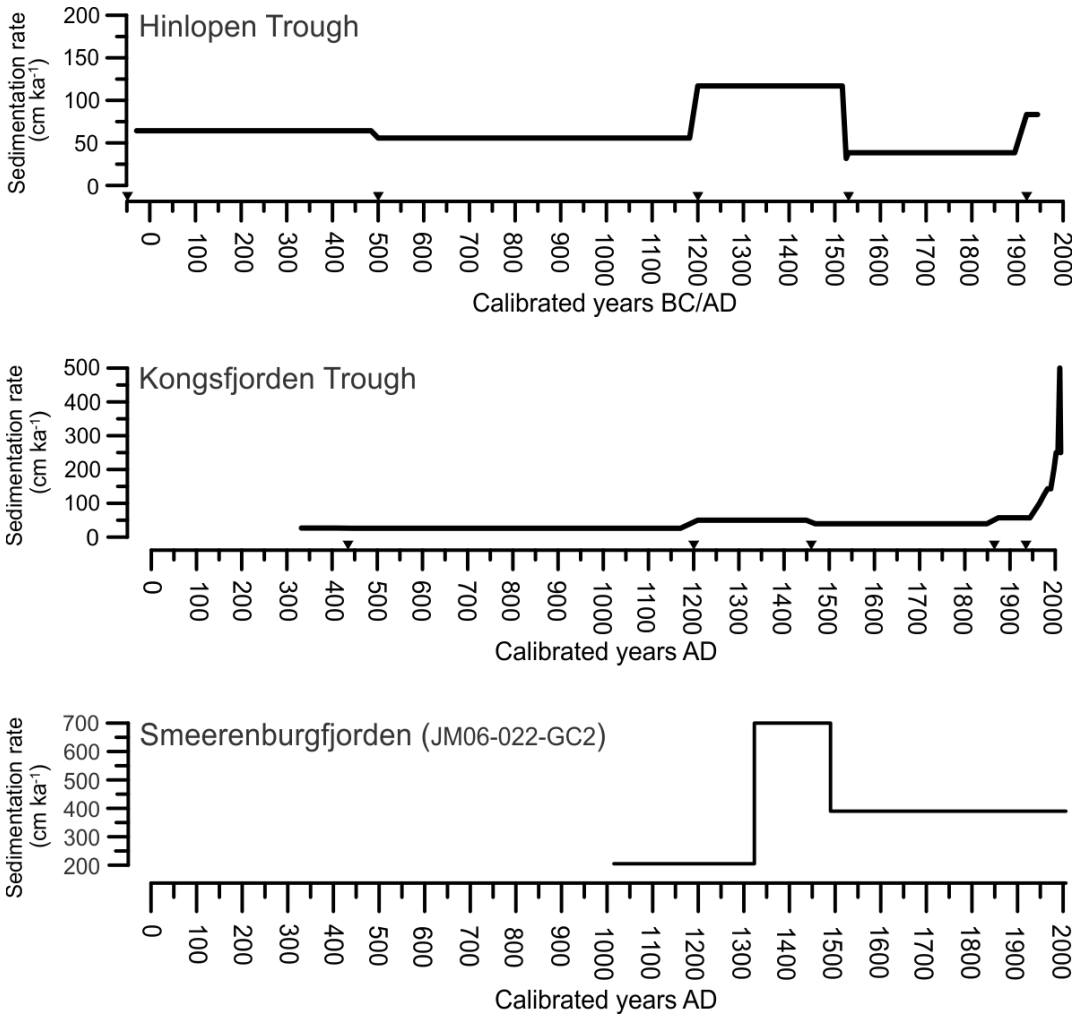

Figure 6.9: *Sedimentation rates from Hinlopen Trough and Kongsfjorden Trough (from Jernas et al., in press) and core JM06-022-G2 in Smeerenburgfjorden.*

Core 23. The mean sedimentation rate for core 23 is 282 cm/cal. ka. Although this rate is in the same order of magnitude as that of core 22, the sedimentation rate is approximately 30% lower in core 23 which may indicate that the accumulation rate decreases rapidly with the distance from the main tidewater glacier front (e.g. Elverhøi et al., 1980). The estimated sedimentation rate for this core is based only on one date and is therefore an average of the whole core length. It is, however, most likely that there have been changes in the sedimentation rate over time, as seen in cores 22 and 24. Core 23 is located in the mid-fjord basin (3 in Figure 6.4) but is still subject to glacial influence as the tidewater glacier Sellströmbreen is located only ~3 km east of the core site (Figure 2.2). The high sedimentation rate is probably a result of sediment-laden glacial meltwater plumes and debris-loaded icebergs passing the core site (e.g. Elverhøi et al., 1980; Powell et al., 2003; Trusel et al., 2010; see *6.4 Provenance and post-glacial sedimentary processes*).

Core 24. The lower ~120 cm of this core have been interpreted as reworked sediments and sedimentation rates were therefore not estimated. In the interval between 7342 – 4764 cal. years BP, the sedimentation rate is 40 cm/cal. ka. The lowest sedimentation rate in core 24 (21 cm/cal. ka) occurred between 4764 – 0 cal. years BP. The mean linear sedimentation rate for the entire core is 27 cm/cal. ka (Table 6.1). Several studies from Svalbard have shown the highest sedimentation rates to occur prior to Holocene followed by generally low rates through the early and mid-Holocene (e.g. Svendsen & Mangerud, 1997; Hald et al., 2004; Ślubowska et al., 2005; Forwick & Vorren, 2009; Forwick et al., 2010; Skirbekk et al., 2010).

Although other studies show generally low accumulation rates through the Mid-Holocene, the sedimentation rates seem to increase towards the latest Holocene and present day (Hald et al., 2004; Ślubowska et al., 2005; Forwick et al., 2010; Skirbekk et al., 2010; Jernas et al., in press). As there are no datings above 100.75 cm (4764 cal. years BP), there is no opportunity to estimate the sedimentation rate with a higher resolution and it is, thus, difficult to say if core 24 also has an increase in sedimentation rate towards the latest Holocene.

Core 49. For core 49, the mean linear sedimentation rate is 32 cm/cal. ka which is a rate similar to those found in core 24. As with core 23, the sedimentation rate was calculated

based only on one date and is probably not truly representative for potential changes in sedimentation rate through time.

The decrease in sedimentation rates out-fjord are most likely related to the distance to the major sediment sources, i.e. rivers, glaciers and icebergs (see *6.4 Provenance and post-glacial sedimentary processes*). Although tidewater glaciers exist along the fjord sides, Smeerenburgbreen in the innermost part of the fjord is by far the largest and its glacier front may be responsible for most of the iceberg production within the fjord as well as meltwater supply. The two innermost basins (3 and 5 in Figure 6.4) may act as sediment traps collecting most of the suspended sediment that enters the fjord in glacial meltwater plumes. The two outermost cores (core 49 and 24) may therefore not receive as much sediment as the inner-fjord cores (core 22 and 23) and are probably mainly influenced by ice-rafted debris (see *6.4.2 Ice rafting*).

Only one other study has investigated the sedimentation rates in Smeerenburgfjorden. Elverhøi et al. (1983) estimated the average sedimentation rate since deglaciation to be 150 cm/ka. Compared to this study, the rate found by Elverhøi et al. (1983) is more similar to the rates found in the inner and mid-fjord than the rates found in the outer fjord. The difference can probably be explained by the fact that Elverhøi et al. (1983) based their estimates on 3.5 kHz echo-sounding profiles. The rates are therefore a mean of the whole fjord, whereas the rates found in this study are more local for each individual core location.

In summary, the sedimentation rates in Smeerenburgfjorden show a strong out-fjord decreasing trend related to the increasing distance from the main sediment source. Average sedimentation rates are lower than rated reported from Kongsfjorden and this may be related to the size and composition of the drainage basin.

6.4 Provenance and post-glacial sedimentary processes

The sediment distribution in a fjord environment is affected by the hydrographic regime (tidal activity, waves, Coriolis effect) as well as its bathymetry (depth and morphology). The sediment entering a fjord is distributed through several different processes including ice-contact processes, fluvial processes, ice rafting by icebergs and sea ice, and deep-water currents (Figure 6.10). After the initial deposition, the sediment can be redistributed through mass wasting (e.g. slides and gravity flows) and wave/tidal activity (Dowdeswell, 1987; Syvitski, 1989; Powell, 2003). In fjords of the Svalbard regime, the main sediment sources are glaciers and rivers (Hambrey, 1994).

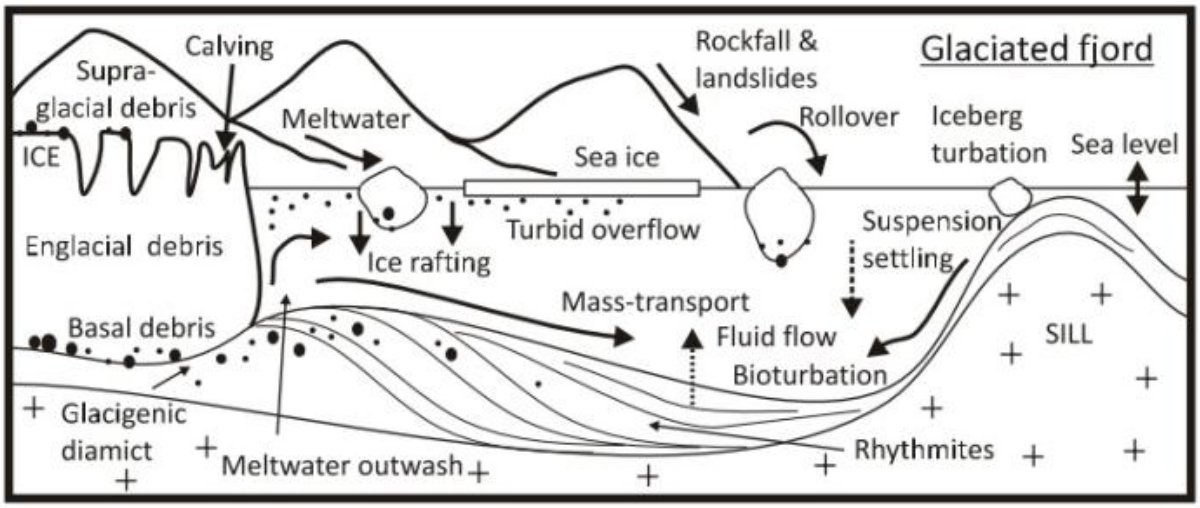

Figure 6.10 *Main processes and products in a glaciated fjord (Howe et al., 2010).*

Through the study of the sediment cores and the acoustic data, it is suggested that the main sedimentary processes in Smeerenburgfjorden since the last deglaciation were/are suspension settling, ice rafting and mass wasting.

6.4.1 Suspension settling

Based on the relatively structureless and homogenous mud found in the six sediment cores, the main sedimentary process in Smeerenburgfjorden is most likely rain-out of fine-grained sediments from glacial meltwater. This process has been reported from other Spitsbergen

fjords, e.g. from Kongsfjorden where Elverhøi et al. (1980) found up to 500 mg/l of sediment in suspension. The sediment-laden freshwater enters the fjord through meltwater tunnels, either subglacially or englacially, at the fronts of the tidewater glaciers (Elverhøi et al., 1980; Powell et al., 2003). The coarser material is deposited in the immediate vicinity of the glacier front, whereas the finer grains are held in suspension and transported further out-fjord (e.g. Syvitski et al., 1987; Svendsen et al., 2002; Powell et al., 2003; Trusel et al., 2010; Figure 6.11 A).

Sediment is also supplied from rivers draining lakes and glaciers situated further up-valley Figure 6.11 A). These (glaci-) fluvial discharges are usually loaded with sediments and thereby also contribute to the suspension rain-out in the fjord (e.g. Zajączkowski & Włodarska-Kowalczuk, 2007; Forwick et al., 2010; Trusel et al., 2010; Szczuciński & Zajączkowski, 2012). Most river runoff occurs in the summer months from June to September, while they are completely frozen in winter (Killingtveit et al., 2003; Plassen et al., 2004; Zajączkowski & Włodarska-Kowalczuk, 2007). Thus, rivers act only intermittently as sediment sources. As most of the sediment sources, i.e. glaciers and rivers, are located on Vasahalvøya, it is reasonable to assume that the sediment succession in the fjord is thickening towards the east. In addition, the Coriolis effect deflects surface currents, i.e. currents carrying suspended sediment, to the right hand side (along the eastern fjord side in Smeerenburgfjorden; cf. Syvitski et al., 1987; Forwick et al., 2010; Skarðhamar & Svendsen, 2010). This may also contribute to a thicker sediment succession along the eastern fjord side in Smeerenburgfjorden. However, as there is only a longitudinal chirp profile and no cross-profile of the fjord, it is not possible to document such an eastward thickening of the sediment succession.

As the meltwater discharge can vary both annually and inter-annually (Svendsen et al., 2002; Cottier et al., 2007, 2010; Nilsen et al., 2008), the amount of sediment introduced to the fjord system fluctuates. In addition, the current regimes and circulation patterns influence where sediment fall-out occurs (e.g. Syvitski et al., 1987). On the chirp profile it is evident that the sediment succession is thinner on bathymetric highs and generally thicker in basins and deeper areas (Figure 4.4).

The influence of currents, and possibly also current reworking, is seen on the generally smooth appearance of the basin seafloor and on the chirp profile. Compared to the R1 reflection, where recessional moraines are seen throughout the profile, relatively few of the

moraines are observed on the seafloor (R2 reflection). Some areas of the seafloor mirror the underlying bathymetry, e.g. the recessional moraines, whereas others only have a smooth surface. Therefore, it is suggested that sedimentation occurs not only through passive suspension settling as this would result in a conformable sediment drape. There are probably other processes involved as well; most likely the current and circulation regimes. As Smeerenburgfjorden has two straits in the west (Danskegattet and Sørgattet; see Figure 2.2), in addition to the fjord mouth, the circulation pattern is most likely different from that of a typical fjord with only one connection to the open ocean. Although the two openings towards the west have shallow water depths, they probably allow some inflow of Atlantic and shelf waters which would influence the circulation in the fjord. Unfortunately, there are no studies of the circulation pattern in the fjord and the amount of AW entering the fjord through Sørgattet and Danskegattet is not known.

Figure 6.11 (next page)*: Illustrative sketch showing* ***A) Suspension settling:*** *tentative extent of sediment in suspension (note that the sediment is brought further out-fjord than the sketch illustrates);* ***B) Ice rafting:*** *sea ice (approximate cover of close drift ice during the winter months based on an average between the years 2005 – 2010; from polarview.met.no) and the drift paths of icebergs (note that the iceberg presumably travel further out-fjord than the sketch illustrates);* ***C) Mass wasting:*** *fjord sides where slope failure occurs (green line) and regions of mass transport deposition (green areas);* ***D) Provenance:*** *summary of the measured properties and whether they increase in the in-fjord or the out-fjord direction. Circles indicate the core locations.*

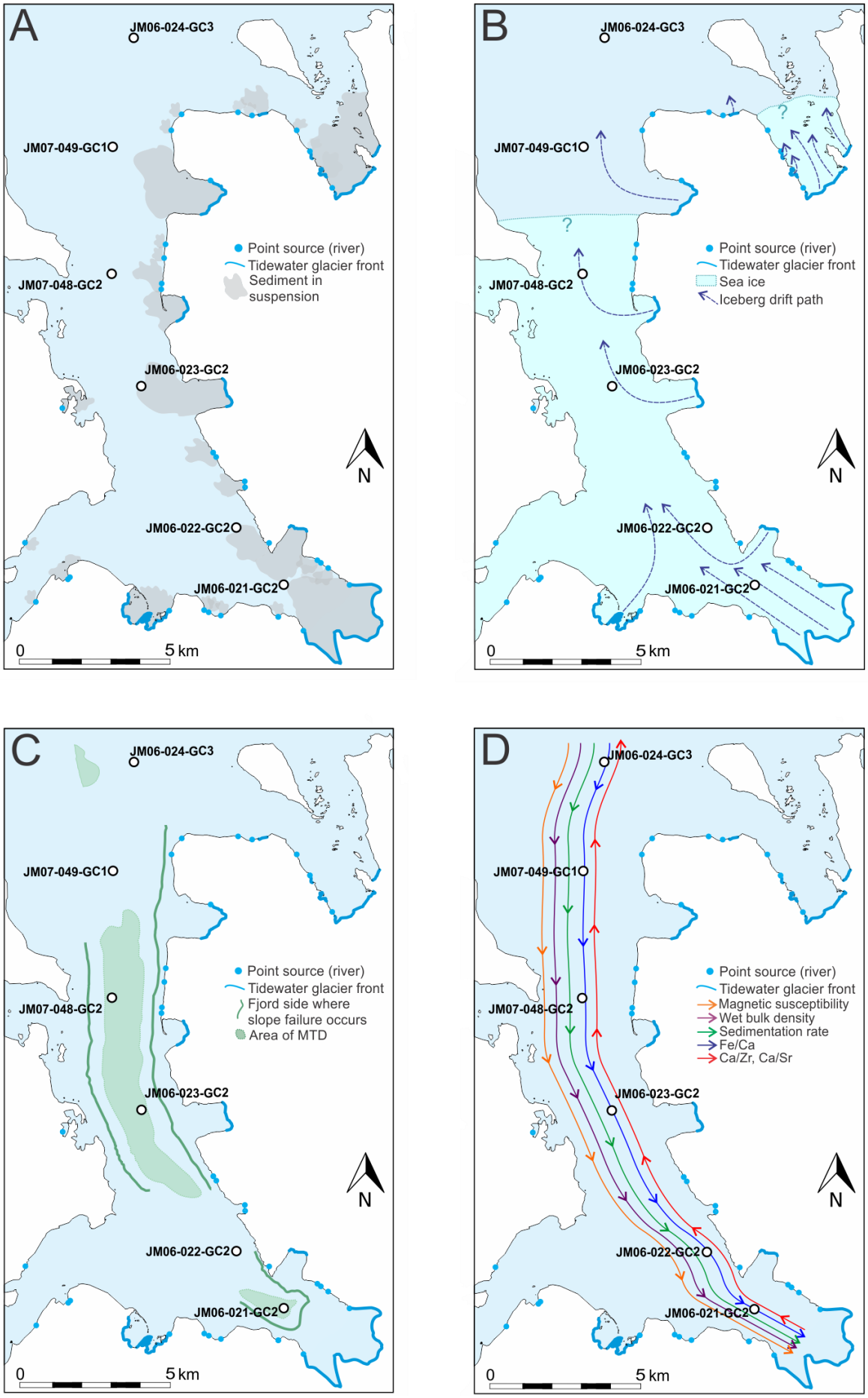
A
JM06-024-GC3
JM07-049-GC1
JM07-048-GC2
JM06-023-GC2
JM06-022-GC2
JM06-021-GC2
Point source (river)
Tidewater glacier front
Sediment in suspension
N
0
5 km
B
JM06-024-GC3
JM07-049-GC1
JM07-048-GC2
JM06-023-GC2
JM06-022-GC2
JM06-021-GC2
Point source (river)
Tidewater glacier front
Sea ice
Iceberg drift path
N
0
5 km
C
JM06-024-GC3
JM07-049-GC1
JM07-048-GC2
JM06-023-GC2
JM06-022-GC2
JM06-021-GC2
Point source (river)
Tidewater glacier front
Fjord side where slope failure occurs
Area of MTD
N
0
5 km
D
JM06-024-GC3
JM07-049-GC1
JM07-048-GC2
JM06-023-GC2
JM06-022-GC2
JM06-021-GC2
Point source (river)
Tidewater glacier front
Magnetic susceptibility
Wet bulk density
Sedimentation rate
Fe/Ca
Ca/Zr, Ca/Sr
N
0
5 km

6.4.2 Ice rafting

Icebergs calving off the tidewater glacier fronts are important for the transport of sediment to the fjord (Figure 6.11 B). From floating icebergs, debris is deposited by; i) rain-out and/or ii) drop as the berg melts, and iii) dumping when the iceberg overturns (e.g. Vorren et al., 1983; Dowdeswell & Dowdeswell, 1989; Figure 6.12). Grounded icebergs can also deposit material and bergs ploughing the seafloor can cause redeposition (Vorren et al., 1983). Tidewater glaciers that are less active produce fewer icebergs as their surface is usually less crevassed than that of surging glaciers (Dowdeswell, 1989). The tidewater glaciers terminating in Smeerenburgfjorden (Figure 2.2) are all characterised as slow-flowing or stagnant and have a total estimated calving intensity of 0.0671 km^3/year (Błaszczyk et al., 2009). For comparison, Kronebreen (Kongsfjorden) alone has an estimated volumetric iceberg flux of 0.3103 km^3/year (Błaszczyk et al., 2009). However, these estimates are based on ASTER images and may not be fully representative of the actual iceberg flux.

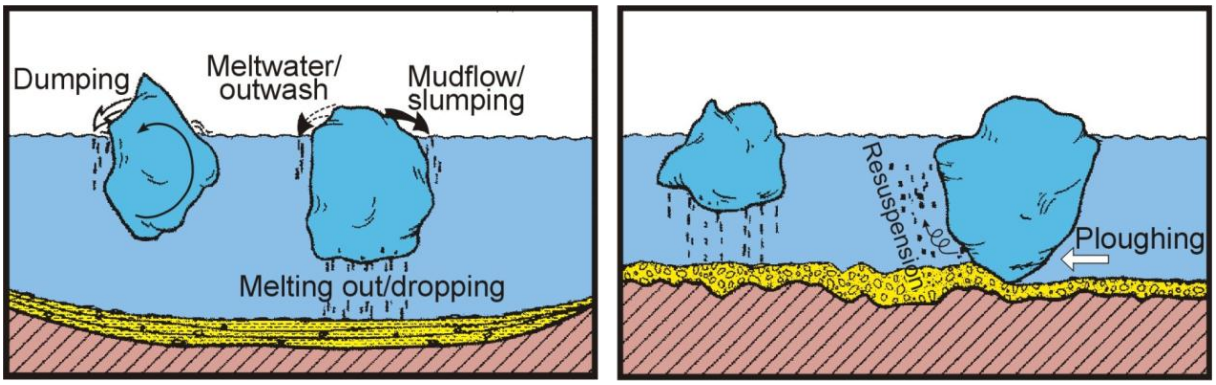

Figure 6.12: *Modes of iceberg rafting. Modified from Vorren et al., 1983.*

The sea-ice conditions in the fjord also affect the calving rate as the winter sea-ice cover at the tidewater glacier front suppresses iceberg calving. The icebergs that are calved off are often trapped within the sea ice and released as the sea-ice cover breaks up in spring (Dowdeswell, 1989). The sea ice is also responsible for ice rafting as it incorporates both suspended sediments as well as beach sediments in areas where the sea ice is shore-fast (Figure 6.11 B). It is likely that shore-fast sea ice occurs in Smeerenburgfjorden as there are several low-lying strand-flats surrounding the fjord (Danskøya, Amsterdamøya, Fuglepynten; Figure 6.4).

Ice-rafted debris is observed in all of the six sediment cores, thus both sea ice and icebergs are probably active transport mechanisms for debris in Smeerenburgfjorden. However, the relative importance of ice rafting as a sedimentation process increases out-fjord (cf. *6.3 Sedimentation rates*). This is related to the large amounts of meltwater entering the fjord in the inner and middle parts, making suspension settling the main sedimentation process and masking the deposited ice-rafted debris (e.g. Dowdeswell & Dowdeswell, 1989; Plassen et al., 2004).

6.4.2.1 Ice Rafted Debris (IRD)

As mentioned earlier (see *5. Lithostratigraphy*), for this study, IRD is defined as grains and clasts exceeding 63 µm (sand and coarser). This is based on observations from the x-radiographs and the results from GRADISTAT (see *Chapter 3.2.7.3*). However, all grains-sizes can be incorporated into icebergs or sea ice and become ice rafted (Gilbert, 1990; Figure 6.13); supraglacial, englacial and subglacial debris of all fractions may be incorporated into the glacier ice and transported in calved icebergs (e.g. Dowdeswell & Dowdeswell, 1989), and sea ice is capable of transporting sizes up to cobbles, e.g. from beach environments (Figure 6.13). However, much of the material transported by sea ice may be clay- and silt-sized as sediment in suspension adfreezes to the sea-ice (Vorren et al., 1983; Gilbert, 1990). This fraction of IRD is difficult to separate from sediment deposited from suspension fall-out and, thus, difficult to quantify (e.g. Hebbeln, 2000; Hass, 2002; Hass et al., 2010).

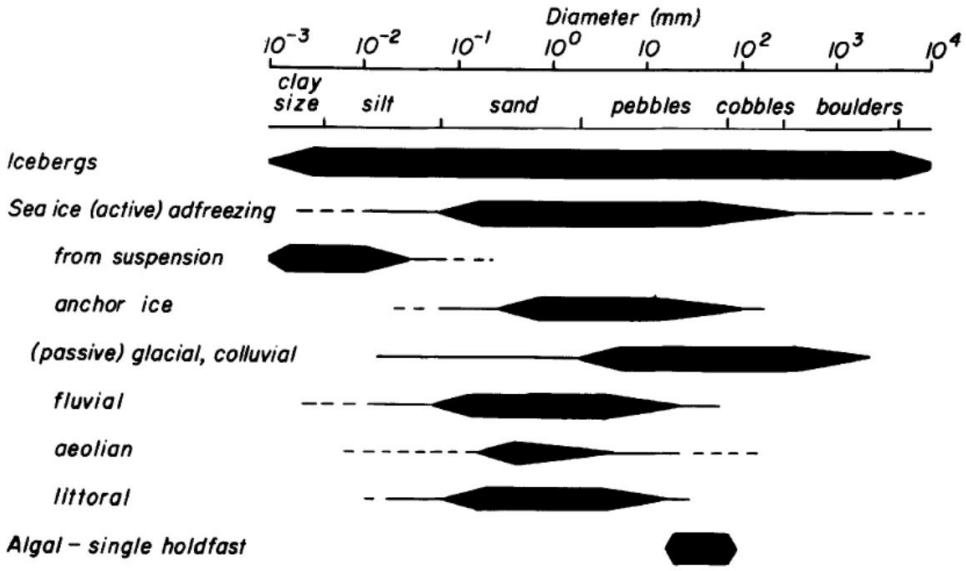

Figure 6.13: *The approximate range of grain-size transported by icebergs, sea ice and vegetation. From Gilbert, 1990.*

6.4.3 Mass wasting

Mass-transport activity is an important process in re-depositing sediments and has been identified in other Spitsbergen fjords (e.g. Plassen et al., 2004; Ottesen & Dowdeswell, 2006; Forwick & Vorren, 2007, 2011b; Włodarska-Kowalczuk et al., 2007; Zajączkowski & Włodarska-Kowalczuk, 2007; Baeten et al., 2010). Fjord topography, the supply of material, the physical properties of the sediment and the releasing mechanism are the main factors controlling slope failures in fjords. Most slope failures in fjords relate to high sediment supply and sediment loading adjacent to glacier fronts or delta areas (Prior et al., 1984; Syvitski et al., 1987; Syvitski, 1989; Włodarska-Kowalczuk et al., 2007; Zajączkowski & Włodarska-Kowalczuk, 2007). However, other factors may also trigger slope failures, such as seismic activity related to postglacial isostatic rebound, glacier surges or meltwater pulses, sea-level fluctuations, storm events and the presence of gas (e.g. Syvitski et al., 1987; Mulder & Cochonat, 1996; Forwick & Vorren, 2007).

Core 21. As mentioned earlier, it is evident from both the swath bathymetry and the chirp data that core 21 is located in an area affected by slope failures (5 in Figure 6.4; Figures 6.5 and 6.11 C). This points towards mass wasting on the distal slope of the LIA moraine possibly related to the high sediment input and loading during the LIA but also to the continued high sedimentation rates during the past c. 150 years (cf. Table 6.1). The irregular and sub-horizontal colour changes seen in core 21 are assumed to be remnants of the original structure which has been deformed during sediment reworking (e.g. Nardin et al., 1979; Mulder & Cochonat, 1996; Mulder, 2011). It is therefore suggested that the sediments in core 21 represent a slump deposit.

Core 48. The presence of bioturbation between the MTD intervals in core 48 indicates that they are four individual events separated by periods of "normal" sedimentation (i.e. suspension settling and ice rafting). The shells found within the MTD intervals are probably reworked and transported downslope along with the sediments. The marked increase in wet bulk density in the MTD intervals points towards cohesive material often associated with debris flows (e.g. Elverhøi et al., 2000). The chaotic appearance of the MTD's on the x-radiographs as well as the lack of grading and poor sorting of the sediment also support the interpretation of debris flow deposits rather than turbidites (e.g. Mulder & Alexander, 2001).

Only two of the debris flows have erosional lower boundaries (Figures 5.9 and 5.11). The lack of any erosional boundaries in the other two MTD's may be due to hydroplaning of the debris flow which reduces bed friction (Elverhøi et al., 2000). The thickness of the MTD's does not exceed 6 cm and they are therefore regarded as relatively small events.

Forwick & Vorren (2007) found that Holocene mass wasting in Svensksunddjupet in outer Isfjorden can be linked to a regional event of postglacial isostatic uplift around 9650 cal. years BP. In addition, events occurring around ~8300 cal years BP and 3000 cal years BP may have been caused by relative sea-level fall and/or presence of gas in the sediments. Smaller mass transport events may have been triggered by meltwater pulses from the nearby Vardebreen (Forwick & Vorren, 2007). As there are no dated intervals in core 48, it is not possible to pinpoint the mass-transport events to any specific time and thus difficult to determine a triggering mechanism with regards to external forces such as sea level fluctuations or tectonics. However, as seen in Figure 6.7, the core penetrates only the uppermost MTD's of a relatively thick sediment succession (~16 m). Therefore, it is reasonable to assume that the events took place relatively late in the Holocene.

Core 24. The lower part of core 24 (410 – 260 cm) has previously been interpreted to consist of reworked sediments. As there are no internal structures or boundaries (apart from the colour changes), it is difficult to estimate how many mass wasting events the interval contains. The two most apparent changes in wet bulk density occur at 383 and ~260 cm and correlate with the two most distinct colour changes (Figure 5.14; top of red interval and top of blue interval respectively). It is suggested that the change at ~260 cm marks the boundary between reworked sediments (below 260 cm) and the overlying sediments that are thought to be in-situ. The change in wet bulk density and colour at 383 cm may mark the boundary between two events. The grain-size distribution shows that both the mass transport deposits are coarsening upwards. This is in opposite to the typical debris flow deposits and turbidites (e.g. Mulder & Alexander, 2001). Due to these opposing signals in the sediment core properties as well as the few traces of mass wasting around the core site, it is difficult to identify the type of process that has deposited these sediments. Although the process cannot be determined, the approximate timing can be estimated. The dated shells in this interval have ages of 10905 and 8695 cal. years BP. This indicates that the first event must have occurred after 10905 cal. years BP and the second after 8695 cal. years BP. It is, therefore, a possibility

that the events were related to seismic activity generated by post-glacial isostatic uplift (cf. Forwick & Vorren, 2007; previous paragraph).

The slide scars and associated debris lobes occur mostly in the middle part of the fjord (Figure 6.11 C). The slides on the eastern fjord side are presumably related to the tidewater glaciers entering the fjord from Vasahalvøya (Sellströmbreen, Frambreen and Kennedybreen; Figure 2.2) and the glacifluvial discharge points and deltas. The rapid accumulation of sediment around these discharges as well as periodic meltwater pulses makes the slope unstable and prone to failure (e.g. Mulder & Cochonat, 1996; Forwick et al., 2010; Trusel et al., 2010). Although NW Spitsbergen is thought to have been distal to the main loading during the Late Weichselian and therefore did not suffer very dramatic postglacial isostatic uplift (Lehman & Forman, 1987; Forman, 1990; Forman et al., 2004), some isostatic rebound is likely to have occurred and may have triggered slope failures (e.g. Stewart et al., 2000). In addition, seismic activity from the fault zone aligned parallel to the north-eastern fjord side (Figure 2.3) may cause slope failures in the fjord. Slope failure occurs along the western fjord side as well, especially off Danskøya and Amsterdamøya. These failures could also be related to meltwater as well as seismic activity. In addition the failures may be related to the oceanic currents and inflow of Atlantic and shelf waters through the straits.

6.4.4 Provenance of sediments

As described above, the Holocene sediments in the fjord are glacimarine sediments mainly deposited through suspension settling, ice rafting and mass wasting. Thus, the provenance of the sediments is the surrounding land areas and the catchments of the glaciers.

The magnetic susceptibility of the sediments in the innermost fjord (in core 21 and 22) range between 86 - 140 (x 10^{-5} SI; Table 5.1). These values are relatively high compared to the magnetic susceptibility usually found for sediments originating from Spitsbergen (e.g. Jessen et al., 2010). As there is a strong gradient of decreasing magnetic susceptibility in the out-fjord direction (Table 5.1), it is reasonable to assume that sediments with higher magnetic susceptibility are derived from the Hornemantoppen granite which only exists in the innermost part of the fjord in the catchment of Smeerenburgbreen (Ohta et al., 2008). The high magnetic susceptibility in cores 21 and 22 probably relate to the high input of suspended sediment originating from Smeerenburgbreen (cf. *6.3 Sedimentation rates*).

The Fe/Ca ratio is thought to record variations in the relative abundance of terrigenous material and biogenic carbonate, respectively (Richter et al., 2006). The Fe/Ca ratio is decreasing in the out-fjord direction in Smeerenburgfjorden (Figure 6.11 D) which means that the amount of terrigenous material decreases whereas biogenic carbonate becomes more abundant in the out-fjord direction. This is also seen in the sediment cores, where the two outermost cores, core 49 and 24, contain large amounts of shells and shell fragments (Figure 5.2). This indicates that terrigenous material is the main component of the inner-fjord cores (cores 21, 22 and partly 23) whereas the outer-fjord cores (cores 48, 49 and 24) are more influenced by biogenic processes. The opposite trend is seen for the Ca/Zr and Ca/Sr ratios which increase in the out-fjord direction (Figure 6.11 D). However, this also indicates a general increase in the Ca-content of the sediments towards the fjord mouth.

In summary, the main sedimentary processes acting in Smeerenburgfjorden are rain-out of fine-grained sediments from turbid meltwater plumes, ice rafting and mass wasting. Sediments are introduced to the fjord through glacial meltwater channels and rivers. The sediment kept in suspension influences the whole fjord. However, most of the material is deposited in the inner part of the fjord, relatively close to the main tidewater glacier fronts (Figure 6.11 A). Ice Rafted Debris is transported both by sea ice and icebergs. IRD occurs throughout the fjord and its relative importance as a sedimentary process increases in the out-fjord direction where the influence of suspended sediment is reduced (Figure 6.11 B). Slope failure occurs along the fjord sides and Mass Transport Deposits (MTD's) are found in the basins. Mass wasting is especially pronounced at discharge points such as deltas (Figure 6.11 C). The sediments in Smeerenburgfjorden originate from the surrounding land areas. Magnetic susceptibility and Fe-content are linked to the Hornemantoppen granite in the inner fjord and show a strong decreasing gradient towards the outer fjord. The Ca-content is linked to biogenic processes and increases out-fjord (Figure 6.11 D).

6.5 Holocene glacial history and climate

In this chapter, the previously discussed topics will be viewed in the light of external forces (Figure 6.1) in order to elucidate the Holocene glacial history and sedimentary environments in Smeerenburgfjorden. The reconstruction of the Holocene glacial history is based mainly on the occurrence of IRD (sand and clast content), physical properties (magnetic susceptibility) and element geochemistry as well as comparison to published data.

The amount of IRD is influenced by several factors; e.g. both glacial retreat and advance may cause enhanced calving and thereby high IRD contents (cf. Forwick et al., 2010). In addition, the IRD content also depends on oceanographic conditions such as surface water temperatures which determine how far icebergs drift before their debris melts out. Furthermore, the amount of IRD in a sample is relative to the supply of suspended sediment (e.g. Elverhøi et al., 1980; Plassen et al., 2004; Forwick et al., 2010). Therefore, when using IRD as a proxy, comparisons to published palaeo-environmental records are necessary.

The division into four main time-slices; late early Holocene; mid-Holocene, late Holocene and latest Holocene, is based on both lithology as well as the physical properties of all cores, but especially the two key cores JM06-022-GC2 and JM06-024-GC3. The age limits between these divisions follow the dated intervals and are rounded to the nearest fifty. The past ~8650 cal. years are based on core 24, whereas core 22 comprises the last ~1200 cal. years. Assuming a constant and continuous sedimentation, the sediments at the base of core JM07-049-GC1 are the oldest found in this study (c. 9300 cal years BP). However, as only one date was obtained from this core, there are larger uncertainties of the age model than in core 24 which has more dated intervals. Core 24 was therefore chosen to represent the oldest sediment. As mentioned previously (cf. *Chapter 6.2*), the two lowermost dates of core 24 were obtained from sediments interpreted to be reworked and the dates were therefore excluded. The oldest, undisturbed, sediments in core 24 have an age of 8650 cal. years BP, and, thus, the Holocene glacial history of Smeerenburgfjorden elucidated in this study begins at this time.

6.5.1 Late early Holocene (8650 – 7350 cal. years BP)

Very little sand (~4%) and no clasts characterise this interval in core 24 (Figures 5.14 and 6.14). A few clasts as well as a somewhat higher sand content (~10%) are found in core 49. Shells and bioturbation occur in both cores. The comparatively low amount of IRD in this interval is probably related to reduced iceberg calving (cf. *6.4.2 Ice rafting*). The low IRD content is consistent with that found in other Spitsbergen fjords for approximately the same time interval; e.g. in Bellsund (Ślubowska-Woldengen et al., 2007), Billefjorden (Baeten et al., 2010), Isfjorden (Forwick & Vorren, 2009) and Kongsfjorden (Skirbekk et al., 2010), as well as on the western Spitsbergen slope (Jessen et al., 2010) and in the eastern part of the Fram Strait (Müller et al., 2012).

On Svalbard, the warmest climatic and oceanographic conditions of the Holocene occurred between c. 10000 – 9000/8800 cal. years BP (e.g. Birks, 1991; Salvigsen et al., 1992; Sarnthein et al., 2003; Hald et al., 2004; Rasmussen et al., 2007, 2012; Forwick & Vorren, 2009). Skirbekk et al. (2010) found that relatively warm climatic conditions prevailed in Kongsfjorden until c. 7200 cal. years BP. The same was found for the Hinlopen Trough (Ślubowska et al., 2005; Ślubowska-Woldengen et al., 2007) and these authors related this to a strong inflow of Atlantic Water at the core sites (Ślubowska et al., 2005; Ślubowska-Woldengen et al., 2007; Skirbekk et al., 2010). As Smeerenburgfjorden is situated between these two locations, it is reasonable to assume that Atlantic Water influenced the environment in Smeerenburgfjorden as well.

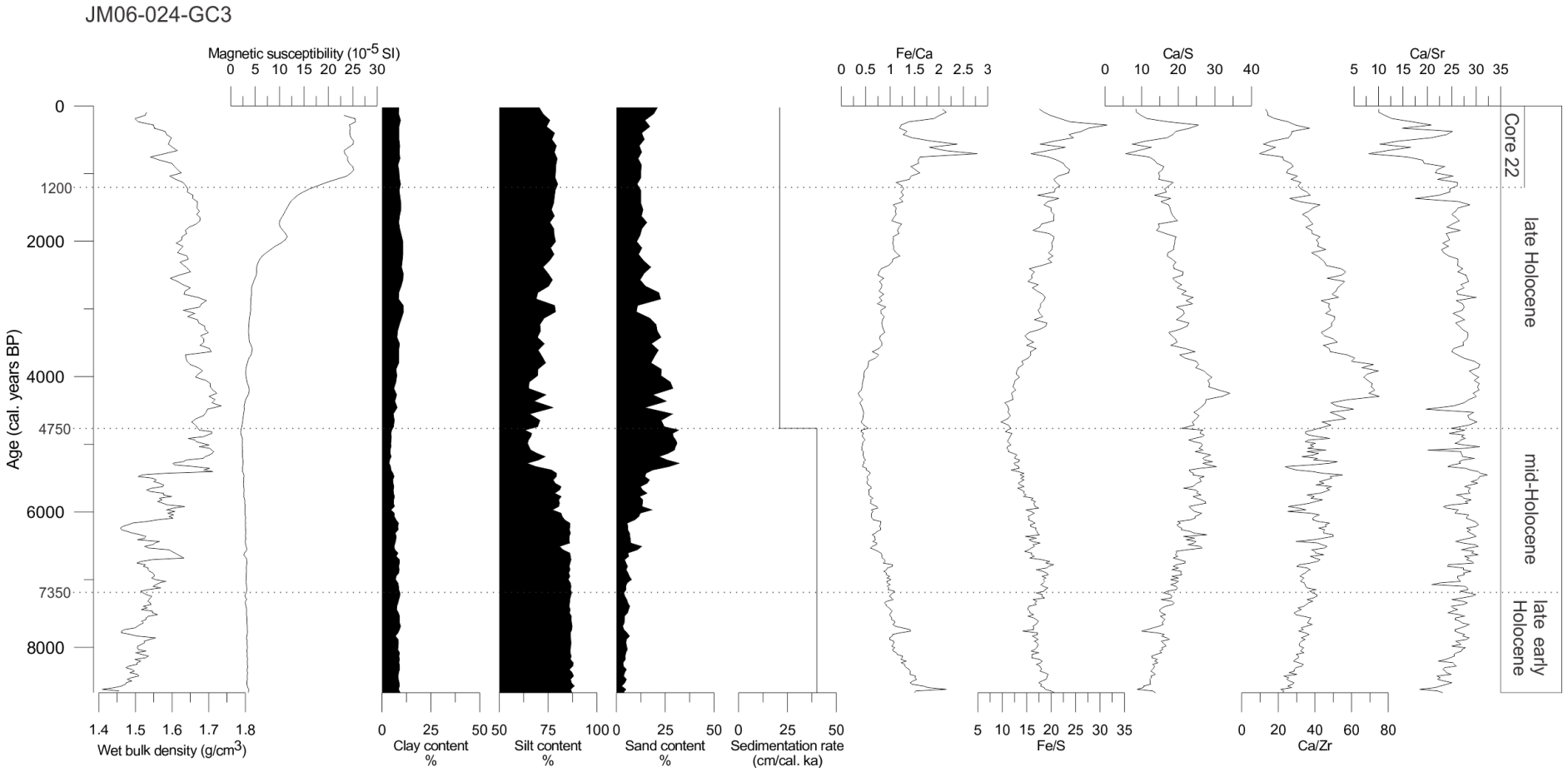

Figure 6.14: *Physical properties, grain-size distribution, sedimentation rates (cm/cal. ka) and element geochemistry for core JM06-024-GC3 plotted against age (cal. years BP). The main subdivisions of the Holocene are indicated and correspond to sub-chapters in the text.*

Müller et al. (2012) postulated that sea surface temperatures during this time period were comparatively warm and that the sea-ice formation was somewhat reduced in the eastern Fram Strait. However, more sea-ice may have formed in the fjords; Forwick & Vorren (2009) and Rasmussen et al. (2012) found indications of increases in the winter sea-ice cover in Isfjorden from c. 9000 cal. years BP. Even so, the main transport mechanism for debris in Isfjorden during this period was icebergs (Forwick & Vorren, 2009). The IRD content in Smeerenburgfjorden is, therefore, suggested to relate to iceberg rafting rather than sea-ice rafting. However, debris transported and deposited by sea-ice should not be excluded as winter sea-ice cover most likely formed in the fjord (e.g. Forwick & Vorren, 2009; Rasmussen et al., 2012). Contrary to the suggestion from Svendsen & Mangerud (1997) that no glacial activity occurred during the early and mid-Holocene, Baeten et al. (2010) found that Nordenskiöldbreen in Billefjorden existed in the early Holocene and that icebergs were the main source of IRD to the fjord at this time. Hald et al. (2004) also found IRD throughout the Holocene record from Van Mijenfjorden and suggested that central Spitsbergen never deglaciated during this period. Similarly, the occurrence of IRD in Smeerenburgfjorden indicates that tidewater glaciers were present at this time. Forwick & Vorren (2009) suggested that remaining ice masses in eastern Spitsbergen and reduced glaciers in western Spitsbergen might indicate that a strong east-west temperature gradient existed during this time. Although Smeerenburgfjorden is situated in western Spitsbergen, the occurrence of IRD indicates that tidewater glaciers were present during the early Holocene. This may indicate that there was a north-south temperature gradient as well.

A stronger influence of Atlantic Water and warmer surface waters may have caused icebergs to melt more rapidly thereby dropping their debris within the fjord (e.g. Forwick et al., 2010). This could explain the difference in IRD content between the cores 49 and 24. As core 49 is located further in-fjord, within the fjord mouth sill and closer to the glacier fronts (e.g. Kennedybreen; Figures 2.2 and 5.1), more icebergs still carrying debris may have passed the core site than for the location of core 24 which is situated in a more open environment.

High magnetic susceptibility of the sediment has previously been related to sediments derived from the Hornemantoppen granite in the innermost part of the fjord, in the catchment of Smeerenburgbreen (see *6.4.4 Provenance of sediments*). As the magnetic susceptibility for this interval is low (3.6×10^{-5} SI; Figure 6.14), it is possible that the sediments did not originate from Smeerenburgbreen. The lithologies of the sediment and the clasts have not been studied in detail and therefore it is not possible to conclude on the provenance of the

icebergs and the sediments. However, as the surface waters may have been warmer during this time interval, it is not unlikely that icebergs and IRD from Smeerenburgbreen did not reach the core sites of cores 49 or 24 before the debris had melted out. The icebergs may, for example, have originated from Kennedybreen (Figure 2.2). All element ratios show an increase in the Ca-content towards the end of the early Holocene (Figure 6.14). This is possibly related to an increased content of biogenic carbonates such as shells and foraminifera. Favourable conditions with high biogenic productivity and foraminifera fluxes have been found for other Spitsbergen fjords for the same time interval (e.g. Hald et al., 2004; Ślubowska et al., 2005; Baeten et al., 2010; Skirbekk et al., 2010; Müller et al., 2012) and may be related to the inflow of Atlantic Water and the increased SST (sea-surface temperature) of 4 °C higher than today (Sarnthein et al., 2003).

6.5.2 Mid Holocene (7350 – 4750 cal. years BP)

In the mid-Holocene, the IRD content increases with both higher sand content and more clasts. The increase in sand content occurs at c. 6200 cal. years BP and continues to rise towards ~5200 cal. years BP where it reaches a maximum which persists throughout this interval (Figure 6.14). The clasts do not follow the trend of the sand content and seem to occur more randomly. The general increase in IRD in this interval is most probably the result of enhanced ice rafting, either by icebergs and/or sea-ice. The sand content increases to 30 % towards the end of the mid-Holocene whereas the magnetic susceptibility is very low and slightly decreasing (Figure 6.14).

Increased IRD contents have been found in sediment cores in other Spitsbergen fjords for the mid-Holocene, e.g. in Billefjorden (Baeten et al., 2010), Van Mijenfjorden (Hald et al., 2004), Isfjorden (Forwick & Vorren, 2009; Rasmussen et al., 2012) and Tempelfjorden (Forwick et al., 2010). In addition, weakened inflow of Atlantic Water (e.g. Ślubowska et al., 2005; Skirbekk et al., 2010; Rasmussen et al., 2012) and an increase in the sea-ice cover has been inferred from both Spitsbergen fjords (e.g. Ślubowska-Woldengen et al., 2007; Baeten et al., 2010; Rasmussen et al., 2012) as well as on the western Svalbard continental margin (Müller et al., 2012) and in the western Barents Sea (Sarnthein et al., 2003). The re-growth of sea-ice was potentially related to decreasing insolation in summer and a general regional cooling at this time (e.g. Birks, 1991; Sarnthein et al., 2003; Hald et al., 2004; Hald & Korsun, 2008; Müller et al., 2012). Hald et al. (2004) postulated that the cooling observed in Van

Mijenfjorden during the mid-Holocene may have been partly due to inflow of colder shelf waters and partly related to a more restricted exchange of water masses between the fjord and the margin due to isostatic uplift of the fjord-mouth sill.

Forwick & Vorren (2009) suggested that the IRD in Isfjorden in the mid-Holocene mainly derived from icebergs. Increased glacial activity in Spitsbergen fjords has been suggested for the mid-Holocene by several authors; from 7500 cal. years BP in Van Mijenfjorden (Hald et al., 2004), from 5600 cal. years BP in Tempelfjorden (Forwick et al., 2010) and from 5400 cal. years BP in Billefjorden (Baeten et al., 2010). In Smeerenburgfjorden, a marked increase in IRD is observed from ~6200 cal. years BP and a further increase around 5200 cal. years BP. The marked increases in sand content may reflect re-growth of the tidewater glaciers in Smeerenburgfjorden. However, the marked change in IRD source is not observed in the magnetic susceptibility or in the Fe-signal (Figure 6.14). This indicates that the IRD originates from a different source than Smeerenburgbreen and may reflect the growth of the other tidewater glaciers in the fjord (Figure 2.2). As increased sea-ice cover is postulated for this period (e.g. Ślubowska-Woldengen et al., 2007; Baeten et al., 2010; Müller et al., 2012; Rasmussen et al., 2012), denser sea-ice cover may have formed in the innermost part of the fjord, trapping calved icebergs and/or suppressing calving from Smeerenburgbreen, and, thus, not allowing debris with higher magnetic susceptibility to reach the outermost core locations. Icebergs calved from the glaciers further out-fjord (Frambreen, Kennedybreen; Figure 2.2) may not have been that restricted by the sea-ice cover.

In Kongsfjorden, Skirbekk et al. (2010) observed a generally colder environment with diminished inflow of Atlantic Water (AW) during the mid-Holocene; however, no change in glacial activity, increase in IRD or decrease in productivity was found. Skirbekk et al. (2010) suggested that this might indicate that only a minor reduction in the inflow of AW occurred or that the inflow of AW had a more seasonal inflow similar to the circulation pattern of today. The IRD increase found for the mid-Holocene in Smeerenburgfjorden may be linked to the general cooling and possible re-growth of both sea-ice and glaciers. However, both in core 49 and 24, an increase in the content of shells and shell fragments occur in this interval. This is also seen in the increasing Ca-content detected in all sediment ratios. Such an increase in productivity would usually indicate more favourable conditions instead of the suggested change to a colder climate. The shells in this interval have not been studied, and it may be that they are species that thrive in somewhat colder and more Arctic conditions. Alternatively, the circulation pattern in Smeerenburgfjorden may have been similar to that described by

Skirbekk et al. (2010) and may have allowed inflow of Atlantic Water creating a favourable environment for molluscs. Smeerenburgfjorden has a fjord mouth sill, but also, as mentioned earlier, two straits opening up towards the west. These factors probably influence both the internal circulation in the fjord as well as the exchange of water masses with the open ocean. This distinguishes Smeerenburgfjorden from other typical fjords which only have one connection to the open ocean, and Smeerenburgfjorden may therefore respond differently to climatic and oceanographic changes.

6.5.3 Late Holocene (4750 – 1200 cal. years BP)

A decreasing trend in the IRD is observed from 4750 until c. 3000 cal. years BP in core 24 (Figure 6.14). This decrease in IRD may be related to reduced iceberg calving. From c. 4200 cal. years BP, a minor increase in magnetic susceptibility and Fe-content occurs. A further increase in these two properties occurs around 2000 cal. years BP and may indicate a change in provenance of the sediments

Forwick & Vorren (2009) found that the IRD in central Isfjorden decreased around 4000 cal. years BP after which ice rafting occurred in equal amounts by sea ice and icebergs. This decrease in IRD was attributed to a more permanent sea-ice cover and/or enhanced formation of shorefast sea-ice. Such an increase in sea-ice would trap icebergs within the fjord and force them to release their debris closer to the calving fronts (Ò Cofaigh & Dowdeswell, 2001; Forwick & Vorren, 2009). Indications of enhanced sea-ice formation in combination with increased IRD contents in this period are found in other Spitsbergen fjords, e.g. in Bellsund (Ślubowska-Woldengen et al., 2007), Billefjorden (Baeten et al., 2010), Kongsfjorden (Skirbekk et al., 2010) and for the western Spitsbergen margin (Müller et al., 2012).

The observed decrease in IRD in Smeerenburgfjorden may be related to the increase in sea-ice cover suggested by Forwick & Vorren (2009). If more of the sea-ice was shorefast during this period, beach material may have been frozen into the ice during winter and brought to the core sites as the sea-ice broke up in late spring and cause the IRD content to remain relatively high. The increase in magnetic susceptibility from c. 4200 cal. years BP may indicate a slightly increased influence from Smeerenburgbreen. Although an increased sea-ice cover would most likely trap icebergs and force them to release their debris in the inner parts of the fjord (e.g. Ò Cofaigh & Dowdeswell, 2001; Forwick & Vorren, 2009), it is possible that the icebergs were released as sea-ice broke up in late spring and that the debris within the

icebergs survived the drift towards the fjord mouth before it was released at the core sites. Alternatively, the icebergs were calved off in a period when sea-ice cover was minimal, e.g. in summer or early autumn.

Müller et al. (2012) found that the sea-ice margin in the eastern Fram Strait has fluctuated during the past 3000 years with periods of both rapid advance and retreat. This was attributed to variations in the inflow of Atlantic Water and/or periods of weaker or stronger westerlies (Müller et al., 2012; Figure 6.15). For glaciers to grow, a net increase in accumulation is required. As the source of moisture to Svalbard is the surrounding ocean, precipitation over Svalbard is influenced by the sea-ice cover (e.g. Svendsen & Mangerud, 1997; Dickson et al., 2000; Müller et al., 2012). Therefore, the variations in the inflow of Atlantic Water and the fluctuations of the sea-ice margin influence glacier growth on Spitsbergen (Müller et al., 2012; Figure 6.15).

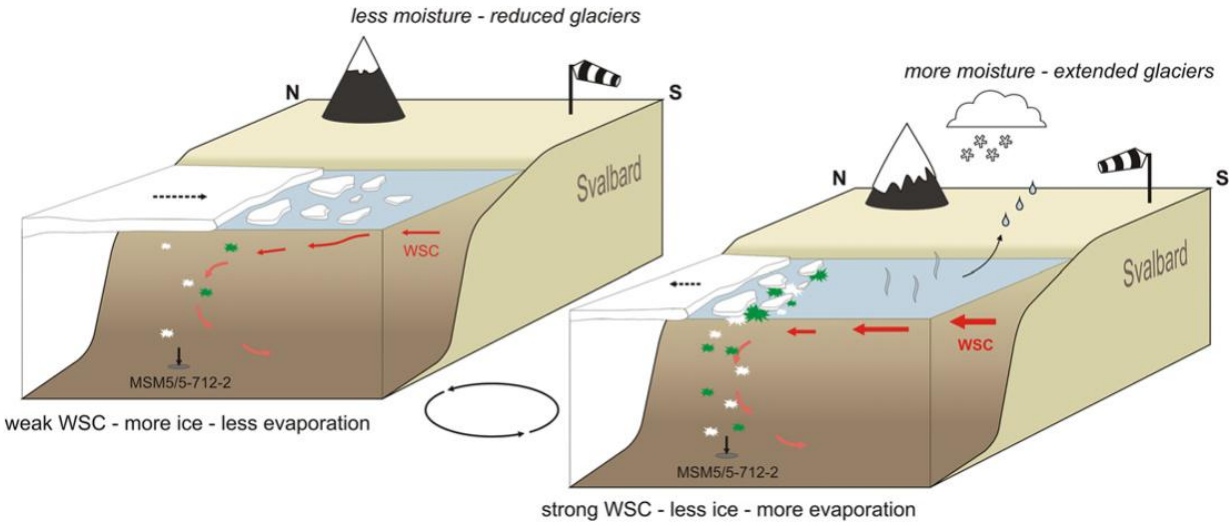

Figure 6.15: *Sketch illustrating fluctuations in sea-ice cover during the past 3000 cal. years BP. Sea-advance (left) and sea-ice retreat (right) due to changes in the inflow of AW and/or the strength of westerlies along the western Spitsbergen margin. In periods when the sea-ice margin retreats, more moisture causes glacier growth on Svalbard. The green and white patches indicate phytoplankton and ice algae productivity, respectively. WSC refers to the West Spitsbergen Current and MSM5/5-712-2 refers to the core used in Müller et al., 2012. From Müller et al. (2012).*

In core 24, the sand content is lower than in the beginning of the late Holocene in the period between 3000 – 1200 cal. years BP. In the same interval, the occurrence of clasts increases (50 – 20 cm depth in Figure 5.14). Around 2000 cal. years BP, a marked increase in magnetic susceptibility and the Fe-content occurs in core 24. A similar increase in magnetic

susceptibility occurs in core 49 (Figure 6.16). As the age model for core 49 is based only on one date, the increase in magnetic susceptibility may have occurred more simultaneously with core 24 than Figure 6.16 shows. An increase is observed in the magnetic susceptibility of core 48 as well (Figure 5.9), but as there are no dated intervals in this core, it is not possible to pinpoint the timing of the increase. However, as there is such an apparent increase in magnetic susceptibility of these three cores, it is likely that it has happened at approximately the same time. As the magnetic susceptibility has been suggested to represent input from the Hornemantoppen granite and Smeerenburgbreen, the observed increase in magnetic susceptibility may relate to increased calving and ice rafting from Smeerenburgbreen. IRD with higher magnetic susceptibility would then be transported to the core sites. The increased calving may relate either to glacial advances or retreats. Forwick et al. (2010) observed an increase in IRD content in Tempelfjorden around 2000 cal. years BP and suggested that this might be related to glacial retreat during the Roman Warm Period. Although no significant increase in IRD is observed in Smeerenburgfjorden for this interval, the increased magnetic susceptibility and Fe-content may indicate increased calving from Smeerenburgbreen possibly related to a glacial retreat which may have occurred as a response to the warming during the Roman Warm Period (~50 BC – AD 500; e.g. Spielhagen et al., 2011; Jernas et al., in press).

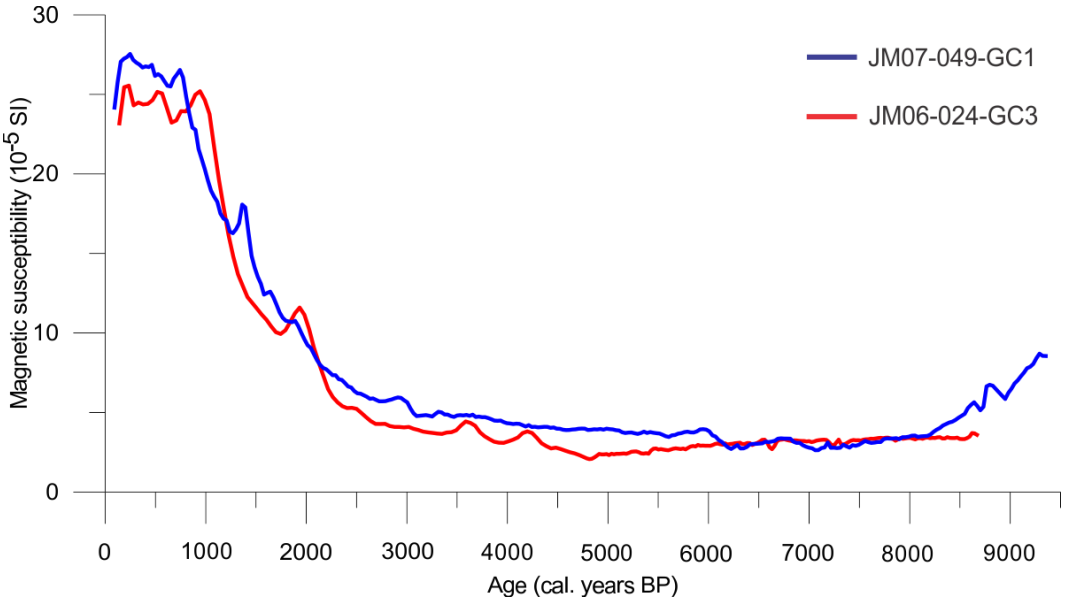

Figure 6.16: *Magnetic susceptibility for the two outermost cores JM07-049-GC1 (blue) and JM06-024-GC3 (red).*

The continued presence of IRD and the increase in magnetic susceptibility and Fe-content towards the end of this time interval (Figure 6.14) indicates that glacial activity remained high. The Roman Warm Period ended around AD 400 and was followed by the Dark Ages Cold Period (DACP; AD 400 – 800; e.g. Spielhagen et al., 2011; Jernas et al., in press). According to Jernas et al. (in press), generally deteriorated conditions with reduced inflow of AW and enhanced inflow of Arctic Water (ArW) occurred in the Hinlopen and Kongsfjorden Troughs at this time. Svendsen & Mangerud (1997) found high input of glacial sediments to Linnèvatnet between AD 400 – 500 and suggested that this period represented one of the glacial maxima that occurred during the late Holocene. It is therefore possible that the increase in magnetic susceptibility towards the end of this interval is related to increased glacial activity and calving from Smeerenburgbreen during the Dark Ages Cold Period. However, as the stratigraphic resolution of core 24 (which spans this time interval) is relatively low, it is not possible to distinguish the Dark Ages Cold Period as one separate event.

6.5.4 Latest Holocene (1200 – 0 cal. years BP; AD 750 - present)

Due to the low stratigraphic resolution of core 49 and 24, it is difficult to identify different climatic signals within this period. However, there is an overall increase in the sand content and a high number of clasts (Figures 5.14 and 6.14). In the same interval, the Fe-content generally increases and a peak in the Ca-content occurs. The highest magnetic susceptibility for both core 49 and 24 occur in this interval. The increase in Fe-content and the high magnetic susceptibility point towards a continued increase in input of icebergs and IRD originating from Smeerenburgbreen and the Hornemantoppen granite. The increased ice rafting may be related both to glacier growth and retreat; glacier retreat may have occurred in the Medieval Warm Period (c. AD 900 – 1500; e.g. Spielhagen et al., 2011) and glacier growth most probably occurred during the Little Ice Age (AD 1500 – 1900; e.g. Svendsen & Mangerud, 1997).

In core 22 and 23, the clast contents are relatively high and stable throughout this interval (Figures 5.4 and 5.8). Due to the 2 cm sample interval of grain-size distribution, frequent peaks in the sand content are distinguishable in core 22 (Figure 6.17). Other than an increase in the sulphur content between c. AD 900 – 1300 and an increase in the Ca-content around AD 1300 – 1400, no apparent trends are observed in the element ratios.

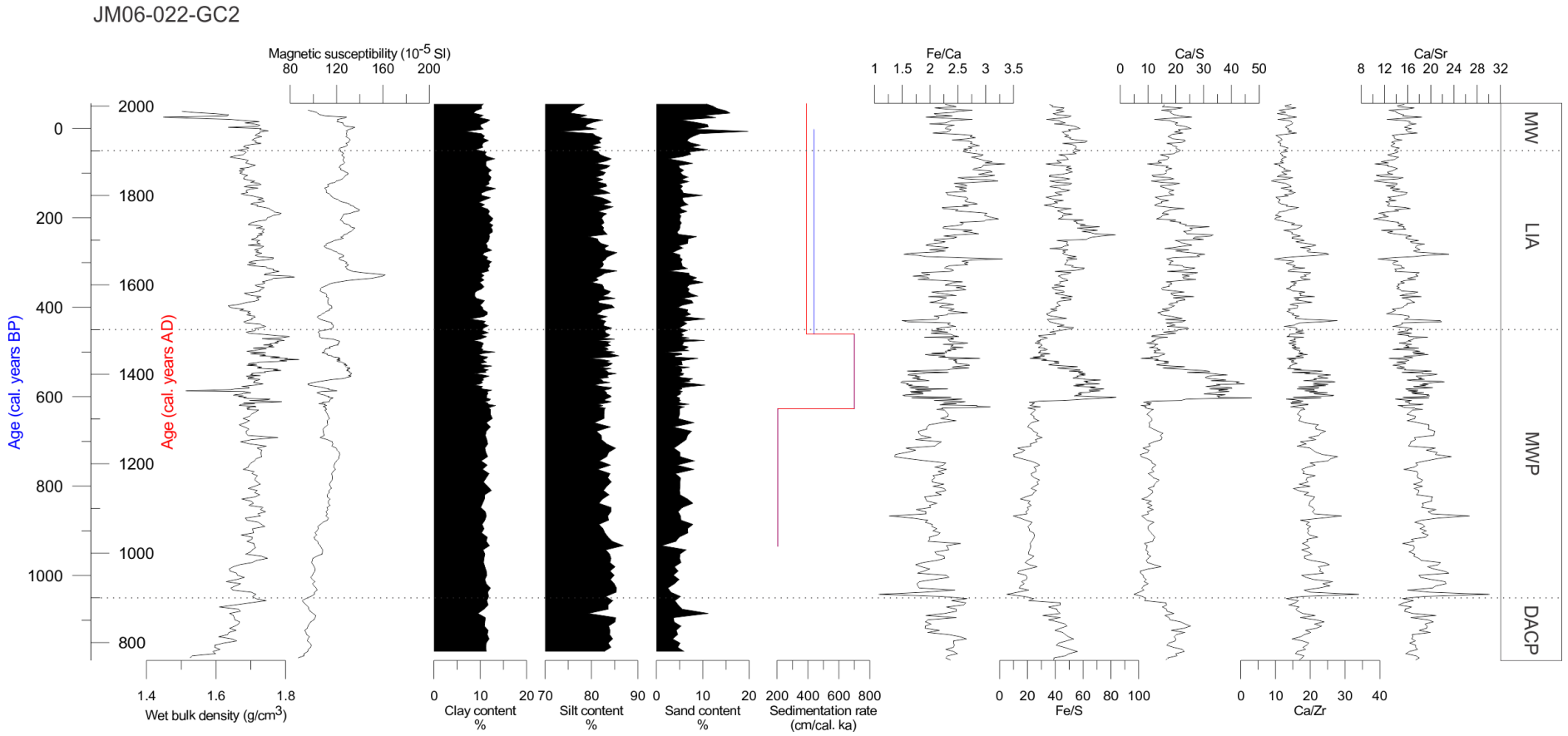

Figure 6.17: *Physical properties, grain-size distribution, sedimentation rates (cm/cal. ka) and element geochemistry for core JM06-022-GC2 plotted against age (cal. years AD and cal. years BP). The main subdivisions of the past ~1200 cal. years are indicated.* ***DACP (AD 400 – 800)*** *= Dark Ages Cold Period;* ***MWP (AD 900 – 1500)*** *= Medieval Warm Period;* ***LIA (AD 1500 – 1900)*** *= Little Ice Age;* ***MW (1900 – present)*** *= Morden Warming.*

6.5.4.1 The Medieval Warm Period (MWP; AD 900 – 1500)

Indications of climatic variability in the Arctic during the Medieval Warm Period have been reported by several studies which show a relative warming around AD ~1000 (Miller et al., 2010 and references therein). In western Spitsbergen, D'Andrea et al. (2012) found that warmer summers occurred in two episodes during the MWP; between AD 1010 – 1060, and 1160 – 1250. In the Fram Strait, higher sea-surface temperatures, strengthened AW inflow and greatly reduced sea-ice conditions have been suggested for the early MWP (AD ~1000; Werner et al., 2011).

Based on lithological and foraminiferal studies, Jernas et al. (in press) found generally ameliorated conditions with high productivity and enhanced inflow of AW in the Hinlopen and Kongsfjorden troughs for the period AD 700 – 1500 and, thus, suggested this period to represent the Medieval Warm Period. During this 800 year period, the interval from AD c. 900 – 1150 was identified as the temperature optimum whereas the maximum biological productivity occurred between AD 1200 and AD 1500 (Jernas et al., in press). In addition, these authors found an increase in IRD and increased sedimentation rates for the interval from c. AD 1200 - 1500 (cf. *6.3 Sedimentation rates*; Figure 6.9) and attributed this to general growth of glaciers and/or glacier surges on Svalbard during this time period. A similar increase in sedimentation rate is found for core 22 in Smeerenburgfjorden (Figure 6.17). In core 22, more frequent peaks in the sand content occur in the period between AD 1200 and 1500 and correspond to the interval of increased IRD in the cores from Hinlopen and Kongsfjorden (Figures 6.17 and 6.18). However, it is reasonable to assume that the sedimentary environment is different in the inner part of the fjord (this study) compared to that of an outer fjord trough (Jernas et al., in press). It is possible that the continued input of suspended sediment from the tidewater glaciers of inner Smeerenburgfjorden is masking some of the IRD input. A small peak in the sand content and an increase in clasts are observed for approximately the same interval (AD c. 1360 – 1420) in core 23 (150 – 120 cm in Figure 5.8). However, the age model of this core is based on only one date and a mean sedimentation rate. The uncertainties of the age model may therefore cause the timing of the IRD increase to vary from the true age. In addition, it is possible that the large accumulation of clasts in this interval (~130 cm in Figure 5.8) may represent IRD dumped from one iceberg rather than a general increase in ice rafting (cf. Vorren et al., 1983).

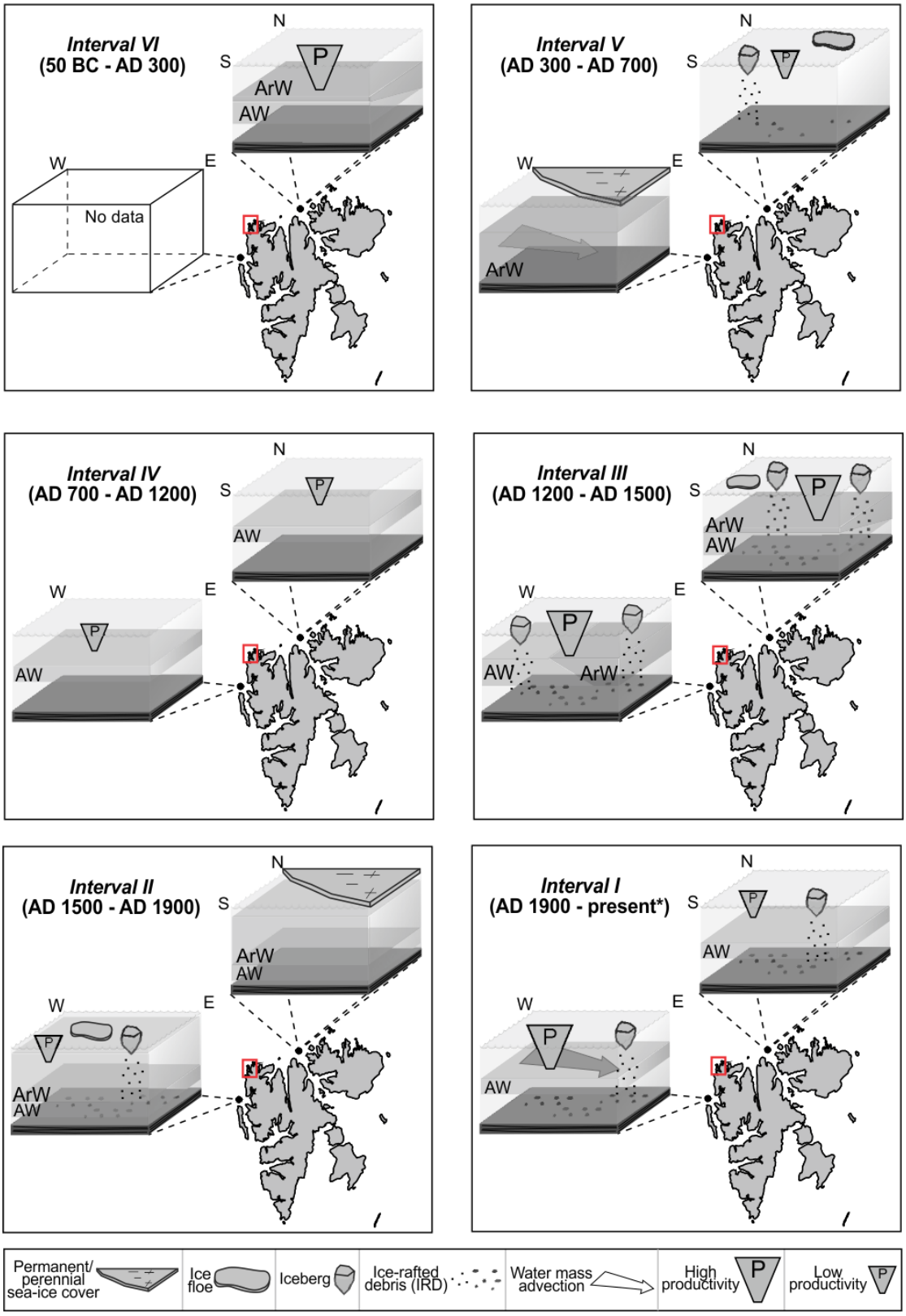

Figure 6.18: *Reconstruction of the palaeoenvironments in the Hinlopen Trough and Kongsfjorden Trough. The time intervals correspond roughly to the time-slices of this study: Interval I = MW; Interval II = LIA; Interval III and IV = MWP; Interval V = DACP; Interval VI = RWP. Smeerenburgfjorden is indicated by the red box. Modified from Jernas et al., in press.*

According to Jernas et al. (in press), the period between AD 1200 – 1500 is suggested to represent a maximum in productivity and the period with the most favourable conditions for benthic foraminifera. In addition, productivity peaks have been identified in the eastern Fram Strait for approximately the same time period (Spielhagen et al., 2011; Werner et al., 2011). In core 22 from Smeerenburgfjorden there is a marked increase in the Ca-content occurring between c. AD 1320 and 1420 (Figure 6.17). As productivity peaks were identified south (Kongsfjorden), north-east (Hinlopen) and west (Fram Strait) of the core site, it is possible that the Ca-increase in Smeerenburgfjorden represents a similar peak in productivity linked to the regional increase in productivity. An increase in productivity and a higher organic flux may possibly be the reason for the increase in sedimentation rate in this interval (Figure 6.9). The increase in Ca-content in Smeerenburgfjorden seems to have occurred relatively abruptly and ends as early as AD ~1420. This is earlier than the productivity peak in Hinlopen and Kongsfjorden which ended around AD 1500, and the peak observed in the Fram Strait which persisted until AD 1650 (Spielhagen et al., 2011; Werner et al., 2011). However, as mentioned earlier, some difference is to be expected between the core sites due to the different environmental and oceanographic settings of the cores used in the other studies. A similar peak in the Ca-content is observed in core 24 (Figure 6.14) for approximately the same interval. As the stratigraphic resolution of core 24 is relatively low, it is difficult to pinpoint the timing of this peak, but it appears to have occurred around AD 1600. It is possible that this Ca-peak also represents enhanced productivity related to the regional increase.

6.5.4.2 The Little Ice Age (LIA; c. AD 1500 – 1900)

The sand content in core 22 increases slightly towards AD 1600 after which the sand content is relatively low until AD 1880. After AD 1880, the sand content increases slightly followed by a significant increase shortly after AD 1900 (Figure 6.17). The clast content is high and relatively stable throughout this period which is interpreted to represent the Little Ice Age (c. AD 1500 - 1900) in Smeerenburgfjorden. The reduced sand content may be a result of colder conditions and more sea-ice cover during this period (Figure 6.19). The Little Ice Age represented the maximum Holocene extent for Svalbard glaciers (e.g. Werner, 1993; Svendsen & Mangerud, 1997; Plassen et al., 2004) and the glacial advances during this period were either climatically induced or related to surges (Plassen et al., 2004).

Based on an ice-core record from Svalbard, Isaksson et al. (2005) suggested that a significant cooling started AD ~1500 and that the coldest period of the Little Ice Age occurred in the period from AD 1760 to AD 1900. In the eastern Fram Strait, a two-phased cooling during the LIA has been identified from a multi-proxy dataset (Werner et al., 2011). The first cooling event occurred around AD 1600 (Bonnet et al., 2010; Werner et al., 2011) and the second around AD 1900 (Werner et al., 2011). Svendsen & Mangerud (1997; and references therein) suggested that the Little Ice Age occurred in response to lower temperatures. However, based on alkenones (small fractions of plankton; Ruddiman, 2001) in a lake core from Kongressvatnet in western Spitsbergen, D'Andrea et al. (2012) postulated that increased heat transport by the West Spitsbergen Current (WSC) commenced around AD 1600 and that the LIA summer temperatures were not especially cold. Rather than cold temperatures, D'Andrea et al (2012) suggested that an increase in precipitation during winter caused the LIA glacial advance. Arctic sea-ice reconstructions performed by Kinnard et al. (2011) suggest that the sea-ice cover during the early LIA was reduced, similarly to that of the early MWP. Furthermore, Kinnard et al. (2011) found that the sea-ice cover generally increased from AD ~1750 towards AD 1900. In addition to cold sea-surface temperatures, Bonnet et al. (2010) suggested a similar reduced sea-ice cover during the LIA which increased towards AD 1900 in the Fram Strait.

In the Hinlopen Trough, Jernas et al. (in press) found that the LIA was dominated by a reduced inflow of Atlantic Water, very low productivity and an extensive sea-ice cover. Although ice rafting occurred, less harsh conditions prevailed in outer Kongsfjorden where relatively favourable environmental conditions and high productivity were sustained by summer advection of AW (Jernas et al., in press; Figure 6.18). The increase in IRD towards AD 1600 in Smeerenburgfjorden (Figure 6.17) may reflect glacial advance related to the first cooling pulse observed by Bonnet et al. (2010) and Werner et al. (2011) in the Fram Strait. The subsequent decrease to a lower, relatively stable, IRD content may be caused by supressed iceberg calving or trapping of icebergs within the sea-ice. Increased sea-ice cover has been suggested for the Hinlopen Trough at this time (Jernas et al., in press; Figure 6.18) and in the eastern Fram Strait, sea-ice cover may have increased during the late LIA (Bonnet et al., 2010; Kinnard et al., 2011). It is therefore possible that enhanced sea-ice formation may have occurred in the fjords as well.

Other studies have inferred that the maximum LIA position was reached around AD 1900 and that general retreat has occurred since (e.g. Werner et al., 1993; Svendsen & Mangerud, 1997;

Plassen et al., 2004). The increase in IRD in Smeerenburgfjorden around AD 1900 may therefore represent the onset of retreat from the maximum extent of the glacier.

6.5.4.3 The Modern Warming (AD 1900 – present)

The Holocene maximum position of Smeerenburgbreen was probably reached around AD 1900 (*Chapter 6.5.4.2*) and is expressed in the LIA moraine in the inner fjord (Figure 4.2 D and 6 in Figure 4.3; Ottesen & Dowdeswell, 2009). Thus, the Modern Warming (AD 1900 – present) represents the retreat from the LIA moraine to the present day terminus of Smeerenburgbreen; a distance of approximately 2.5 - 3 km (Figure 4.3). The recessional moraines within the LIA moraine were deposited during this retreat (Figures 4.2 D and 6.3; e.g. Ottesen & Dowdeswell, 2009) and are therefore the most recent morphological features in the fjord. The mean retreat rate of Smeerenburgbreen was 87.5 m/year during the Modern Warming, whereas the mean rate during the last deglaciation was 140 m/year (cf. *Chapter 6.1*). The different retreat rates are probably the result of the different glacier configurations of the two periods; during the deglaciation the insolation was higher (Berger & Loutre, 1991), the inflow of Atlantic Water was stronger and the water masses were warmer (e.g. Rasmussen et al., 2012), the sea level was higher (e.g. Forman et al., 2004) and the ice was thicker (cf. Landvik et al., 2003) than during the past 100 years.

The glacial retreat following the Little Ice Age is also seen in the IRD record of core 22, which has the highest sand content of the entire core length (Figure 6.17). Generally the sand content increases towards the core top, with the two most distinct peaks occurring around AD 1940 and AD 1990.

Werner et al. (2011) observed an increasing influence of AW in the Fram Strait already from AD 1850. However, due to continued cold surface conditions, icebergs and sea ice were still present at the core site (see Werner et al., 2011 for location). A strong warming around AD 1900 was observed in an ice-core record from Svalbard (Isaksson et al., 2005) and Kinnard et al. (2011) suggested a general decrease in the sea-ice cover from c. AD 1900. Werner et al. (2011) suggested that an abrupt warming event occurred around AD 1930 in the Fram Strait; this warming is also seen in instrumental data from Svalbard (Førland et al., 2009; Werner et al., 2011; Figure 2.4). Spielhagen et al. (2011 and references therein) postulated that the strongest inflow of AW to the Arctic Ocean occurred during the past 30 years. In western Spitsbergen, D'Andrea et al. (2012) found that the period between AD 1987 and AD 2009

experienced especially warm summer temperatures and that the temperatures in this period are unprecedented in Svalbard during the past 1800 years. Jernas et al. (in press) found that generally warmer conditions with increased productivity and inflow of Atlantic Water prevailed in the Kongsfjorden Trough at this time and that the sea-ice cover in Hinlopen was spatially and/or temporally reduced.

In addition to intensified calving related to glacier retreat, a reduction in the sea-ice cover, as suggested by Kinnard et al. (2011), may have allowed more icebergs to be transported further out in Smeerenburgfjorden. The peak in sand content around AD 1940 in core 22 may reflect glacial retreat and increased calving related to the abrupt warming in AD 1930 suggested by Spielhagen et al. (2011). The high sand content during the last ~30 years may also be related to increased calving and retreat caused by the most recent warming suggested by D'Andrea et al. (2012) and Spielhagen et al. (2011). However, due to uncertainties in the age model, care should be taken when pinpointing singular peaks to specific years. In addition, the fjord may have a more local response to regional climatic changes.

In summary, based on variations in IRD content and physical and geochemical properties, the palaeoclimatc conditions in Smeerenburgfjorden are relatively similar to findings from other western Spitsbergen fjords as well as to the western Svalbard continental margin. The discrepancies between the fjord records may be due to regionalism as well as differences between the methods, proxies and dating material used.

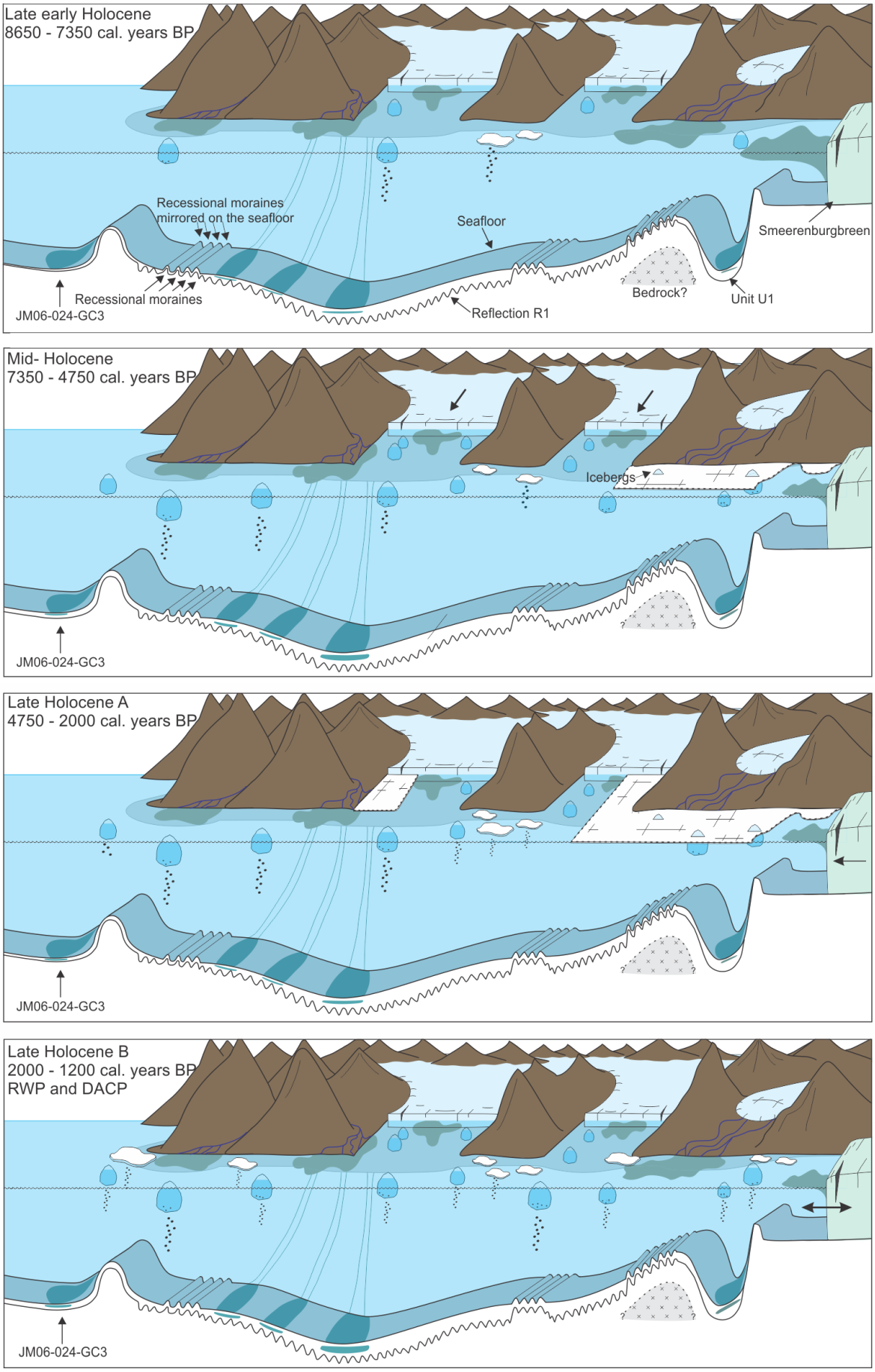
Late early Holocene
8650 - 7350 cal. years BP
Recessional moraines
mirrored on the seafloor
Seafloor
Smeerenburgbreen
Recessional moraines
JM06-024-GC3
Reflection R1
Bedrock?
Unit U1
Mid- Holocene
7350 - 4750 cal. years BP
Icebergs
JM06-024-GC3
Late Holocene A
4750 - 2000 cal. years BP
JM06-024-GC3
Late Holocene B
2000 - 1200 cal. years BP
RWP and DACP
JM06-024-GC3

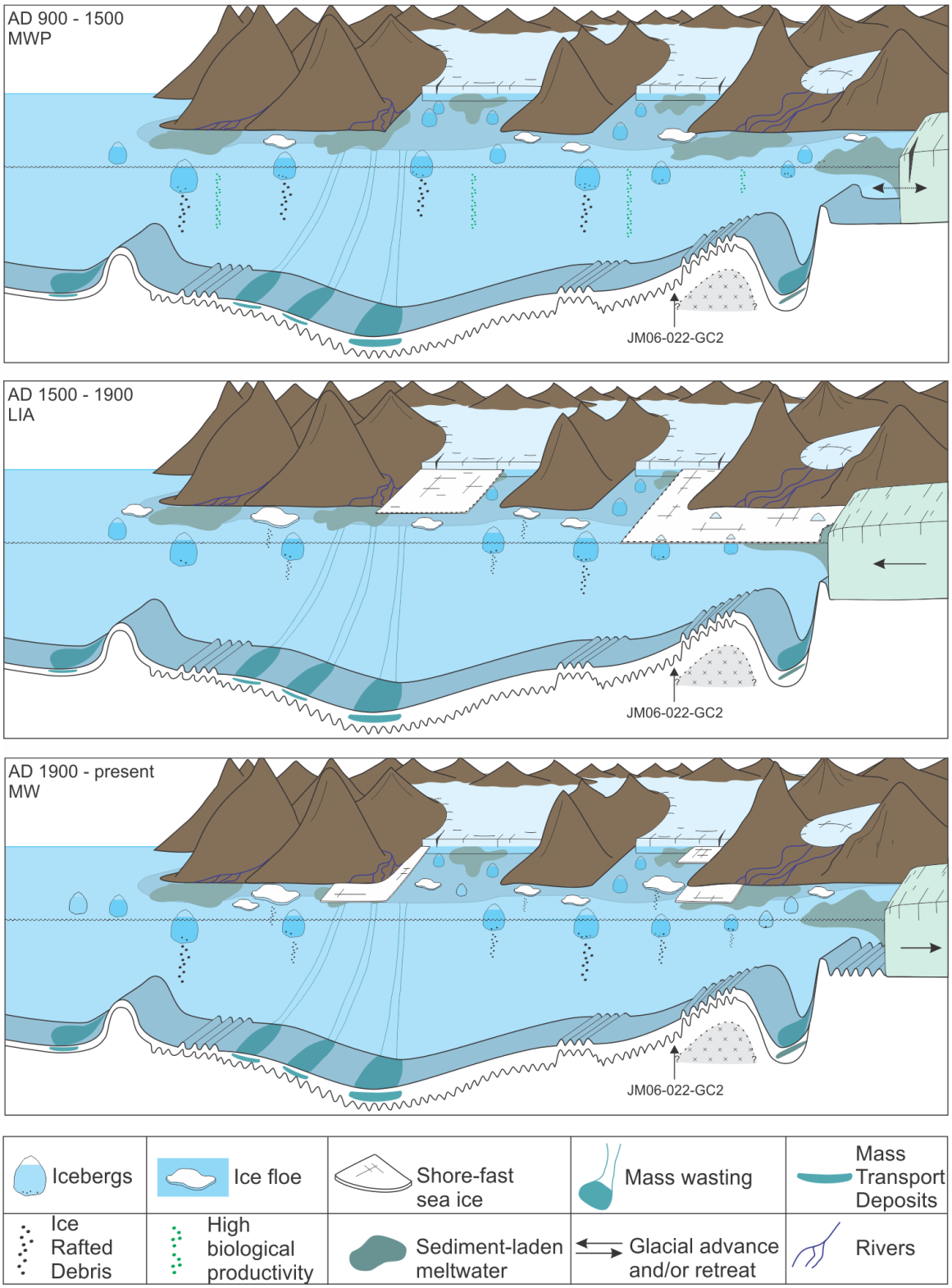

Figure 6.19: *Illustrative sketches of the main sedimentary processes and palaeoenvironments in Smeerenburgfjorden for the different time-slices discussed in the text. The core used to reconstruct the specific time-slices is indicated with an arrow. RWP = Roman Warm Period (50 BC – AD 400); DACP = Dark Ages Cold Period (AD 400 – 800); MWP = Medieval Warm Period; LIA = the Little Ice Age; MW = the Modern Warming.*

7. Summary and conclusions

Six sediment cores from Smeerenburgfjorden, northwest Spitsbergen, were analysed and correlated with swath bathymetry and chirp data in order to elucidate the Holocene sedimentary processes and to reconstruct the Holocene palaeoenvironments of the fjord and adjacent areas.

- The large-scale bathymetry is divided into three main basins. Sills occur at the fjord mouth and in the inner fjord, the latter being a bedrock sill. Further in-fjord, a transverse ridge represents the maximum position of Smeerenburgbreen during the Little Ice Age (LIA). Two sets of recessional moraines occur: 1) Recessional moraines deposited between the bedrock sill and the fjord mouth during the last deglaciation. These moraines are only visible in shallower parts; 2) recessional moraines between the LIA and the present position of Smeerenburgbreen.
- Chirp data reveal the continuous occurrence of recessional moraines also in the deeper parts; between the inner bedrock sill and the fjord mouth, and also demonstrate that they are masked by younger sediments.
- Assuming that the recessional moraines were deposited annually, the mean retreat rate of the glacier front was ~140 m/year during the last deglaciation. The retreat of the ice front from its LIA maximum position was ~87.5 m/year.
- The chirp data allow a general distinction of two seismic reflections; the lower reflection represents the sub-surface of a glacial till and the upper represents the present day seafloor. One sedimentary unit is defined between the two reflections. The unit is generally thinning towards the fjord mouth and comprises several internal reflections. Some of these are interpreted to reflect MTD's and others represent changes in grain-size.
- Sedimentation rates decrease strongly in the out-fjord direction, most likely related to the increasing distance from the main sediment source Smeerenburgbreen at the fjord head.
- The dominating sedimentary processes in Smeerenburgfjorden are suspension settling from turbid meltwater plumes entering the fjord at the front of tidewater glaciers and river mouths, as well as ice rafting by icebergs and sea-ice. The relative importance of ice rafting increases in the out-fjord direction where the influence of suspended

sediment decreases. Mass-transport activity occurs along the fjord sides, but is most prominent off river deltas and tidewater glaciers.

- Magnetic susceptibility and Fe-content decrease out-fjord and are suggested to reflect variations in sediment input from Smeerenburgbreen eroding into the Hornemantoppen granite. The out-fjord increase of Ca-contents is most probably linked to the amount of biogenic carbonates in the cores.
- Recessional moraines in the outer part of Smeerenburgfjorden were deposited prior to 8650 cal. years BP. At least two mass wasting events occurred at the fjord mouth, either from the fjord mouth sill or from the adjacent shallow areas off Amsterdamøya.
- Ice rafting was low in the outer fjord between 8650 and 7350 cal. years BP and most likely occurred from icebergs. However, the ice-rafted debris (IRD) most probably derived from more local tide-water glaciers because warmer surface waters forced icebergs to release their debris in the vicinity of the glaciers.
- Ice rafting – presumably from icebergs and sea ice – increased around 6200 cal. years BP and reached a maximum around 5200 cal. years BP. However, the sea-ice cover may have been suppressing iceberg calving so that icebergs from Smeerenburgbreen were trapped in the inner fjord. The increase in glacial activity and sea-ice formation was possibly related to a general regional cooling. Although conditions may have been cooler, favourable conditions for molluscs still existed.
- Smeerenburgbreen became more active from c. 2000 cal. years BP. The increasing glacial activity may have been related to glacial retreat during the Roman Warm Period (50 BC – AD 400) and glacial advance during the Dark Ages Cold Period (AD 400 – 800).
- Increased ice rafting, higher sedimentation rates and a peak in productivity characterises the last part of the Medieval Warm Period (AD 1300 – 1500).
- Increased ice rafting related to the Little Ice Age glacier growth occurred until AD 1600. It was subsequently reduced until AD 1880 when Smeerenburgbreen's retreat from the LIA maximum position commenced.

References

Andersen, B.G., Mangerud, J., Sørensen, R., Reite, A., Sveian, H., Thoresen, M. & Bergstrøm, B., 1995. Younger Dryas ice-marginal deposits in Norway. *Quaternary International*, **28**, pp. 147-169, http://dx.doi.org/10.1016/1040-6182(95)00037-J

Andersen, E.S., Dokken, T.M., Elverhøi, A., Solheim, A. & Fossen, I., 1996. Late Quaternary sedimentation and glacial history of the western Svalbard continental margin. *Marine Geology*, **133**, pp. 123-156

Avaatech XRF, 2012. Avaatech XRF Core Scanner, URL: www.avaatech.com

Azetsu-Scott, K. & Syvitski, J.P.M., 1999. Influence of melting icebergs on distribution, characteristics and transport of marine particles in an East Greenland fjord. *Journal of Geophysical Research*, **104(C3)**, pp. 5321-5328, doi: 10.1029/1998JC900083

Baeten, N.J., 2007. Late Weichselian and Holocene sedimentary processes and environments in Billefjorden, Svalbard. Master's thesis at the Faculty of Science, Department of Geology, University of Tromsø, November 2007.

Baeten, N.J., Forwick, M., Vogt, C. & Vorren, T.O., 2010. Late Weichselian and Holocene environments and glacial activity in Billefjorden, Svalbard. *In:* Howe, J.A., Austin, W.E.N., Forwick, M. & Paetzel, M. (eds) *Fjord systems and archives*. Geological Society, London, Special Publications, **344**, pp. 207-223, doi: 10.1144/SP344.15

Batchelor, C.L., Dowdeswell, J.A. & Hogan, K.A., 2011. Late Quaternary ice flow and sediment delivery through Hinlopen Trough, Northern Svalbard margin: Submarine landforms and depositional fan. *Marine Geology*, **284**, pp. 13-27, doi: 10.1016/j.margeo.2011.03.005

Benn, D.I. & Evans, D.J.A., 2010. *Glaciers and glaciation*. Second edition. London: Hodder Education

Berger, A. & Loutre, M.F., 1991. Insolation values for the climate of the last 10 million years. *Quaternary Science Reviews*, **10**, pp- 297-317, doi: http://dx.doi.org/10.1016/0277-3791(91)90033-Q

Birks, H., 1991. Holocene vegetational history and climatic change in west Spitsbergen – plant macrofossils from Skardtjørna, an Arctic lake. *The Holocene*, **1(3)**, pp. 209-218, doi: 10.1177/095968369100100303

Blaszczyk, M., Jania, J.A. & Hagen, J.O., 2009. Tidewater glaciers of Svalbard: Recent changes and estimates of calving fluxes. *Polish Polar Research*, **30(2)**, pp. 85-182

Blott, S.J. & Pye, K., 2001. Gradistat: A grain size distribution and statistics package for the analysis of unconsolidated sediments. *Earth Surface Processes and Landforms*, **26**, pp. 1237 – 1248, doi: 10.1002/esp.261

Bonnet, S., de Vernal, A., Hillaire-Marcel, C., Radi, T. & Husum, K., 2010. Variability of sea-surface temperature and sea-ice cover in the Fram Strait over the last two millennia. *Marine Micropaleontology*, **74**, pp. 54-74, doi: 10.1016/j.marmicro.2009.12.001

Boulton, G.S., 1986. Push-moraines and glacier-contact fans in marine and terrestrial environments. *Sedimentology*, **33(2)**, pp. 677 - 698

Bowman, S., 1990. *Radiocarbon dating*. Berkley and Los Angeles: University of California Press

Brouwer, P., 2003*. Theory of XRF, getting acquainted with the principles*. The Netherlands, PANalytical B.V.

Carter, L., 2009. Charting the seafloor: Multibeam echo sounding, *Te Ara – the Encyclopedia of New Zealand.* URL: http://www.teara.govt.nz/en/charting-the-sea-floor/4 (updated 2 March 2009) [viewed 20 July 2012]

Cilas, Cilas Particle Size Analyzer, URL: http://www.particle-size-analyser.com/cilas_1180_particle.htm#

Cottier, F.R., Nilsen, F., Inall, M.E., Gerland, S., Tverberg, V. & Svendsen, H., 2007. Wintertime warming of an Arctic shelf in response to large-scale atmospheric circulation. *Geophysical Research Letters*, **34**, doi: 10.1029/2007GL029948

Cottier, F.R., Nilsen, F., Skogseth, R., Tverberg, V., Skarðhamar, J. & Svendsen, H., 2010. Arctic fjords: a review of the oceanographic environment and dominant physical processes. *In:* Howe, J.A., Austin, W.E.N., Forwick, M. & Paetzel, M. (eds.) *Fjord systems and archives*. Geological Society, London, Special Publications, **344**, pp. 35-50, doi: 10.1144/SP344.4

Dallmann, W.K., Ohta, Y., Elvevold, S. & Blomeier, D., 2002. Bedrock map of Svalbard and Jan Mayen. Norsk Polarinstitutt Temakart No. 33

Dickson, R.R., Osborn, T.J., Hurrell, J.W., Meincke, J., Blindheim, J., Adlandsvik, B., Vinje, T., Alekseev, G. & Maslowski, W., 2000. The Arctic Ocean response to the North Atlantic Oscillation. *Journal of Climate*, **13**, pp. 2671-2696, doi: http://dx.doi.org/10.1175/1520-0442(2000)013<2671:TAORTT>2.0.CO;2

Domack, E.W. & McClennen, C.E., 1996. Accumulation of glacial marine sediments in fjords of the Antarctic Peninsula and their use as late Holocene paleoenvironmental indicators. *In:* Ross, R.M., Hofmann, E.E. & Quetin, L.B. (eds.)

Foundations for ecological research west of the Antarctic Peninsula. Antarctic Research Series, **70**, pp. 135-154

Dowdeswell, J.A., 1987. Processes of glacimarine sedimentation. *Progress in physical geography*, **11 (1)**, pp. 52 – 90, doi: 10.1177/03913338701100103

Dowdeswell, J.A. & Dowdeswell, E.K., 1989. Debris in icebergs and rates of glaci-marine sedimentation: observations from Spitsbergen and a simple model. *Journal of Geology*, **97(2)**, pp. 221-231, doi: jstor.org/stable/30065541

Dyke, A.S. & Savelle, J.M., 2000. Major end moraines of Younger Dryas age on Wollaston Peninsula, Victoria Island, Canadian Arctic: implications for palaeoclimate and for formation of hummocky moraine. *Canadian Journal of Earth Sciences*, **37(4)**, pp. 601-619, doi: 10.1139/e99-118

D'Andrea, W.J., Vaillencourt, D.A., Balascio, N.L., Werner, A., Roof, S.R., Retelle, M. & Bradley, R.S., 2012. Mild Litte Ice Age and unprecedented recent warmth in an 1800 year lake sediment record from Svalbard. *Geology*, **40(11)**, pp. 1007-1010, doi: 10.1130/G33365.1

Elverhøi, A., Liestøl, O. & Nagy, J., 1980. Glacial erosion, sedimentation and microfauna in the inner part of Kongsfjorden, Spitsbergen. *In:* Geological and geophysical research in Svalbard and on Jan Mayen. *Norsk Polarinstitutt Skrifter 172*, pp. 33-58

Elverhøi, A., Lønne, Ø. & Seland, R., 1983. Glaciomarine sedimentation in a modern fjord environment, Spitsbergen. *Polar Research*, **1(2)**, pp. 127-149

Elverhøi, A., Andersen, E.S., Dokken, T., Hebbeln, D., Spielhagen, R., Svendsen, J.I., Sørflaten, M., Rørnes, A., Hald, M. & Forsberg, C.F., 1995. The growth and decay of the Late Weichselian ice sheet in western Svalbard and adjacent areas based on provenance studies of marine sediments. *Quaternary Research,* **44**, pp. 303-316

Elverhøi, A., Harbitz, C.B., Dimakis, P., Mohrig, D., Marr, J. & Parker, G., 2000. On the dynamics of subaqueous debris flows. *Oceanography*, **13(3)**, pp. 109-117, doi: http://dx.doi.org/10.5670/oceanog.2000.20

Forman, S.L., Mann, D.H. & Miller, G.H., 1987. Late Weichselian and Holocene relative sea-level history of Brøggerhalvøya, Spitsbergen. *Quaternary Research*, **27**, pp. 41-50

Forman, S.L., 1990. Post-glacial relative sea-level history of northwestern Spitsbergen, Svalbard. *Geological Society of America Bulletin*, **102(11)**, pp. 1580-1590, doi: 10.1130/0016-7606(1990)102<1580:PGRSLH>2.3.CO;2

Forman, S.L., Lubinski, D.J., Ingòlfsson, Ò., Zeeberg, J.J., Snyder, J.A., Siegert, M.J. & Matishov, G.G., 2004. A review of postglacial emergence on Svalbard, Franz Josef Land and Novaya Zemlya, northern Eurasia. *Quaternary Science Reviews*, **23**, pp. 1391-1434, doi: 10.1016/j.quascirev.2003.12.007

Forwick, M. & Vorren, T.O., 2007. Holocene mass-transport activity and climate in outer Isfjorden, Spitsbergen: marine and subsurface evidence. *The Holocene*, **17(6)**, pp. 707-716, doi: 10.1177/0959683607080510

Forwick, M. & Vorren, T.O., 2009. Late Weichselian and Holocene sedimentary environments and ice rafting in Isfjorden, Spitsbergen. *Palaeogeography, Palaeoclimatology, Palaeoecology*, **280**, pp. 258-274, doi: 10.1016/j.palaeo.2009.06.026

Forwick, M., Vorren, T.O., Hald, M., Korsun, S., Roh, Y., Vogt, C. & Yoo, K.-C., 2010. Spatial and temporal influence of glaciers and rivers on the sedimentary environment in Sassenfjorden and Tempelfjorden. *In:* Howe, J.A., Austin, W.E.N., Forwick, M. & Paetzel, M. (eds.) *Fjord systems and archives*. Geological Society, London, Special Publications, **344**, pp. 163-193, doi: 10.1144/SP344.13

Forwick, M. & Vorren, T.O., 2011a. Stratigraphy and deglaciation of the Isfjorden area, Spitsbergen. *Norwegian Journal of Geology,* **90**, pp. 163-179

Forwick, M. & Vorren, T.O., 2011b. Mass wasting in Isfjorden, Spitsbergen. *In:* Yamada, Y., Kawamura, K., Ikehara, K., Ogawa, Y., Urgeles, R., Mosher, D., Chaytor, J. & Strasser, M. (eds.) *Submarine Mass Movements and Their Consequences*. Advances in Natural and Technological Hazards Research, **31**, 711-722. Springer Verlag

Førland, E.J. & Hanssen-Bauer, I., 2003. Climate variations and implications for precipitation types in the Norwegian Arctic. Norwegian Meteorological Institute Report no. 24/02 Klima. http://met.no/filestore/klima-02-24.pdf

Førland, E.J., Benestad, R.E., Flatøy, F., Hanssen-Bauer, I., Haugen, J.E., Isaksen, K., Sorteberg, A. & Ådlandsvik, B., 2009. Climate development in North Norway and the Svalbard region during 1900-2100. Norsk Polarinstitutt Rapportserie nr. 128

Gammelsrød, T. & Rudels, B., 1983. Hydrographic and current measurements in the Fram Strait, August 1981. *Polar Research*, **1(2)**, pp. 115-126

GEOTEK, 2000. Geotek Multi-Sensor Core Logger (MSCL) Manual

Gilbert, R., 1990. Rafting in glacimarine environments. *In:* Dowdeswell, J.A. & Scourse, J.D. (eds.) *Glacimarine Environments: Processes and Sediments*. Geological Society, London, Special Publications, **53**, pp. 105-120, doi: 10.1144/GSL.SP.1990.053.01.06

Hagen, J.O., Liestøl, O., Roland, E. & Jørgensen, T., 1993. Glacier atlas of Svalbard and Jan Mayen. Norsk Polarinstitutt Meddelelser nr. 129

Hald, M., Ebbesen, H., Forwick, M., Godtliebsen, F., Khomenko, L., Korsun, S., Olsen, L.R. & Vorren, T.O., 2004. Holocene paleoceanography and glacial history of the West Spitsbergen area, Euro-Arctic margin. *Quaternary Science Reviews*, **23**, pp. 2075-2088, doi: 10.1016/j.quascirev.2004.08.006

Hald, M. & Korsun, S., 2008. The 8200 cal. yr BP event reflected in the Arctic fjord, Van Mijenfjorden, Svalbard. *The Holocene*, **18(6)**, pp. 981-990, doi: 10.1177/0959683608093536

Hambrey, M., 1994. Glacial environments. London: UCL Press

Hass, H.C., 2002. A method to reduce the influence of ice-rafted debris on a grain size record from northern Fram Strait, Arctic Ocean. *Polar Research*, **21(2)**, pp. 299-306

Hass, H.C., Kuhn, G., Monien, P., Brumsack, H.-J. & Forwick, M., 2010. Climate fluctuations during the past two millennia as recorded in sediments from Maxwell Bay, South Shetland Islands, West Antarctica. *In:* Howe, J.A., Austin, W.E.N., Forwick, M. & Paetzel, M. (eds.) *Fjord systems and archives*. Geological Society, London, Special Publications, **344**, pp. 243 - 260, doi: 10.1144/SP344.17

Hebbeln, D., 2000. Flux of ice-rafted detritus from sea ice in the Fram Strait. *Deep-Sea Research II*, **47**, pp. 1773-1790, doi: http://dx.doi.org/10.1016/S0967-0645(00)00006-0

Hisdal, V., 1998. Svalbard: Nature and history. Norsk Polarinstitutt Polarhåndbok No. 12

Hjelstuen, B.O., Haflidason, H., Sejrup, H.P. & Lysså, A., 2009. Sedimentary processes and depositional environments in glaciated fjord systems – Evidence from Nordfjord, Norway. *Marine Geology*, **258**, pp. 88-99, doi: 10.1016/j.margeo.2008.11.010

Holtedahl, H., 1967. Notes on the formation of fjords and fjord-valleys. *Geografiska Annaler. Series A, Physical Geography*, **49(2)**, pp. 188-203, http://www.jstor.org/stable/520887

Howe, J.A., Austin, W.E.N., Forwick, M., Paetzel, M., Harland, R. & Cage, A.G., 2010. Fjord systems and archives: a review. *In:* Howe, J.A., Austin, W.E.N., Forwick, M. & Paetzel, M. (eds.) *Fjord systems and archives*. Geological Society, London, Special Publications, **344**, pp. 5-15, doi: 10.1144/SP344.2

Hughen, K., Lehman, S., Southon, J., Overpeck, J., Marchal, O., Herring, C. & Turnbull, J., 2004. ^{14}C Activity and Global Carbon Cycle Changes over the Past 50.000 Years. *Science,* **303**, pp. 202-207

Humlum, O., Instanes, A. & Sollid, J.L., 2003. Permafrost in Svalbard: a review of research history, climatic background and engineering challenges. *Polar Research*, **22(2)**, pp. 191-215

Ingólfsson, Ó., 2011. Fingerprints of Quaternary glaciations on Svalbard. *In:* French, M.I.P. et al. (eds*) Ice-marginal and periglacial processes and sediments*. Geological Society, London, Special Publications*,* **354***,* pp. 15-31

Isaksson, E., Kohler, J., Pohjola, V., Moore, J., Igarashi, M., Karlöf, L., Martma, T., Meijer, H., Motoyama, H., Vaikmäe & van de Wal, R.S.W., 2005. Two ice-core $\delta^{18}O$ records from Svalbard illustrating climate and sea-ice variability over the last 400 years. *The Holocene*, **15(4)**, pp. 501-509, doi: 10.1191/0959683605hl820rp

Jakubas, D., Gluchowska, M., Wojczulanis-Jakubas, K., Karnovsky, N.J., Keslinka, L., Kidawa, D., Walkusz, W., Boehnke, R., Cisek, M., Kwasniewski, S. & Stempniewicz, L., 2011. Foraging effort does not influence body condition and stress level in little auks. *Marine Ecology Progress Series*, **432**, pp. 277-290, doi: 10.3354/meps09082

Jernas, P., Klitgaard-Kristensen, D., Husum, K., Wilson, L. & Koç, N. (in press). Palaeoenvironmental changes of the last two millennia on the western and northern Svalbard shelf.

Jessen, S.P., Rasmussen, T.L., Nielsen, T. & Solheim, A., 2010. A new Late Weichselian and Holocene marine chronology for the western Svalbard slope 30,000-0 cal years BP. *Quaternary Science Reviews*, **29**, pp. 1301-1312, doi: 10.1016/j.quascirev.2010.02.020

Kempf, P., Forwick, M., Laberg, J.S. & Vorren, T.O. (in prep.). Late Weichselian and Holocene sedimentary processes and glacier activity in Van Keulenfjorden

Kessler, M.A., Anderson, R.S. & Briner, J.P., 2008. Fjord insertion into continental margins driven by topographic steering of ice. *Nature Geoscience*, **1(6)**, pp. 365-369, doi: 10.1038/ngeo201

Killingtveit, Å., Pettersson, L-.E. & Sand, K., 2003. Water balance investigations in Svalbard. *Polar Research*, **22(2)**, pp. 161-174

Kinnard, C., Zdanowicz, C.M., Fisher, D.A., Isaksson, E., de Vernal, A. & Thompson, L.G., 2011. Reconstructed changes in Arctic sea ice over the past 1,450 years. *Nature*, **479**, pp.509-513, doi: 10.1038/nature10581

Koç, N., Klitgaard-Kristensen, D., Hasle, K., Forsberg, C.F. & Solheim, A., 2002. Late glacial palaeoceanography of Hinlopen Strait, northern Svalbard. *Polar Research*, **21 (2)**, pp. 307-314, doi: 10.1111/j.1751-8369.2002.tb00085.x

Kongsberg Maritime, 2003. EM 300 30 kHz multibeam echo sounder product specifics

Landvik, J.Y., Mangerud, J. & Salvigsen, O., 1987. The Late Weichselian and Holocene shoreline displacement on the west-central coast of Svalbard. *Polar Research*, **5(1)**, pp. 29-44

Landvik, J.Y., Bondevik, S., Elverhøi, A., Fjeldskaar, W., Mangerud, J., Salvigsen, O., Siegert, M.J., Svendsen, J.I. & Vorren, T.O., 1998. The last glacial maximum of Svalbard and the Barents Sea area: Ice sheet extent and configuration. *Quaternary Science Reviews*, **17**, pp. 43-75

Landvik, J.Y., Brook, E., Gualtieri, L., Raisbeck, G., Salvigsen, O. & Yiou, F., 2003. Northwest Svalbard during the last glaciation: Ice-free areas existed. *Geology*, **31(10)**, pp. 905-908, doi: 10.1130/G19703.1

Landvik, J.Y., Ingólfsson, Ó., Mienert, J., Lehman, S.J., Solheim, A., Elverhøi, A. & Ottesen, D., 2005. Rethinking Late Weichselian ice-sheet dynamics in coastal NW Svalbard. *Boreas*, **34**, pp. 7-24, doi: 10.1080/03009480510012809

Lehman, S.J. & Forman, S.L., 1987. Glacier extent and sea level variation during the Late Weichselian on northwest Spitsbergen. *Polar Research*, **5**, pp. 271-272

Lehman, S.J. & Forman, S.L., 1992. Late Weichselian glacier retreat in Kongsfjorden, west Spitsbergen, Svalbard. *Quaternary Research*, **37**, pp.139-154

Liestøl, O., 1972. Submarine moraines off the west coast of Spitsbergen. *Norsk Polarinstitutt Årbok 1970,* pp. 165-168

Liestøl, O., 1977. Årsmorener foran Nathorstbreen? *Norsk Polarinstitutt Årbok 1976*, pp. 361-363

Lønne, I., 2005. Faint traces of high Arctic glaciations: an early Holocene ice-front fluctuation in Bolterdalen, Svalbard. *Boreas*, **34**, pp. 308-323, doi: 10.1080/03009480510012971

Mangerud J., Bolstad M., Elgersma A., Helliksen D., Landvik J.Y., Lycke A.K., Lønne I., Salvigsen O., Sandahl T. & Sejrup H.P., 1987. The Late Weichselian glacial maximum in western Svalbard. *Polar Research,* **5(3)**, pp. 275-278

Mangerud, J., Dokken, T., Hebbeln, D., Heggen, B., Ingólfsson, Ó., Landvik, J.Y., Mejdahl, V., Svendsen J.I. & Vorren, T.O., 1998. Fluctuations of the Svalbard-Barents Sea Ice Sheet during the last 150 000 years. *Quaternary Science Reviews,* **17**, pp. 11-42

Mangerud, J., Bondevik, S., Gulliksen, S., Hufthammer, A. K. and Høisæter, T., 2006. Marine ^{14}C reservoir ages for 19th century whales and molluscs from the North Atlantic. *Quaternary Science Reviews* **25**, pp. 3228-3245, doi: 10.1016/j.quascirev.2006.03.010

Mangerud, J. & Landvik, J.Y., 2007. Younger Dryas glaciers in western Spitsbergen: smaller than during the Little Ice Age. *Boreas*, **36(3)**, pp. 278-285, doi: 10.1080/03009480601134827

Miller, G.H., Brigham-Grette, J., Alley, R.B., Andreson, L., Bauch, H.A., Douglas, M.S.V., Edwards, M.E., Elias, S.A., Finney, B.P., Fitzpatrick, J.J., Funder, S.V., Herbert, T.D., Hinzman, L.D., Kaufman, D.S., MacDonald, G.M., Polyak, L., Robock, A., Serreze, M.C., Smol, J.P., Spielhagen, R., White, J.W.C., Wolfe, A.P. & Wolff, E.W., 2010. Temperature and precipitation history of the Arctic. *Quaternary Science Reviews*, **29**, pp. 1679-1715, doi: 10.1016/j.quascirev.2010.03.001

Mosher, D. C. & Simpkin, P. G., 1999. Status and trends of marine high-resolution seismic reflection profiling: data acquisition. *Geoscience Canada,* **26(4)**, pp. 174-188

Mulder, T. & Cochonat, P., 1996. Classification of offshore mass movements. *Journal of Sedimentary Research*, **66(1)**, pp. 43-57, doi: 1073-130X/96/066-43/$03.00

Mulder, T. & Alexander, J., 2001. The physical character of subaqueous sedimentary density flows and their deposits. *Sedimentology*, **48(2)**, pp. 269-299, doi: 10.1046/j.1365-3091.2001.00360.x

Mulder, T., 2011. Chapter 2 - Gravity processes and deposits on continental slope, rise and abyssal plains*. In:* HüNeke, H. & Mulder, T. (eds.): *Developments in sedimentology, Deep-Sea Sediments*, Elsevier, **63**, pp. 25-148, doi: 10.1016/B978-0-444-53000-4.00002-0

Müller, J., Werner, K., Stein, R., Fahl, K., Moros, M. & Jansen, E., 2012. Holocene cooling culminates in sea ice oscillations in Fram Strait. *Quaternary Science Reviews*, **47**, pp. 1-14, doi: 10.1016/j.quascirev.2012.04.024

Nardin, T.R., Hein, F.J., Gorsline, D.S. & Edwards, B.D., 1979. A review of mass movement processes, sediment and acoustic characteristics, and contrasts in slope and base-of-slope systems versus canyon-fan-basin floor systems. *The Society of Economic Paleontologists and Mineralogists (SEPM) Special Publication*, **27**, pp. 61-73

Nesje, A. & Whillans, I.M., 1994. Erosion of Sognefjord, Norway. *Geomorphology*, **9(1)**, pp. 33-45, http://dx.doi.org/10.1016/0169-555X(94)90029-9

Nilsen, F., Cottier, F., Skogseth, R. & Mattsson, S., 2008. Fjord-shelf exchanges controlled by ice and brine production: The interannual variation of Atlantic Water in Isfjorden, Svalbard. *Continental Shelf Research*, **28**, pp. 1838-1853, doi: 10.1016/j.csr.2008.04.015

Ó Cofaigh, C. & Dowdeswell, J.A., 2001. Laminated sediments in glacimarine environments: diagnostic criteria for their interpretation. *Quaternary Science Reviews*, **20**, pp. 1411-1436, doi: http://dx.doi.org/10.1016/S0277-3791(00)00177-3

Ohta, Y., Hjelle, A. & Dallmann, W.K., 2007. Geological map Svalbard 1:100 000, sheet A4G, Vasahalvøya. Norsk Polarinstitutt Temakart No. 40

Ohta, Y., Hjelle, A. & Dallmann, W.K., 2008. Geological map Svalbard 1:100 000, sheet A5G, Magdalenefjorden. Norsk Polarinstitutt Temakart No. 41

Ottesen, D., Dowdeswell, J.A. & Rise, L., 2005. Submarine landforms and the reconstruction of fast-flowing ice streams within a large Quaternary ice sheet: The 2500-km-long Norwegian-Svalbard margin (57°-80°N). *Geological Society of America Bulletin*, **117(7/8)**, pp. 1033-1050, doi: 10.1130/B25577.1

Ottesen, D. & Dowdeswell, J.A., 2006. Assemblages of submarine landforms produced by tidewater glaciaers in Svalbard. *Journal of Geophysical Research*, **111**, F01016, doi: 10.1029/2005JF000330

Ottesen, D., Dowdeswell, J.A., Landvik, J.Y. & Mienert, J., 2007. Dynamics of the Late Weichselian ice sheet on Svalbard inferred from high-resolution sea-floor morphology. *Boreas*, **36**, pp. 286-306, doi: 10.1080/03009480701210378

Ottesen, D., Dowdeswell, J.A., Benn, D.I., Kristensen, L., Christiansen, H.H., Christensen, O., Hansen, L., Lebesbye, E., Forwick, M. & Vorren, T.O., 2008. Submarine landform characteristic of glacier surges in two Spitsbergen fjords. *Quaternary Science Reviews*, **27**, pp. 1583 - 1599

Ottesen, D. & Dowdeswell, J.A., 2009. An inter-ice-stream glaciated margin: Submarine landforms and a geomorphic model based on marine-geophysical data from Svalbard. *Geological Society of America Bulletin*, **121(11/12)**, pp. 1647-1665, doi: 10.1130/B26467.1

Plassen, L., Vorren, T.O. & Forwick, M., 2004. Integrated acoustic and coring investigation of glacigenic deposits in Spitsbergen fjords*. Polar Research*, **23(1)**, pp. 89-110

Powell, R.D., 2003. Subaquatic landsystems: Fjords. *In:* Evans, D.J.A. (ed.) *Glacial landsystems.* London: Arnold, pp. 313-347

Prior, D.B., Bornhold, B.D. & Johns, M.W., 1984. Depositional characteristics of a submarine debris flow. *The Journal of Geology*, **92(6)**, pp. 707-727, doi: http://www.jstor.org/stable/30070502

Queens University Belfast, The ^{14}CRONO Centre for Climate the Environment and Chronology, URL: http://chrono.qub.ac.uk/

Quinn, R., Bull, J. M. & Dix, J. K., 1998. Optimal processing of marine high-resolution seismic reflection (Chirp) data. *Marine Geophysical Researches,* **20**, pp. 13-20, doi: 10.1023/A:1004349805280

Rasmussen, T.L., Thomsen, E., Ślubowska, M.A., Jessen, S., Solheim, A. & Koç, N., 2007. Paleoceanographic evolution of the SW Svalbard margin (76°N) since 20,000 ^{14}C yr BP. *Quaternary Research*, **67**, pp.100-114, doi: 10.1016/j.yqres.2006.07.002

Rasmussen, T.L., Forwick, M. & Mackensen, A., 2012. Reconstruction of inflow of Atlantic Water to Isfjorden, Svalbard during the Holocene: Correlation to climate and seasonality. *Marine Micropaleontology*, **94-95**, pp. 80-90, doi: 10.1016/j.marmicro.2012.06.008

Reimer, P. J. & Reimer, R. W., 2001. A marine reservoir correction database and on-line interface. *Radiocarbon,* **43 (2A)**, pp. 461-463

Reimer, P. J., Baillie, M. G. L., Bard, E., Bayliss, A., Beck, J. W., Blackwell, P. G., Ramsey, C. B., Buck, C. E., Burr, G. S., Edwards, R. L., Friedrich, M., Grootes, P. M.,Guilderson, T. P., Hajdas, I., Heaton, T. J., Hogg, A. G., Hughen, K. A., Kaiser., K. F., Kromer, B., McCormac, F. G., Manning, S. W., Reimer, R. W., Richards, D. A., Southon, J. R., Talamo, S., Turney, C. S. M., van der Plicht, J. and Weyhenmeyer, C. E., 2009. *Radiocarbon,* **51***,* pp. 1111-1150

Richter, T.O.,van der Gaast, S., Koster, B., Vaars, A., Gieles, R., deSttigter, H.C., De Haas, H. & van Weering, T.C.E., 2006. The Avaatech XRF Core Scanner: technical description and applications to NE Atlantic sediments. *In:* Rothwell, R.G. 2006. *New Techniques in Sediment Core Analysis.* Geological Society, London, Special Publications, **267**, pp. 39-50, doi: 0305-8719/06/$15.00

Ruddiman, W.F., 2001. Earth's Climate: Past and future. W.H. Freeman & Co., England

Saloranta, T.M. & Svendsen, H., 2001. Across the Arctic front west of Spitsbergen: high-resolution CTD sections from 1998-2000. *Polar Research*, **20(2)**, pp. 177-184

Salvigsen, O., 1977. Radiocarbon datings and the extensions of the Weichselian ice-sheet on Svalbard. *Norsk Polarinstitutt Årbok,* **1976***,* pp. 209-224

Salvigsen, O., Elgersma, A., Hjort, C., Lagerlund, E., Liestøl, O. & Svensson, N.-O., 1990. Glacial history and shoreline displacement on Erdmannflya and Bohemflya, Spitsbergen, Svalbard. *Polar Research*, **8(2)**, pp. 261-272

Salvigsen, O., Forman, S.L. & Miller, G.H., 1992. Thermophilous molluscs on Svalbard during the Holocene and their paleoclimatic implications. *Polar Research*, **11(1)**, pp. 1-10

Sarnthein, M., Van Kreveld, S., Erlenkeuser, H., Grootes, P.M., Kucera, M., Pflaumann, U. & Schulz, M., 2003. Centennial-to-millennial-scale periodicities of Holocene climate and sediment injections off the western Barents shelf, 75°N. *Boreas*, **32**, pp. 447-461, doi: 10.1080/03009480310003351

Schock, S. G., LeBlanc, L. R. & Mayer, L. A., 1989. Chirp subbottom profiler for quantitative sediment analysis. *Geophysics,* **54(4)**, pp. 445-450.

Skarðhamar, J. & Svendsen, H., 2010. Short-term hydrographic variability in a stratified Arctic fjord. *In:* Howe, J.A., Austin, W.E.N., Forwick, M. & Paetzel, M. (eds.) *Fjord systems and archives*. Geological Society, London, Special Publications, **344**, pp. 51-60, doi: 10.1144/SP344.5

Skirbekk, K., Klitgaard-Kristensen, D., Rasmussen, T.L., Koç, N. & Forwick, M., 2010. Holocene climate variations at the entrance to a warm Arctic fjord: evidence from Kongsfjorden trough, Svalbard. *In:* Howe, J.A., Austin, W.E.N., Forwick, M. & Paetzel, M. (eds) *Fjord systems and archives*. Geological Society, London, Special Publications, **344**, pp. 289-304, doi: 10.1144/SP344.20

Skogseth, R., Haugan, P.M. & Jakobsson, M., 2005. Watermass transformations in Storfjorden. *Continental Shelf Research*, **25**, pp. 667-695, doi: 10.1016/j.csr.2004.10.005

Ślubowska, M.A., Koç, N., Rasmussen, T.L. & Klitgaard-Kristensen, D., 2005. Changes in the flow of Atlantic water into the Arctic Ocean since the last deglaciation: Evidence from the northern Svalbard continental margin, 80°N. *Paleoceanography*, **20**, pp. 1-16, doi: 10.1029/2005PA001141

Ślubowska-Woldengen, M., Rasmussen, T.L., Koç, N., Klitgaard-Kristensen, D., Nilsen, F. & Solheim, A., 2007. Advection of Atlantic Water to the western and northern Svalbard shelf since 17,500 cal yr BP. *Quaternary Science Reviews*, **26**, pp. 463-478, doi: 10.1016/j.quascirev.2006.09.009

Spielhagen, R.F., Werner, K., Aagaard Sørensen, S., Zamelczyk, K., Kandiano, E., Budeus, G., Husum, K., Marchitto, T.M. & Hald, M., 2011. Enhanced modern heat transfer to the Arctic by warm Atlantic Water. *Science*, **331**, pp. 450-453, doi: 10.1126/science.1197397

Stewart, I.S., Sauber, J. & Rose, J., 2000. Glacio-seismotectonics: ice sheets, crustal deformation and seismicity. *Quaternary Science Reviews*, **19**, pp. 1367-1389, doi: http://dx.doi.org/10.1016/S0277-3791(00)00094-9

Stuiver, M. & Reimer, P.J., 1986-2011. CALIB Radiocarbon Calibration, URL: http://calib.qub.ac.uk/calib/ (Last updated 10/03/2012)

Stuiver, M., Reimer, P. J., 1993. Extended ^{14}C database and revised CALIB 3.0 ^{14}C calibration program. *Radiocarbon,* **35 (1)**, pp. 215-230

Svendsen, H., Beszczynska-Møller, A., Hagen, J.O., Lefauconnier, B., Tverberg, V., Gerland, S., Ørbæk, J.B., Bischof, K., Papucci, C., Zajaczkowski, M., Azzolini, R., Bruland, O., Wiencke, C., Winther, J.-G. & Dallmann, W., 2002. The physical environment of Kongsfjorden-Krossfjorden, an Arctic fjord system in Svalbard. *Polar Research*, **21(1)**, pp. 133-166

Svendsen, J.I. & Mangerud, J., 1992. Paleoclimatic inferences from glacial fluctuations on Svalbard during the last 20 000 years. *Climate Dynamics*, **6**, pp. 213-220

Svendsen, J.I., Elverhøi, A. & Mangerud, J., 1996. The retreat of the Barents Sea Ice Sheet on the western Svalbard margin. *Boreas*, **25(4)**, pp. 244-256

Svendsen, J.I. & Mangerud, J., 1997. Holocene glacial and climatic variations on Spitsbergen, Svalbard. *The Holocene*, **7(1)**, pp. 45-57, doi: 10.1177/095968369700700105

Syvitski, J.P.M., Burrell, D.C. & Skei, J.M., 1987. Fjords: Processes and products. New York: Springer-Verlag

Syvitski, J.P.M., 1989. On the deposition of sediment within glacier-influenced fjords: oceanographic controls. *Marine Geology*, **85**, pp. 301-329, http://dx.doi.org/10.1016/0025-3227(89)90158-8

Szczuciński, W. & Zajączkowski, M., 2012. Factors controlling downward fluxes of particulate matter in glacier-contact and non-glacier contact settings in a subpolar fjord (Billefjorden, Svalbard). *In:* Li, M.Z., Sherwood, C.R. & Hill, P.R. (eds.) *Sediments, morphology and sedimentary processes on continental shelves. Advances in technologies, research and applications*. International Association of Sedimentologists, Special Publications, **44**, pp. 369-386

Tjallingii, R., Röhl, U., Kölling, M. & Bickert, T., 2007. Influence of the water content on X-ray fluorescence core-scanning measurements in soft marine sediments, *Geochem. Geophys, Geosyst.,* **8 Q02004**, doi:10.1029/2006GC001393

Trusel, L.D., Powell, R.D., Cumpston, R.M. & Brigham-Grette, J., 2010. Modern glacimarine processes and potential future behaviour of Kronebreen and Kongsvegen polythermal tidewater glaciers, Kongsfjorden, Svalbard. *In:* Howe,

J.A., Austin, W.E.N., Forwick, M. & Paetzel, M. (eds.) *Fjord systems and archives*. Geological Society, London, Special Publications, **344**, pp. 89-102, doi: 10.1144/SP344.9

Vorren, T.O., Hald, M., Edvardsen, M. & Lind-Hansen, O-.W., 1983. Glacigenic sediments and sedimentary environments on continental shelves: General principles with a case study from the Norwegian shelf. *In:* Ehlers, J. (ed.): *Glacial Deposits in North-West Europe*. Balkema, Rotterdam, pp. 61-73

Weber, M.E., Niessen, F., Kuhn, G. Wiedicke, M., 1997. Calibration and application of marine sedimentary physical propertie susing a multi-sensor core logger. *Marine Geology*, **136(3-4)**, pp. 151-172, doi: http://dx.doi.org/10.1016/S0025-3227(96)00071-0

Weltje, G. J. & Tjallingii, R., 2008. Calibration of XRF core scanners for quantitative geochemical logging of sediment cores: Theory and application. *Earth and Planetary Science Letters,* **274**, pp. 423-438. doi:10.1016/j.epsl.2008.07.054

Werner, A., 1993. Holocene moraine chronology, Spitsbergen, Svalbard: lichenometric evidence for multiple Neoglacial advances in the Arctic. *The Holocene*, **3(2)**, pp. 128-137, doi: 10.1177/095968369300300204

Werner, K., Spielhagen, R.F., Bauch, D., Hass, C.H., Kandiano, E. & Zamelczyk, K., 2011. Atlantic Water advection to the eastern Fram Strait – multiproxy evidence for late Holocene variability. *Palaeogeography, Palaeoclimatology, Palaeoecology*, **308**, pp. 264-276, doi: 10.1016/j.palaeo.2011.05.030

Włodarska-Kowalczuk, M., Szymelfenig, M. & Zajączkowsksi, M., 2007. Dynaminc sedimentary environments of an Arctic glacier-fed river estuary (Adventfjorden, Svalbard. II: Meio- and macrobenthic fauna. *Estuarine, Coastal and Shelf Science*, **74**, pp. 274-284, doi:10.1016/j.ecss.2007.04.017

Worsley, D. & Aga, O. J., 1986. Evolution of an arctic archipelago, the geological history of Svalbard. *Det norske stats oljeselskap a.s*

Zajączkowsksi, M. & Włodarska-Kowalczuk, M., 2007. Dynamic sedimentary environments of an Arctic glacier-fed river estuary (Adventfjorden, Svalbard). I. Flux, deposition and sediment dynamics. *Estuarine, Coastal and Shelf Science*, **74**, pp. 285-296, doi: 10.1016/j.ecss.2007.04.015

8. References